

# **Waterjet Cutting up to 900 MPa**

Von dem Fachbereich Maschinenbau  
der Universität Hannover  
zur Erlangung des akademischen Grades

Doktor-Ingenieur  
genehmigte Dissertation  
von

M.SC. Eng. Mostafa Ahmed Kamel Mohamed  
geboren am 19. April 1968 in Kena, Ägypten

2004

Referent, Betreuer  
Referent  
Mitprüfer

Prof. Dr.-Ing. H. Louis  
Prof. Dr.-Ing. Gerhard Poll  
Prof. Dr.-Ing. Fr.-W. Bach

Vorsitz der Prüfungskommission: Prof. Eduard Reithmeier

Tag der Promotion: 21.07.2004

# DANKSAGUNG

Diese Arbeit entstand während meiner Anwesenheit als Stipendiat der ägyptischen Regierung am Institut für Werkstoffkunde der Universität Hannover.

Dem Leiter des Instituts, Prof. Dr.-Ing. Fr.-W. Bach möchte ich meinen Dank für die Themenstellung und die Unterstützung während dieser Zeit aussprechen. Ebenso möchte ich Herrn Prof. Dr.-Ing. Dr.-Ing. E.h. mult H. Haferkamp danken, der die Leitung des Instituts bis zum 31.03.2001 innehatte und mir in diesem Zeitraum ebenfalls seine Unterstützung gewährte.

Mein besonderer Dank gilt Herrn Prof. Dr.-Ing. H. Louis. Durch viele wertvolle Anregungen und Diskussionen sowie durch seine engagierte und vorbildliche Unterstützung auf fachlicher und persönlicher Ebene hat er wesentlich zum Gelingen dieser Arbeit beigetragen. Ebenso bedanke ich mich für die Übernahme des Korreferats.

Herrn Prof. Dr.-Ing. Gerhard Poll, Leiter des Institutes für Maschinenelemente, Konstruktionstechnik und Tribologie der Universität Hannover, danke ich für die Übernahme des zweiten Korreferats und die daraus entstandenen Anregungen.

Weiterhin danke ich den Mitarbeitern, die mir durch ihre fachliche und technische Unterstützung eine große Hilfe waren. Besonders hervorheben möchte ich hierbei Herrn Dipl.-Ing. Frank Pude für seine permanente fachliche Ratschläge und beistand bei aller Angelegenheiten. Mein Dank gilt auch Herrn Dipl.-Ing. Alexander Schenk für die fachliche Unterstützung sowie Herrn Bernd Schuster für die hervorragende technische Unterstützung. Des Weiteren gilt mein Dank Herrn Dr.-Ing. Stefan Brandt, Herrn Dr.-Ing. Dirk Barenbrock, Herrn Dipl.-Ing. C. Biskup, Frau Baden, Herrn Dr.-Ing. Wolfgang Milchers, Herrn Dipl.-Ing. Dirk Peter, Herrn Dipl.-Ing. Manfred Pfitzner, Herrn Dr.-Ing. Christoph von Rad, Herrn Dipl.-Ing. Thomas Senne, Herrn Dr.-Ing. Phan Tan Tai und Frau S. Tanenzer (in alphabetischer Reihenfolge).

Mein ganz besonderer Dankes gilt meine Eltern, auch meiner Frau Soumaia Mahmoud, für ihre Unterstützung und das die von ihnen aufgebrachte Verständnis während des Entstehens dieser Arbeit.

Am Ende möchte ich mir bei der ägyptischen Regierung bedanken, die mir die Gelegenheit gegeben hat, hier in Deutschland promovieren zu dürfen.

Hannover, im Juli 2004

Mostafa Mohanmed

# CONTENTS

<b>Nomenclature</b>	<b>VII</b>
<b>Abstract</b>	<b>X</b>
<b>Zusammenfassung</b>	<b>XII</b>
<b>1 Introduction</b>	<b>1</b>
<b>2 State of the art</b>	<b>3</b>
2.1 Historical development of waterjet technology	3
2.2 Pressure generation system	
2.2.1 Plunger pump	4
2.2.2 Intensifier pump	5
2.2.3 Multi-Stage pump	6
2.3 Thermodynamic behaviour of water	7
2.3.1 Phase diagram of ice	7
2.3.2 Compressibility of water	9
2.3.3 Adiabatic heating	11
2.4 Waterjet structure	12
2.5 Cutting result	16
2.5.1 Plain waterjet	16
2.5.2 Abrasive waterjet	19
2.6 Cutting quality and material removal mechanisms	23
2.6.1 Mechanism in liquid impact erosion	23
2.6.2 Mechanism in abrasive waterjet cutting	24
2.6.3 Cutting quality	27
2.7 Modelling of waterjet cutting processes	28
2.7.1 Modelling of plain waterjet cutting for metals	29
2.6.2 Modelling of abrasive waterjet cutting for metals	32
<b>3 Experimental procedure</b>	<b>35</b>
3.1 Experimental setup	35
3.1.1 900 MPa Cutting systems	35

3.1.2	An alternative systems for fundamentals investigations	39
3.1.3	Abrasive waterjet cutting system	40
3.2	Tested materials	41
3.3	Measurements	42
3.3.1	Depth of cut	42
3.3.2	Surface roughness	43
3.3.3	Temperature	44
3.3.3.1	Plain waterjet	45
3.3.3.2	Abrasive waterjet	47
3.4	Surface and wear particle examination	48
3.4.1	Surface examination	48
3.4.2	Wear particle examination	49
<b>4</b>	<b>Materials behaviour</b>	<b>50</b>
4.1	Effect of standoff distance	50
4.2	Effect of traverse rate (loading time)	54
4.3	Effect of loading pressure	60
4.4	Effect of nozzle diameter	61
4.5	Effect of types of materials	63
4.5.1	Behaviour of Aluminium	63
4.5.2	Behaviour of Armco-Iron	67
4.5.3	Behaviour of Zinc	69
4.6	Surface inspection and cutting mechanisms	71
4.6.1	Surface inspection	71
4.6.2	Cutting mechanism for WJ and AWJ	74
<b>5</b>	<b>Test results</b>	<b>76</b>
5.1	Plain waterjet	76
5.1.1	Effect of pressure in the depth of cut	76
5.1.2	Effect of nozzle diameter in the depth of cut	79
5.1.3	Effect of traverse rate in the depth of cut	81
5.1.4	Cutting quality at pressure 900 MPa	82
5.2	Abrasive waterjet	83

5.2.1 Effect of pressure in the depth of cut	83
5.2.2 Abrasive waterjet optimising	84
5.2.2.1 Optimizing the abrasive flow rate	84
5.2.2.2 Optimizing the waterjet nozzle diameter	86
5.2.3 Effect of traverse rate in the depth of cut	87
<b>6 A thermographical map of the tool and workpiece</b>	<b>88</b>
6.1 A Thermographical map at plain waterjet	88
6.1.1 Effect of nozzle diameter on the maximum temperature	88
6.1.2 Effect of pressure on the maximum temperature	91
6.2 A Thermographical map at abrasive waterjet	92
6.2.1 Effect of pressure on the maximum temperature	92
<b>7 Modelling of plain waterjet cutting</b>	<b>97</b>
7.1 The energy model	97
7.2 The semi-empirical model	105
<b>8 Outlook and conclusions</b>	<b>109</b>
8.1 A 900 MPa Cutting system technology	109
8.2 Conclusions	110
<b>References</b>	<b>113</b>

# NOMENCLATURE

$A_m$	cutting area	[mm <sup>2</sup> ]
$a$	constant	-
$b$	constant	-
$b_t$	width of cut	[mm]
$c$	constant	-
$c_k$	characteristic velocity	-
$d$	constant	-
$d_a$	abrasive particle diameter	[mm]
$d_f$	focus diameter	[mm]
$d_j$	jet diameter	[mm]
$d_n$	nozzle diameter	[mm]
$E$	modulus of compressibility	[N/m <sup>2</sup> ]
$E_{ab}$	absorbed energy in the materials	[J]
$E_e$	exiting Energy	[J]
$E_{exp}$	exit particle energy	[J]
$E_{exw}$	exit waterjet energy	[J]
$E_f$	friction energy	[J]
$E_i$	input energy by waterjet	[J]
$E_q$	heat energy	[J]
$E_r$	materials resistance energy	[J]
$F_d$	friction drag force	[N]
$H$	hardness	-
$H_a$	abrasive particle hardness	-
$K$	maximum depth of cut	[mm]
$l_c$	waterjet core length	[mm]
$l_f$	abrasive focus length	[mm]
$m_a$	abrasive flow rate	[g/s]
$m_p$	mass of debris particles	[kg]
$m_w$	mass flow rate of water	[kg/min]
$n$	constant	-

$N_a$	abrasive particle number	-
$N_m$	Machinability number	-
$P$	pressure	[MPa]
$P_c$	threshold pressure	[MPa]
$S$	standoff distance	[mm]
$T$	temperature	[°C]
$T$	time	[s]
$v$	velocity	[m/s]
$v_a$	abrasive velocity	[m/s]
$v_c$	critical velocity	[m/s]
$V_f$	traverse rate	[m/s]
$v_i$	impact velocity	[m/s]
$v_j$	jet velocity	[m/s]
$\rho$	density	[kg/m <sup>3</sup> ]
$\rho_a$	abrasive particle density	[kg/s]
$\rho_E$	environment density	[kg/m <sup>3</sup> ]
$\rho_f$	fluid density	[kg/m <sup>3</sup> ]
$\rho_m$	water density	[kg/m <sup>3</sup> ]
$\sigma$	strength of materials	[MPa]
$\sigma_c$	compressive strength	[MPa]
$\sigma_m$	tensile strength	[MPa]
$\sigma_s$	shear strength	[MPa]
$\sigma_y$	yield strength	[MPa]
$\varphi$	Jet (Particle) impact angle	[°]
$\lambda$	regression parameter	-
$\varepsilon$	specific energy	[J/mm]
$\varepsilon_s$	strain	-
$\mu_f$	coefficient of friction	-
$\nu$	liquid dynamic viscosity	[N.s/m <sup>2</sup> ]



## **Subscripts**

a	Abrasive
f	Focus
j	Jet
n	Nozzle
p	Particle
w	Water

## **Abbreviations**

WJ	Plain Waterjet
AWJ	Abrasive Waterjet

# **ABSTRACT**

## **Waterjet Cutting up to 900 MPa**

Waterjet and abrasive waterjet are successfully used nowadays in several processes and field of applications. They can be used for cutting, drilling, turning, milling and surface preparation of every standard technical material as well as super-alloys and high-tech non-metal compounds as a result of the steady increase of pressure level and reliability of high pressure pumps. Commercially available systems are used at maximum working pressure of 420 MPa. The increase of pressure up to 900 MPa gives a possibility:

- To increase cutting efficiency with plain waterjet,
- to increase efficiency with abrasive waterjet,
- to increase the field of application of plain waterjet for cutting purposes even to metallic materials.

Using waterjet for cutting materials in the case of abrasive waterjet the mechanism of cutting is well examined and understood. In contrary to that when using plain waterjet the cutting mechanism is quite different. This thesis describes the cutting equipment, the possibility of reducing abrasive material and the cutting of smaller curves in the case of plain waterjet as well as in the case of abrasive waterjet at working pressure up to 900 MPa. The thesis intensively discusses the mechanism of the material cutting process for metallic material {which cover three types of crystal structure known for metals, aluminium as ductile material of face centered cubic, (fcc), Armco-iron of body centered cubic, (bcc), representing the materials having less ductile and zinc of closed packed hexagonal structure, (hcp), representing brittle materials} when using plain waterjet. To handle water at high pressure up to 900 MPa it is necessary to look at the fundamentals of physical of water, however at room temperature (20°C) the water freezes at a pressure of 888 MPa. This thesis discuss the thermodynamic behaviour of water like ice formation, the compressibility, the adiabatic heating in order to prevent the risk of water freezing

at pressure of 900 MPa. Although plain waterjet and abrasive waterjet cutting are often classified as cold process, the temperature distribution caused by the cutting with both plain waterjet and abrasive waterjet was measured. In the case of plain waterjet cutting two models, the energy model and the semi-empirical model, were derived to describe the relationship between the operating conditions and the maximum depth of cut. The experimental verification of the both models proved that there is a good correlation between the experimental and the calculated depth of cut for the different tested materials. Finally, the thesis describes some remaining difficulties, either in the development or manufacture of the ultrahigh pressure cutting system at working pressure up to 900 MPa, in its usage or from the scientific point of view is presented.

**Key words**

waterjet, abrasive waterjet, 900MPa, cutting mechanism, temperature, models.

# Zusammenfassung

## Wasserstrahlschneiden bis 900 MPa

Wasser- und Wasserabrasivstrahlen werden heutzutage erfolgreich in vielen industriellen Prozessen und Anwendungsbereichen benutzt. Sie können zum schneiden, bohren, drehen, prägen und zur Oberflächenvorbereitung verwendet werden. Die bearbeitbaren Materialien umfassen jedes technische Standardmaterial sowie Super-Legierungen und moderne Nichtmetall-Verbundwerkstoffe. Im Handel erhältliche Systeme werden momentan mit maximalen Betriebsdrücken bis 420 MPa benutzt. Eine Zunahme des Arbeitsdrucks bis zu 900 MPa eröffnet die Möglichkeit,

- die Leistungsfähigkeit von Reinwasserstrahlen zu erhöhen und damit die Schnitttiefe sowie die Anzahl der damit bearbeitbaren Werkstoffe zu vergrößern, sowie
- die Leistungsfähigkeit von Wasserabrasivstrahlen erhöhen, und somit bezüglich der Schnittgeschwindigkeit in direkte Konkurrenz zu thermischen Verfahren zu positionieren.

Der Schneidprozess bei den Wasserabrasivstrahlverfahren ist gut untersucht und größtenteils verstanden. Der Abtragsmechanismus beim Reinwasserstrahlen ist demgegenüber sehr verschieden. Die vorliegende Arbeit beschreibt die nötige maschinelle Ausrüstung, das Potential zum Einsparen von Abrasivmaterial sowie zur Verkleinerung des minimalen Schnittkurvenradius bei der Anwendung von Drücken über 600 MPa. Die These befasst sich intensiv mit dem Mechanismus des Schneidprozesses für metallische Materialien (für die drei Kristallstrukturen kfz, krz und hdp beispielhaft untersucht an Aluminium, Armco-Eisen sowie Zink, sortiert nach abnehmender Duktilität). Um Wasser unter Hochdruck bis zu 900 MPa handhaben ist es notwendig die Physikalischen Grundlagen zu betrachten, da Wasser bei Raumtemperatur (20°C) bei einem Umgebungsdruck von 888 MPa zu Eis wird. In dieser Arbeit werden das thermodynamische Verhalten bei der

Eisbildung, die Kompressibilität und die adiabatische Erwärmung zwecks Verhinderung der Eisbildung diskutiert. Obgleich Wasser- und Wasserabrasivstrahlen häufig als kalte Prozesse eingestuft werden, wurde die Temperaturverteilung, die beim Schneiden mit Wasser- und Wasserabrasivstrahlen verursacht wurde, gemessen. Im Fall des Wasserstrahles wurden ein Energiemodell und ein halb-empirische Modell abgeleitet, um das Verhältnis zwischen den Betriebsbedingungen und der maximalen Tiefe des Schnittes zu beschreiben. Die experimentelle Überprüfung der beiden Modelle ergab, dass es eine gute Wechselbeziehung zwischen der experimentellen und errechneten Tiefe des Schnittes für die unterschiedlichen geprüften Materialien gibt. Schließlich beschreibt die These einige restliche Schwierigkeiten, die sich in Entwicklung und Bereitstellung eines Ultrahochdruckschneidsystems bis zu 900 MPa Betriebsdruck vom wissenschaftlichen Gesichtspunkt her ergeben.

#### **Schlüsselwörter**

Wasserstahl, Wasserabrasivstrahlen, 900MPa, Schneidmechanismus, Temperatur, Modelle.



# 1. INTRODUCTION

Recently, the waterjet technology has become used extensively in many areas of industry. With plain waterjet applications the waterjet itself is used as the tool to machine the materials. In the case of cutting the waterjet fulfils three functions: cutting, cooling and removal of cutting debris. It is used in the automotive industry to cut carpets as well as for cutting nappies in paper industry but until today their cutting abilities are limited to cut soft and non-metallic materials. The common way to cut metallic materials with waterjet is to add abrasive to the waterjet. This technology is widely used and is called abrasive waterjet cutting. Almost every kind of material can be cut with this technology. But the maximum working pressure limited to 420 MPa is currently state of the art. However recent researches propose to extend the application range of this technology by increasing the working pressures above 420 MPa. The increase of pressure gives the possibility to:

- Increase efficiency of waterjet and abrasive waterjet,
- reduce the abrasive consumption,
- cut thin metal plates with waterjet only and
- increase the application field (e.g. aeronautics, automotive etc.).

So the aim of this thesis is to investigate the potential of using waterjet cutting and abrasive waterjet cutting at working pressure above 420 MPa. It is planned to describe the cutting equipment and optimize the machining process for different metallic materials as well as different machining parameters such as pressure, nozzle diameter, standoff distance and traverse rate in order to increase production rates, possibility of reducing the abrasive material and cutting relatively smaller curves in the case of abrasive waterjet as well as plain waterjet and enhance cutting quality. It is planned in this study to increase the working pressure up to 900 MPa, the physical limit of water, because at higher pressure levels liquid water at room temperature (20°C) becomes ice. The cutting mechanism in the case of abrasive

waterjet cutting is well examined and understood. In contrary to that when using plain waterjet the cutting mechanism is quite different. Therefore, the study will lead to a deeper understanding of the cutting mechanism when metallic materials are cut by plain waterjet, which will contribute an efficient employment of this technology and extent the field of applications. The effect of the thermal stress accompanied to the cutting process should be considered because high temperature can damage the target materials. Although plain waterjet and abrasive waterjet cutting are often classified as cold process, the present study discusses the temperature generated during the cutting process with plain waterjet and abrasive waterjet.

Several theoretical attempts were made to model the abrasive waterjet cutting but little attention was exerted to model the plain waterjet cutting especially in the cutting process of metals. Appropriate models are presented to determine optimized process conditions in plain waterjet. Besides, revealing of some remaining difficulties, either in the development or manufacture of the ultrahigh pressure cutting system, in its usage or from the scientific point of view, will be considered to complete the recognition of the remaining requirements.

This thesis consists of eight chapters. Chapter 1 includes the introduction and the aim of this thesis. Chapter 2 contains literature review and state of the art for waterjet technology at working pressure above 420 MPa. Chapter 3 describes the experimental apparatus used in this study. Cutting mechanism for waterjet is presented in chapter 4. Chapter 5 includes test results where process optimizing parameters are discussed. Chapter 6 presents the measurement of the temperature generated during the cutting process with plain waterjet and abrasive waterjet. Plain waterjet modeling is presented in chapter 7. Then outlook and conclusions are given in chapter 8.



## **2. STATE OF THE ART**

This chapter presents a detailed survey that concerned with the potential of using waterjet and abrasive waterjet with pressure up to 900 MPa. The specific advantages, existing systems and tests done so far are described. Beside, the thermodynamic behaviour of water like ice formation, the compressibility, the adiabatic heating, the obtainable cutting quality and the main cutting mechanism are discussed. Finally the state of the art in the modelling for plain waterjet and abrasive waterjet are described.

### **2.1 Historical Development of Waterjet Technology**

In ancient Egypt, river branches were diverted to wash out soil in search of gold and other minerals. This was possible because this excavation did not require high energy-dense flows. Harder formations, such as coal, required the directing of river flow through pipes to focus the energy for washing out and carrying the coal. Recently, the water was used in the gold production in order to clear away contaminants and ashes to separate gold from soft rock. Due to the increase of the pressure values of waterjet the productivity increased and this extended the application to the coal mines in which the hydraulic power was used for breaking out and transporting coal. In the USSR and the USA, tests with water canons were carried out to break harder rock, where the pulsating loads were produced by pressure up to 1000 MPa [1-4].

At present most applications in the mining industry are operated by mechanical-hydraulic equipments. The waterjet supports the mechanical and tribological behaviour of the tools where the tools life increased. The application of waterjet for cleaning began in the casting industry in the 30's. The casting mould was cleaned with relatively low pressure pump. The pumps were developed to produce higher pressures to extend their range of application in cleaning and material removal. In ship-building, the application of waterjet ranged from cleaning (8 - 20 MPa

At the end of the 60's, the first pump (pressure amplifiers) was built with maximum pressures of 400 MPa and small flow rates (4 l/min.). It was used to cut soft materials (wood, plastic, paper foamed etc.). Thus the waterjet entered into the production engineering.

The addition of abrasive material, by injection system at the end of the 70's and using bypass system in the middle of the 80's, expanded the application type of the waterjet to cut nearly all conventional and composite materials. Higher traverse rate, thicker materials and better edge quality could be achieved. A new technology was born that was called Abrasive Waterjet Machining.

## **2.2 Pressure Generation System**

In order to obtain high pressure suitable for waterjet machining, there are different kinds of pump system can be used. Normally the waterjet is generated by pressurizing the water with a high pressure plunger or intensifier pump as explained below.

### **2.2.1 Plunger pump**

In the case of plunger pump a continuous increase in the pressure level starting from 6 MPa, in the middle of 1950s up to 300 MPa at the end of 1990s took place, [5]. Figure 2.1 shows this development. The increase of pressure levels of the plunger pumps, which are normally connected with higher flow rates compared to intensifier pumps, opened a wider field of effective applications like shipyard cleaning, removal of concrete, nuclear applications.

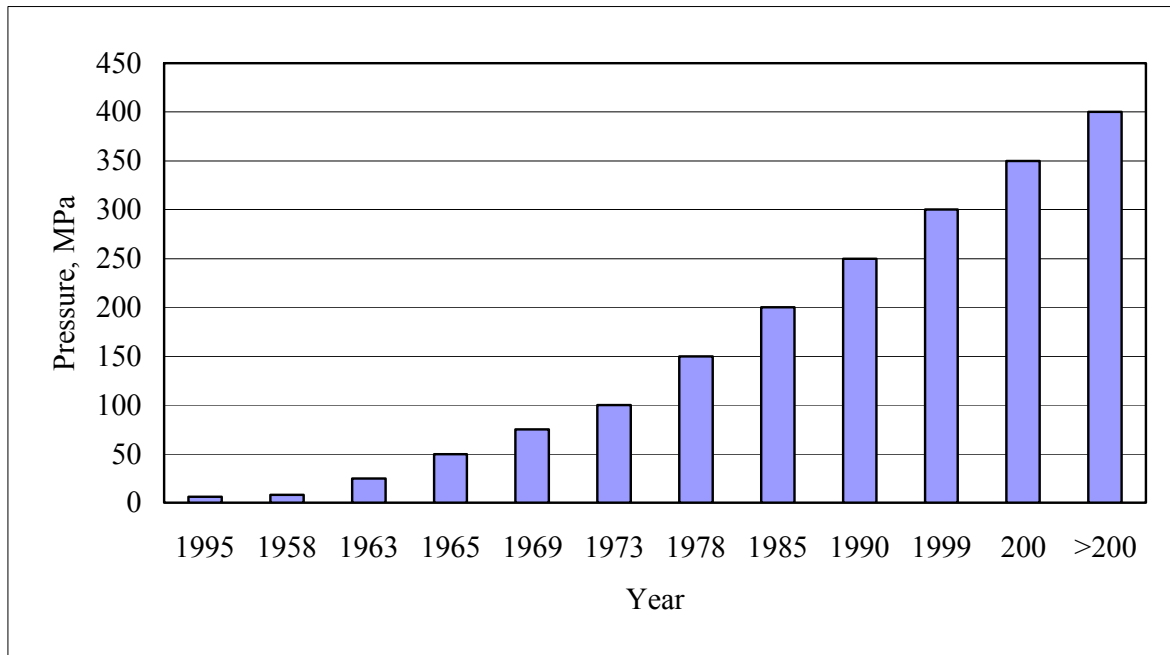


Fig. 2.1: Increase of pressure level for plunger pumps, [5].

### 2.2.2 Intensifier pump

The significant spreading of waterjet cutting technology started when intensifier pumps entered the market. From then – the 70s – until now the reliability of intensifier pumps has continuously increased but the pressure level for practical applications remained at a value of about 420 MPa for many years.

#### a) Conventional intensifier pump

The output pressure of the intensifier pump is determined by the inlet hydraulic oil pressure and the pressure intensification ratio. This ratio is defined as the area of the oil-side piston divided by the area of the pressurized water side plunger, Figure 2.2(a). Normally this ratio is 20. It was [6-8] reported that, an intensification ratio of 33:1 was used in a 690 MPa intensifier pump.

#### b) Modified autofrettage pump

Pressure-controlled pumps normally are used for waterjet cutting. Autofrettage pumps are flow controlled. A modified autofrettage pump (1000 MPa) of a pressure intensification ratio of 50:1 was used, [8-10].

### 2.2.3 Multi-Stage pump

An increased water pressure can be obtained by increasing the inlet pressure of the intensifier pump. This can be done by the additional pre-aligned plunger pump as shown in Figure 2.2(b) or using multi-stage intensifier pumps. For example,[12], was used pre-aligned plunger pump with a pressure of 70 MPa was used as step 1 and intensifier pump as step 2 to produce pressure level 900 MPa. Another way by using two intensifier pumps with transmission ratio 20:1, a 690 MPa intensifier pump, [13], was developed. A development of the UHDE intensifiers pump to pressures of up to 700 MPa has been developed by 2-stage intensifier pump [14]. Table 2.1 shows a summary of previous work carried out with pressures above 420 MPa. All these systems were used for laboratory investigation or in the beginning of practical use. The pressure above 420 MPa can be considered as a challenge for materials and components of these systems.

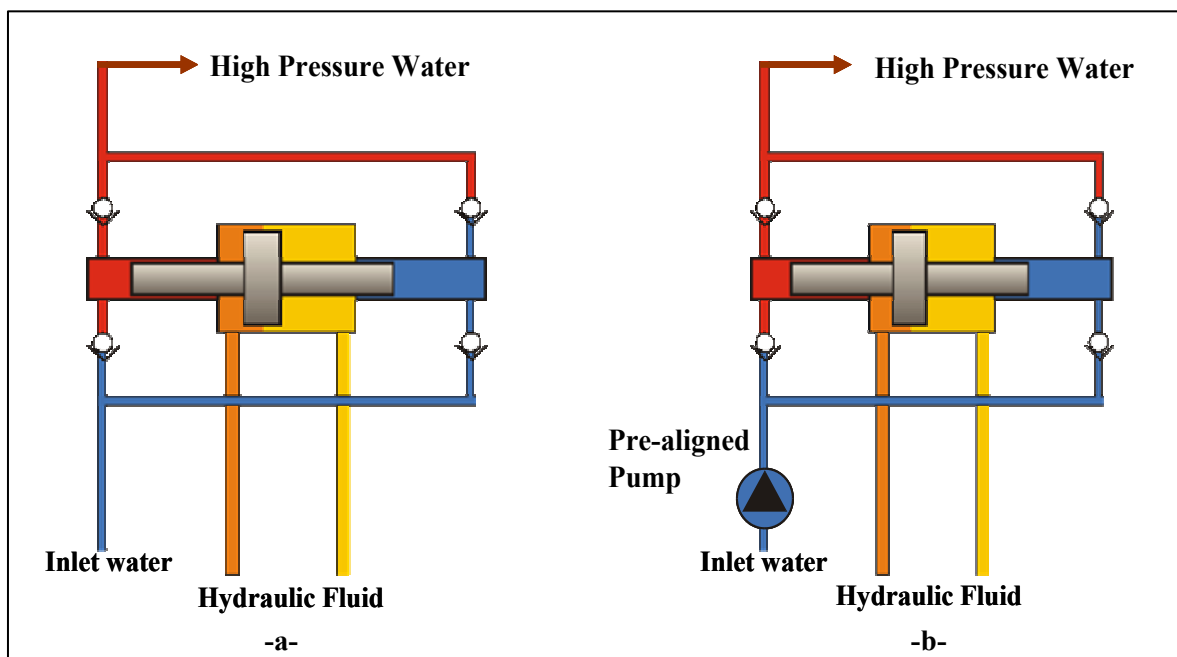


Fig. 2.2(a): Intensifier pump (Different pressure intensification ratios).

Fig. 2.2(b): Intensifier pump (In combination with a pre-aligned pump).

Table 2.1: Summary of previous work with pressure above 420 MPa.

No.		1	2	3	4	5	6
Pump	Step 1	Plunger Pump, 70 MPa	Hydraulic Oil pump	Intensifier	Hydraulic Oil pump	Hydraulic Oil pump	Hydraulic Oil pump
	Step 2	Intensifier	Intensifier	Intensifier	Intensifier	Intensifier	Intensifier
Area Ratio		73:1	87:1	20:1	33.3:1	25.4:1	50:1
$P_{max}$ , MPa		900	1000	690	690	520	1000
$d_{max}$ , mm		0.25	0.15	0.2	0.229	0.38	0.1
Abrasive		•			•	•	•
Additive		•	•		•		
Reference		Oweinah, [12]	Imanaka, [15]	Raghavan and Ting, [13]	Hashish, [6-8]	John and Kevin, [16]	Trieb, [9-11]

## 2.3 Thermodynamic Behaviour of Water

To handle water at high pressure up to 900 MPa, three physical aspects should be taken into consideration. These aspects are the phase diagram of ice, the compressibility and the adiabatic heating.

### 2.3.1 Phase diagram of ice

When working at high pressure (900 MPa) it is necessary to look at the fundamentals of water-phases. The understanding of phase diagrams for water is extremely important to define the limits of the working pressure. For example at high pressure of 1000 MPa the liquid water is expected to freeze at room temperature. All of the natural ice on earth is hexagonal ice (Ice I). Ice I is the normal form of ice by freezing water at atmospheric pressure. The water substance display a many range of solid phases, and all of these are referred to the forms of ice. Most of these phases can be produced by the application of high pressures. The first high pressure phase was discovered a century ago, [17-18], in a programmed study of the pressure-volume-temperature relationships of various materials and these phases were named as Ice II and Ice III. This discovery was extended in experiments [19-20] carried out at pressure up to 2 GPa and led to the discovery of Ices V and VI. The phase diagram of ice, [21-22], is shown in Figure 2.3. It can be

concluded from Figure 2.2 that the important phase for waterjet at working pressure above 400 MPa is Ice V and Ice VI. The first point is the phase of ice V formation with a slope line which begins at (T, P) (258.31K, 377MPa) and ends at (273.31K, 632.4 MPa) but normally the supply water temperature for waterjet cutting is at room temperature so there is no dangerous from phase Ice V. The first point is the phase of Ice VI formation with a slope line which begins at (T, P) (273.31K, 632.4 MPa) and ends at (355K, 2216 MPa), however at room temperature (293.31K) the phase transition pressure is 888 MPa. The slop line equation, [23], to estimation exactly the freeze point of the phase VI is:

$$\frac{P_{ice\_VI}}{P_n} = 1 - 1.07476 \left( 1 - \left( \frac{T}{T_n} \right)^{4.6} \right) \rightarrow (2-1)$$

where  $P_n = 632.4$  MPa, and  $T_n = 273.31$ K

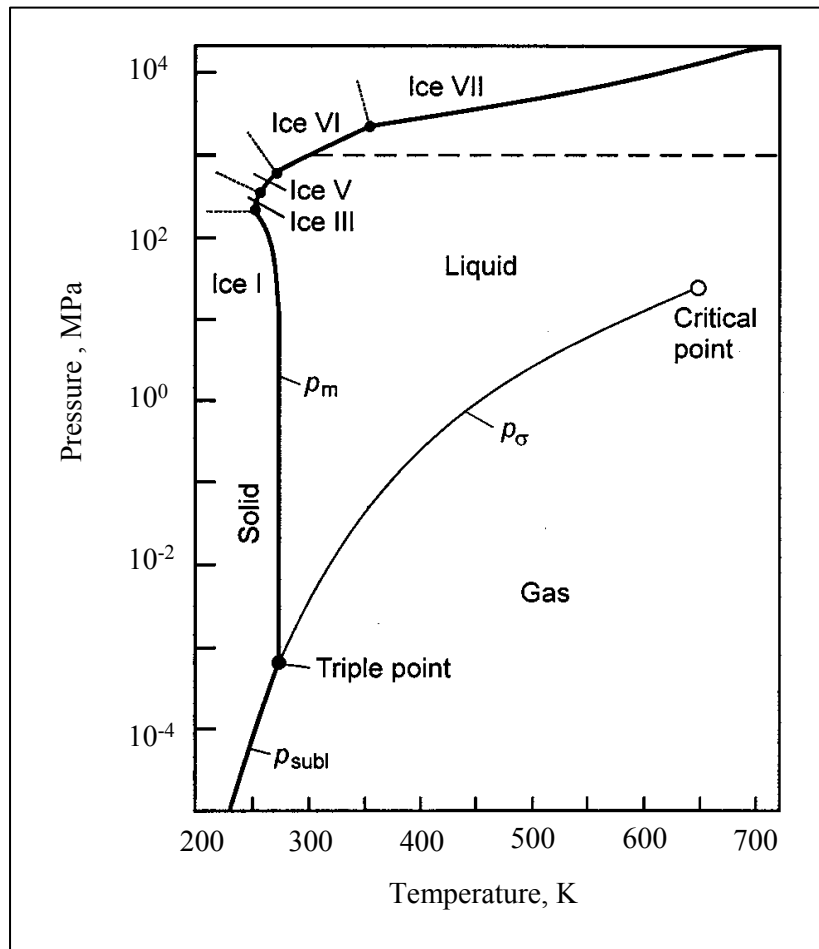


Fig. 2.3: The phase-boundary curves of water in a pressure-temperature diagram, [22].

### 2.3.2 Compressibility of water

In physics liquids are normally considered to be incompressible media. This simplification can be used for most technical applications. But this is not practicable in the field of high pressure applications ( $> 100$  MPa). It is report that the pressure has an essential larger influence on density than temperature, [24-25]. Therefore, density is handled in the following considerations as a plain function of pressure. There are two different equations to calculate the density form. The first equation is:

$$\frac{dp}{E} = \frac{d\rho}{\rho}$$

, where E is the modulus of compressibility, [26]. This state equation after integration becomes:

$$\rho = \rho_0 e^{p/E} \rightarrow (2-2)$$

where the constant factor are ( $E = 4.07 \cdot 10^9$  N/m<sup>2</sup> and  $\rho_0 = 1.02 \cdot 10^3$  kg/m<sup>3</sup>)

The second equation is [27]:

$$\rho = \rho_0 \left( \frac{P + E}{P_0 + E} \right)^{\frac{1}{n}} \rightarrow (2-3)$$

where the constant factors are ( $E = 3.047 \cdot 10^8$  N/m<sup>2</sup>,  $\rho_0 = 1.02 \cdot 10^3$  kg/m<sup>3</sup> and  $n = 7.15$ ). The calculated values referred to equations (2-2) and (2-3) for the density at different pressure is shown in Figure 2.4. The change in the percentage volume as a function of the pressure which data estimated from equations (2-3) is shown in Figure 2.5.

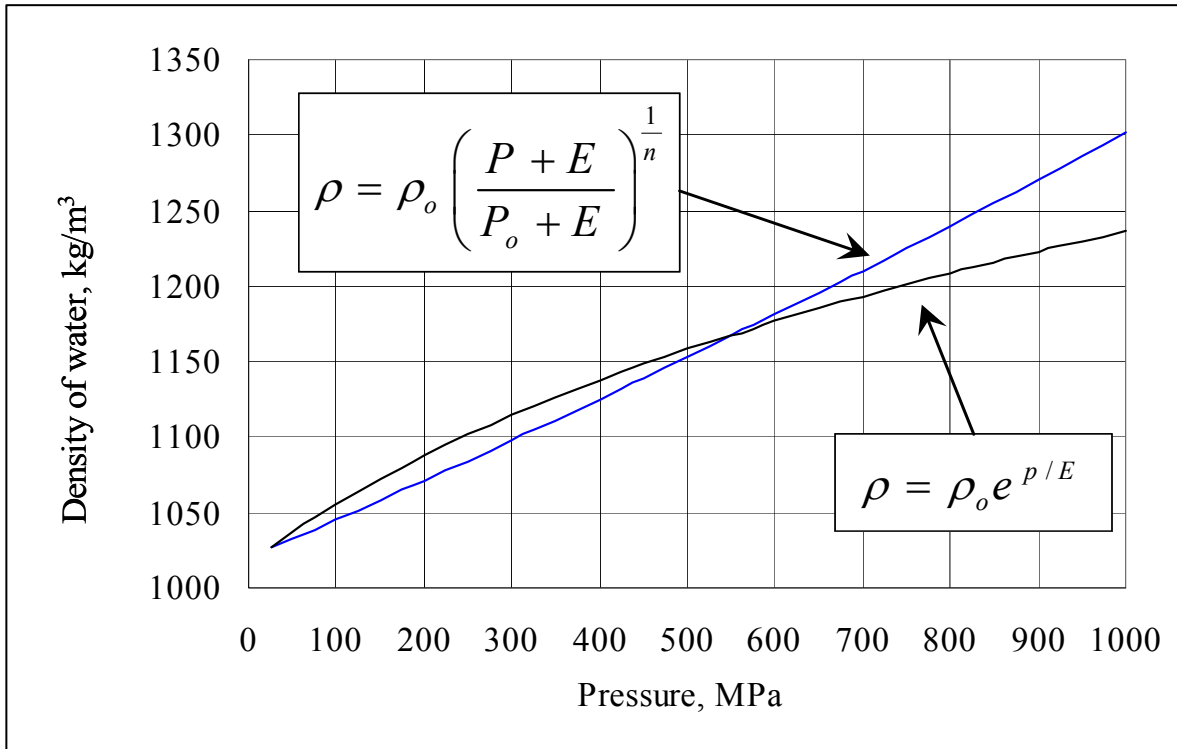


Fig. 2.4: Dependence of density of water on pressure.

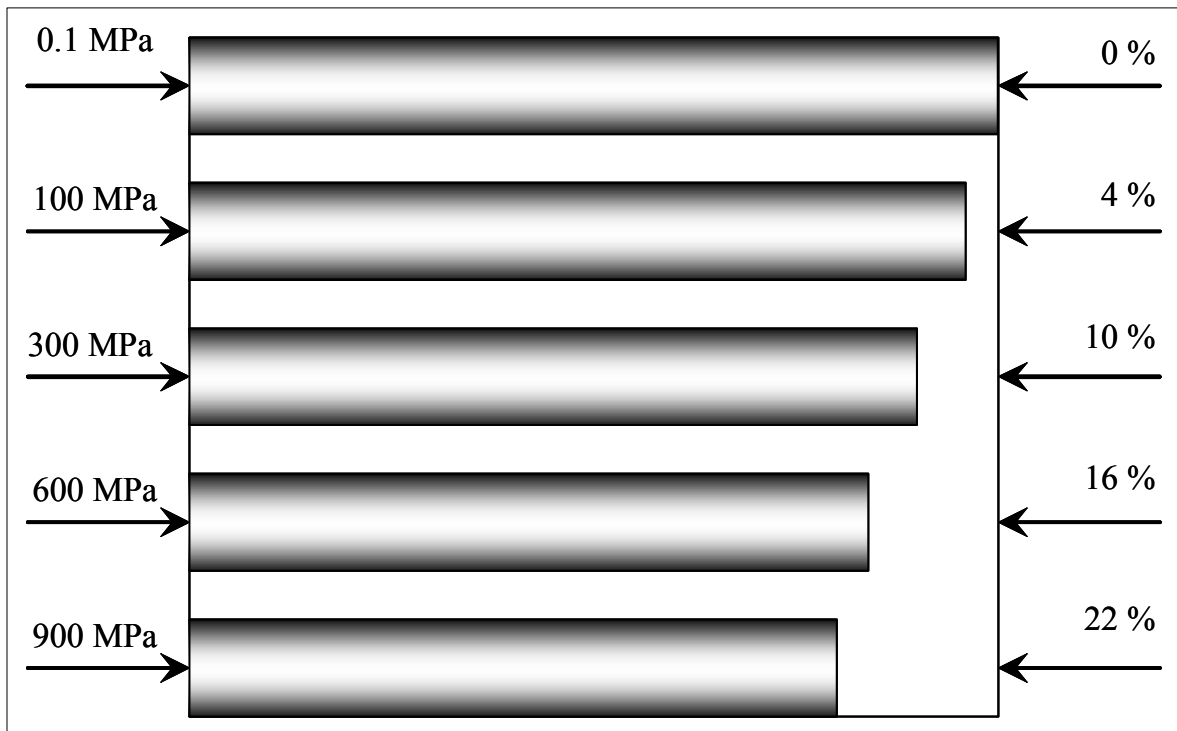


Fig. 2.5: The percentage volume change (data estimated from equation 2.3).



### 2.3.3 Adiabatic heating

Heating of water due to adiabatic compression will increase the temperature of water by approximately  $3^{\circ}\text{C}/100\text{ MPa}$ . The rise of temperature during adiabatic compression for water of different temperatures is shown in Figure 2.6, [28] and the effect of adiabatic heating on pressure ice formation, (data estimated from equation 2.1) is shown table 2.2. This adiabatic heating decreases the risk of ice formation for example increase the pressure ice formation from 691 MPa to 1050 MPa at water inlet temperature  $5^{\circ}\text{C}$  and from 888 MPa to 1322 MPa at water inlet temperature  $20^{\circ}\text{C}$ . In practical application even when the water temperature at the inlet is at room temperature by friction in the machine intensifier, couplings and in the hoses the temperature will rise, this means the risk of freezing at 900 MPa and water at inlet temperature can be ignored.

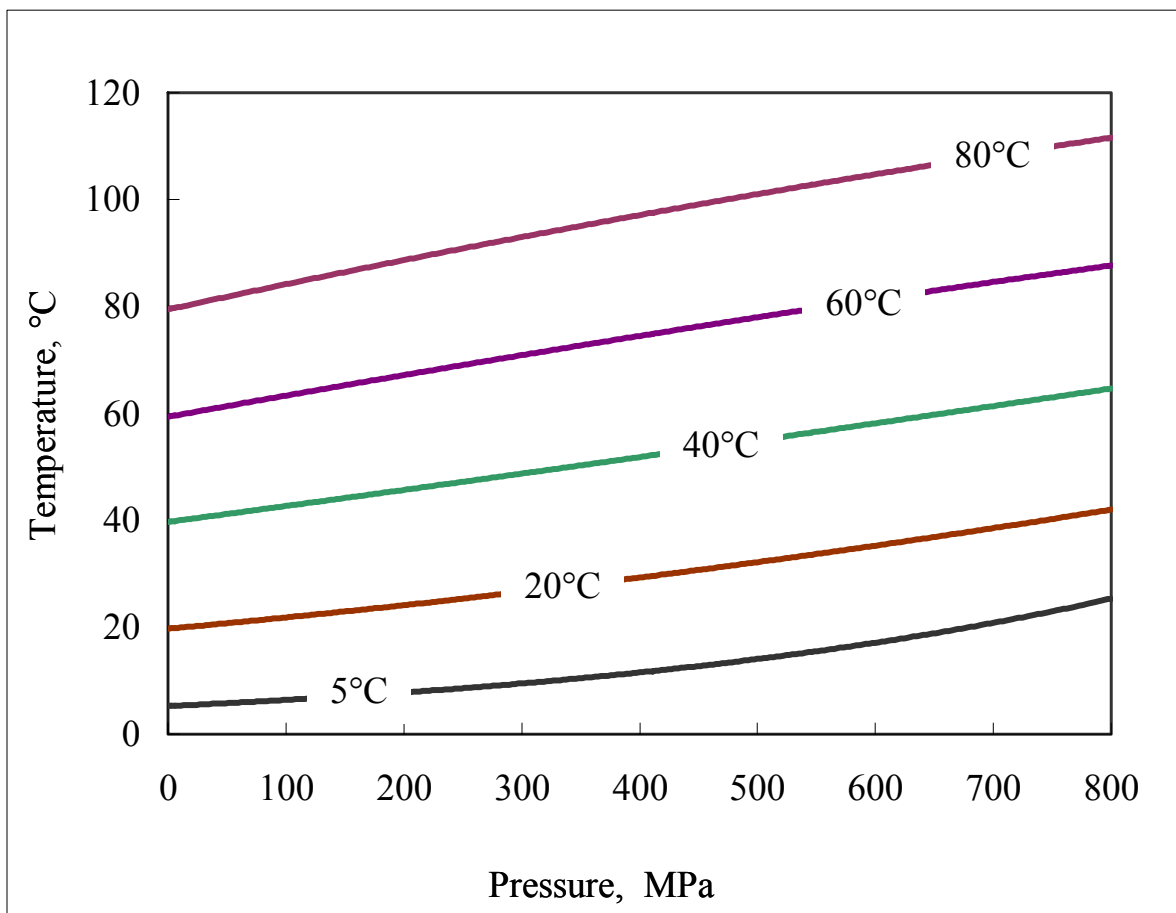


Fig. 2.6: Temperature rise during adiabatic compression of water, [28].

Table 2.2: Shown the effect of the adiabatic heating in the pressure ice formation.

Temperature	Pressure ice formation without adiabatic heating	Pressure ice formation with adiabatic heating
5° C	691 MPa	1050 MPa
10° C	754 MPa	1135 MPa
15° C	821 MPa	1226 MPa
20° C	888 MPa	1322 MPa

## 2.4 Waterjet Structure

During the present study on the topic of plain waterjet erosion, it was determined that a thorough understanding of plain waterjet and liquid impact mechanisms will benefit the application of plain waterjet, especially in cutting and removal. In the plain waterjet process, the critical operating parameters are jet structure, nozzle geometry, nozzle diameter, pressure, traverse rate, and standoff distance. Many researchers [29-32] contributed to the study of waterjet former. In the waterjet former the hydraulic energy of the pressurized water is converted into kinetic energy of the water through the nozzle. The waterjet is mainly structured as follows Figure 2.7.

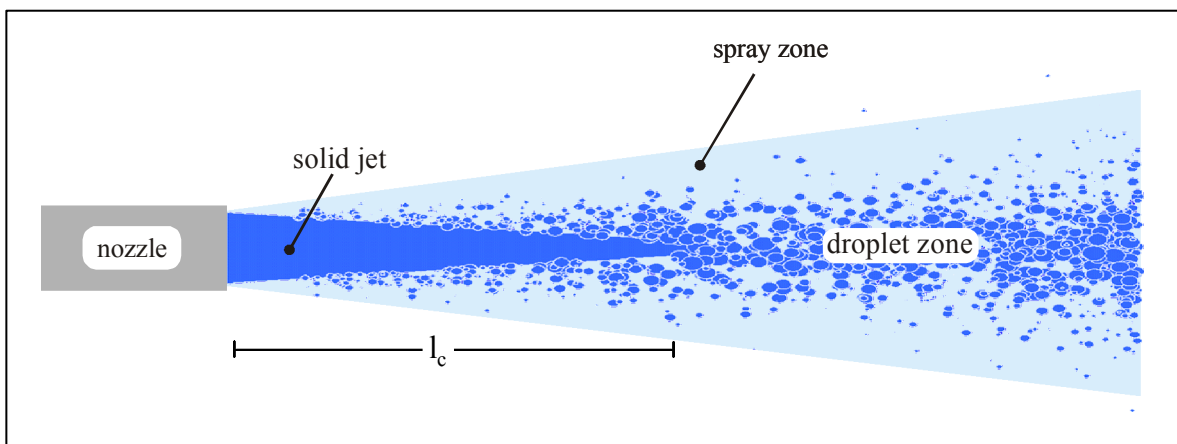


Fig. 2.7: WJ disintegration, [33].

The waterjet consists of a solid jet core zone which gradually disintegrates into fluid packets (droplets). The third zone is surrounding the jet and contains very small droplets (spray zone) at low energy levels that normally do not damage workpiece material, [34]. The length of the jet's solid core is mainly dependant on the inner turbulence of the jet. Consequently, the most significant factor be controlled during jet formation is the turbulence content of the fluid flow. The disintegration caused by flow turbulence is called primary disintegration. At wider standoff distances, the fluid packets continue to disaggregate due to aerodynamic effects; this is then called secondary disintegration. Several values estimated from measurements of the distance of the jet core  $l_c$  are published, [29, 35, 36], respectively

$$73 < \frac{l_c}{d_n} < 135, \quad \rightarrow (2.4), [29]$$

$$50 < \frac{l_c}{d_n} < 125, \quad \rightarrow (2.5), [35]$$

$$20 < \frac{l_c}{d_n} < 150 \quad \rightarrow (2.6), [36]$$

The values of the jet core length are depending on the diameter of nozzle,  $d_n$ .

More investigations were carried out, [37-38], to calculate the jet core length, where they found the density ratio of fluid and environment medium could be considered as additional measured variable, so that the length of the core jet can be calculated as:

$$l_c = k_1 d_n \sqrt{\frac{\rho_F}{\rho_E}} \quad \rightarrow (2.7)$$

where  $k_1$  is constant and equal to 7.15 and 15.8 according to [37-38] respectively,  $\rho_F$  is density of fluid and  $\rho_E$  is density of environment so that for waterjet in air a core length about 200 and 500 the nozzle diameters.

Experimental investigation has been developed, [39], to produce cutting fluid jet with long coherent length by shooting the waterjet into atmosphere with different pressure (ranging between 120 hpa and 1300 hpa) and compositions (regular air, helium, methane and argon) under working conditions of waterjet pressure of 96 MPa and 36  $\mu\text{m}$  nozzle diameter. It is found that the coherent length of waterjet in air is approximately 100 the nozzle diameter. It is reported that when jets are shot into low density media (a very light gas like helium) their coherent length is enhanced several times and the jets shot into lower pressure have a slightly longer coherent length with comparison with higher ambient pressure. This is due to the fact that at high ambient pressure the atmospheric gas would act with more force on the surface of the jet making the interaction between the jet and its surrounding more intensive.

The broad dispersion of the results with the individual authors is to be essentially due to two effects. On the one hand geometry of the related nozzles has substantial influence on the rate of disintegration of the jet, [40], on the other hand the operating pressure that affects the Reynolds number.

The cause of the jet decay may be attributed to the reciprocal effect of the environment medium and the turbulence inside the jet. It was found that, [41], the density ratio of jet and environment medium of crucial influence on the mechanism of the jet decay. With a density ratio ( $\rho_F/\rho_E$ ) of less than 500, the reciprocal effect of the environment is of crucial importance, while for larger density ratio the turbulence is considered as the driving force of the decay. For waterjet in air, the density ratio is about 800, so that the jet decay takes place due to turbulence. The turbulent disturbances expand within the jet and leave it, as soon as their kinetic energy exceeds the surface energy of the medium. As a result of that, it is expected, [41], that the maximum droplet size is occurring at the end of the liquid core.

On the bases of the discussion of the waterjet structure, it can be concluded that different flow regions may result in different loading of the materials and related material removal mechanisms. Firstly, material destruction is caused by the

stagnation pressure, while in the other; the impact pressure resulting from the impact of single liquid volumes is the cause of the destruction. These two effects of high speed liquid jets are simulated by one jet only. With growing distance from the nozzle (standoff distance), the load of a specimen changes correspondingly from the quasi-static stagnation pressure of the compact jet to the pulsed discontinuous impact pressure of the impact of the single drops therefore the standoff distance plays a great role in determining the material removal mechanism. On other hand, it seems to be a consensus on the existence of an optimum standoff distance at which the mass removal rate is maximum as shown in Figure 2.8.

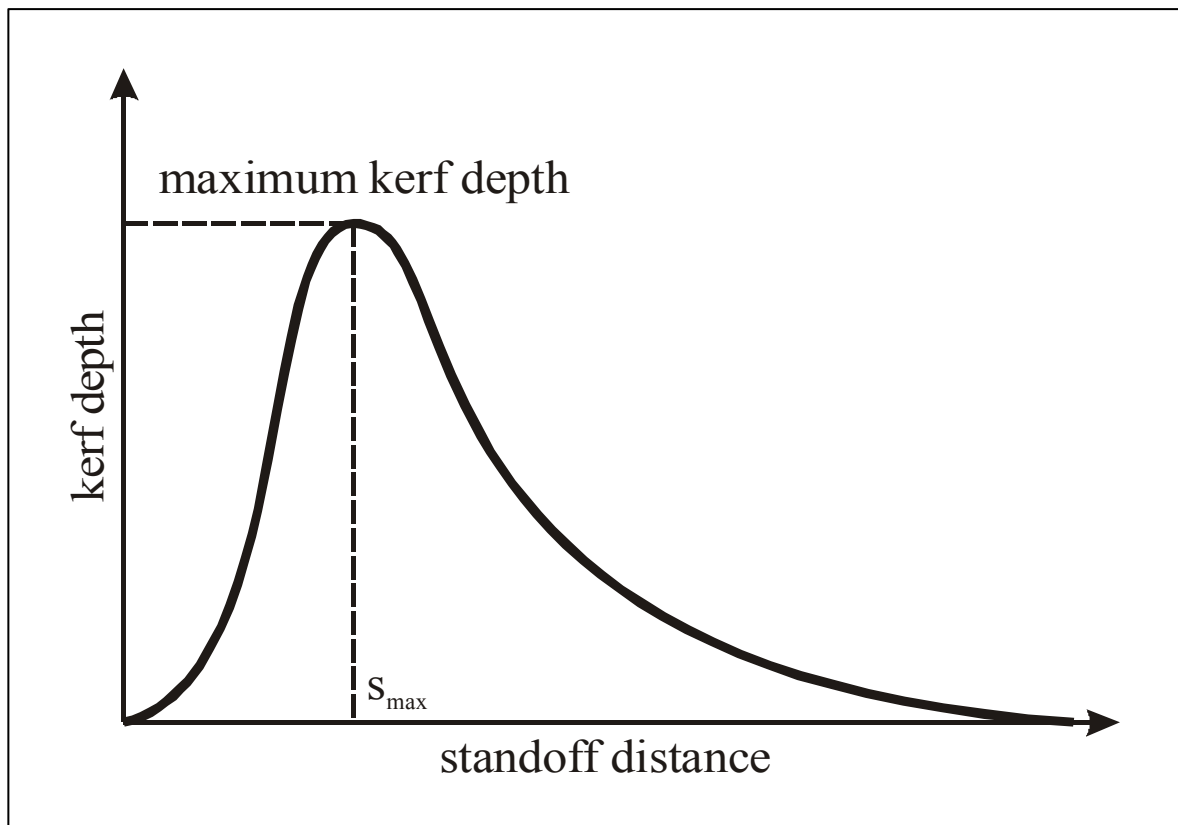


Fig. 2.8: Kerf depth =  $f$  (standoff distance), [34].

## 2.5 Cutting Result

In this section the cutting results for plain waterjet and abrasive waterjet so far is presented.

### 2.5.1 Plain waterjet

The influence of the pressure on the depth of cut for different metallic materials at 0.15 mm nozzle diameter, 3 mm standoff distance, 66 mm/min traverse rate and pressure up to 1000 MPa is shown in Figure 2.9, [15]. It is clear that the liquid jets represent a fairly effective cutting tool for some metallic materials. The depth of cut of lead increased from 1 mm at pressure of 120 MPa to 22 mm at pressure of 1000 MPa and from 0.4 mm at pressure 600 MPa to 1.5 mm at 1000 MPa for brass. Extrapolation of the curve shown in this Figure indicates that there is a threshold pressure below which little or no cutting could be achieved. Mild steel requires a pressure of 600 MPa to produce significant effect at traverse rate of 66 mm/min.

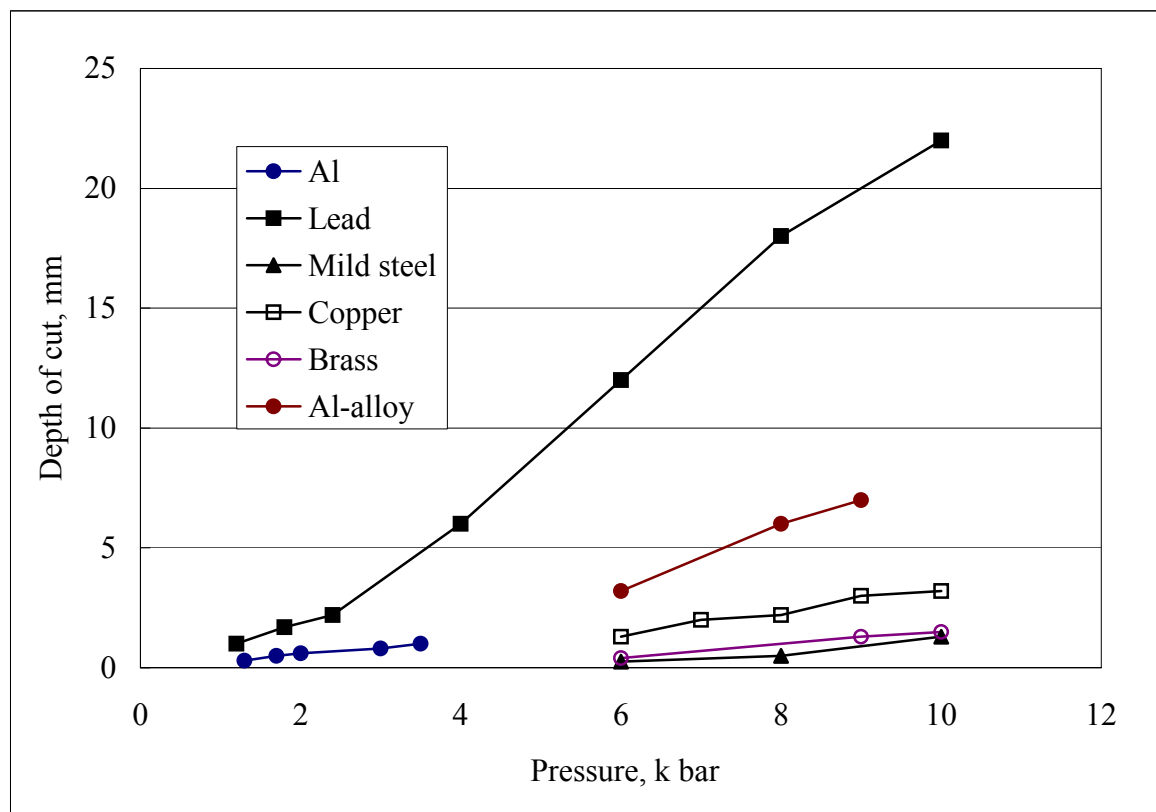


Fig. 2.9: Influence of pressure in depth of cut at different metallic materials, [15].

Experiments were carried out to cut metals such as AlMgSi1.0 and non-metals as CFK (Carbon-fiber reinforced plastic), GFK (Glass-fiber reinforced plastic) and PVC at 0.18 mm nozzle diameter, 120 mm/min traverse rate and pressure up to 900 MPa, where the results are shown in Figure 2.10, [12]. The depth of cut increased with increasing the working pressure for all materials tested. For example, the depth of cut increased from 5.8 mm at pressure of 300 MPa to 25 mm at pressure of 900 MPa for PVC which represents an increase of about 430 %. So, it is worthy to increase the working pressure.

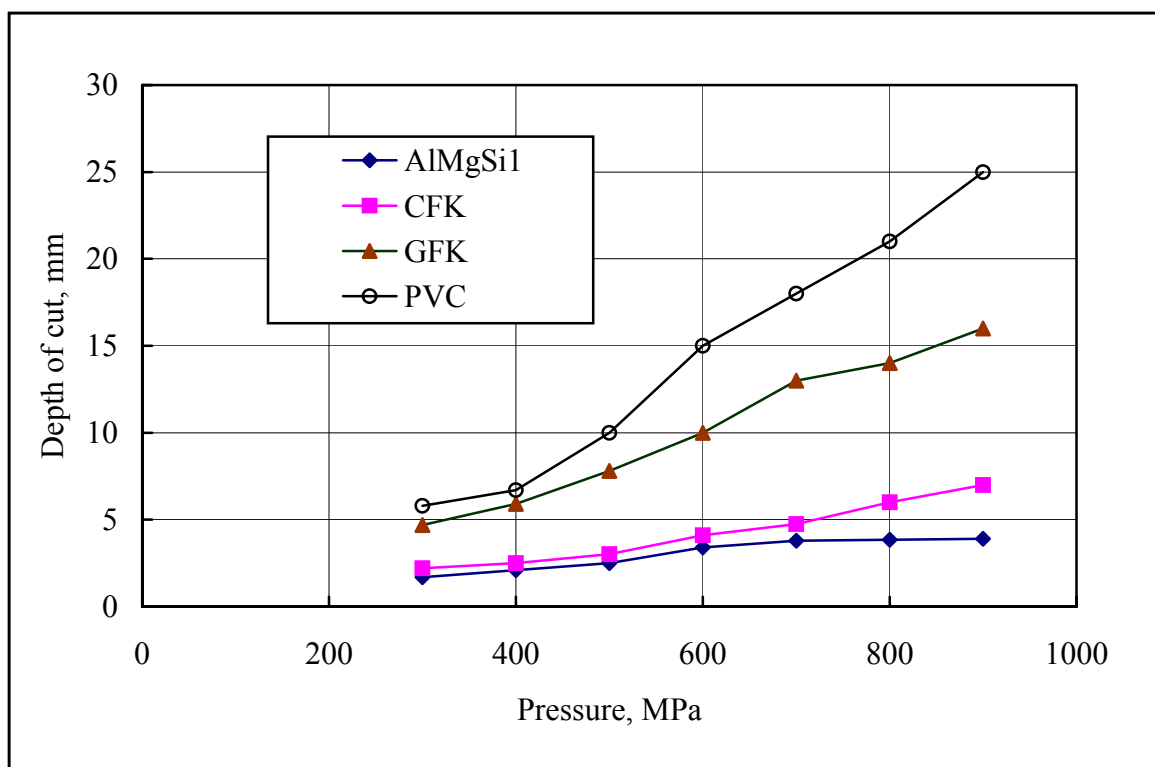


Fig. 2.10: Effect of pressure on depth of cut for metals and non-metallic materials, [12].

Cutting of thin sheet metals from aluminium using 1.69 mm/s traverse rate, 0.178 mm nozzle diameter, different standoff distance and pressure up to 690 MPa is shown in Figure 2.11, [6]. The Figure shows that with increasing pressure a shorter standoff distance is more effective due to the increase of the waterjet diameter with increasing the standoff distance.

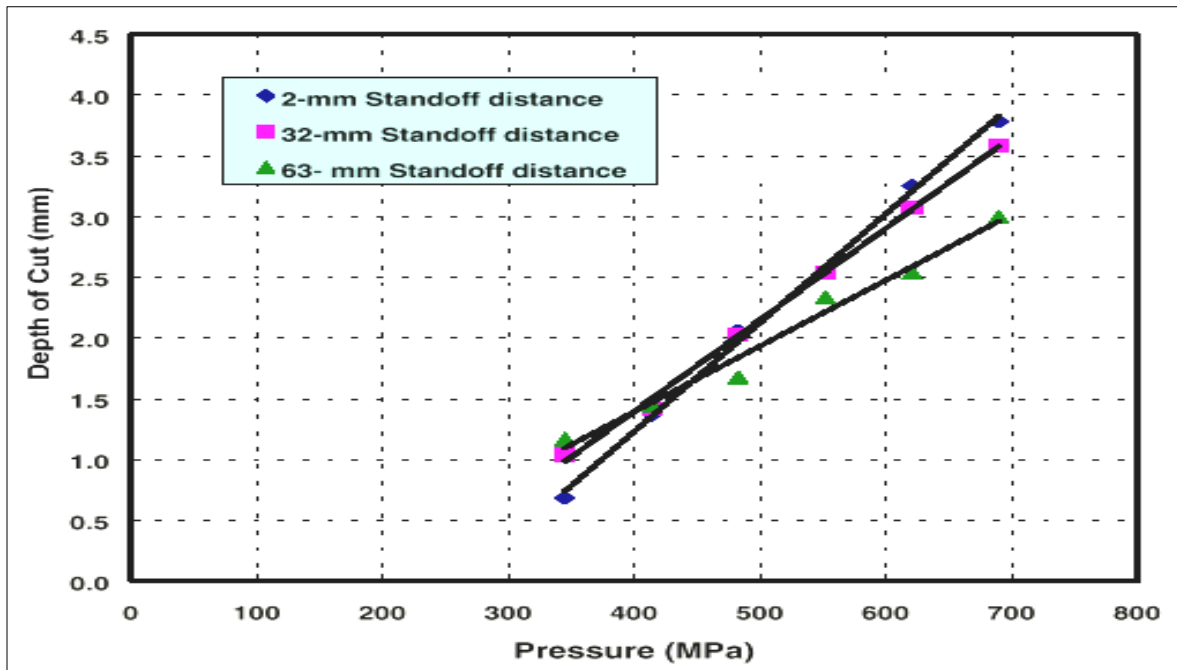


Fig. 2.11: Cutting of thin (1.6-mm) aluminium, [6].

Figure 2.12 shows the influence of cutting speed (traverse rate) on the cutting depth at a standoff distance between orifice and workpiece of 5 mm and 0.1 mm nozzle diameter [9]. Generally, the depth of cut decreased with increasing cutting speed. For example the value of the depth of cut decreased from 6 to about 3.5 mm at 25 and 100 mm/min respectively for aluminium at 800 MPa working pressure.

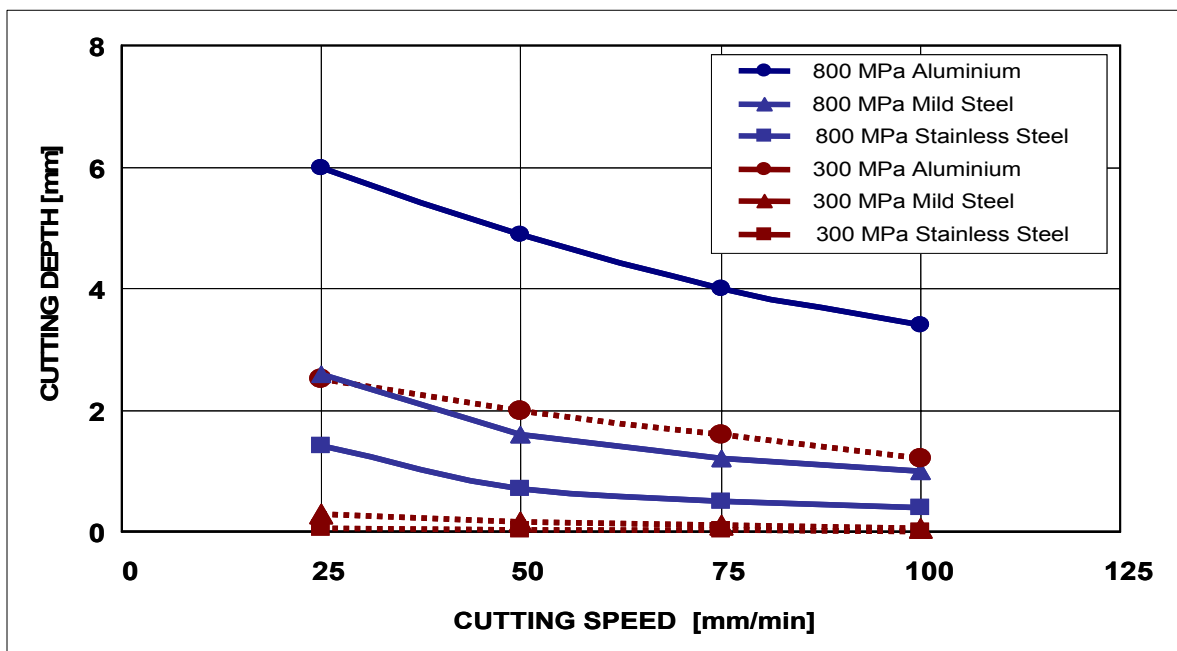


Fig. 2.12: Depth of cut for different materials at 800 MPa and 300 MPa, [9].



## 2. 5.2 Abrasive waterjet

To optimization the abrasive focus length, the results of the calculation of the minimal abrasive focus length at working pressure up to 1000 MPa is shown in Figure 2.13, [42]. It was assumed that the time required to accelerate the abrasive particle is independent of the jet pressure and equals ca.  $10^{-4}$  s. The abrasive focus length can be calculated from the following formula:

$$l_f = v_a t \quad \rightarrow (2.8)$$

where  $v_a$  is the abrasive particle velocity and  $t$  is the time required to accelerate the abrasive particle. The length of the abrasive focus is 80 mm and 140 mm at pressures of 300 and 1000 MPa respectively. It can be seen that the value of the length of the abrasive focus calculated is high due to assuming that the velocity of abrasive particle equals to the velocity of waterjet. It was found that, [43-47] the ratio between the velocity of the abrasive particle and the waterjet velocity was between “0.5 to 0.85”.

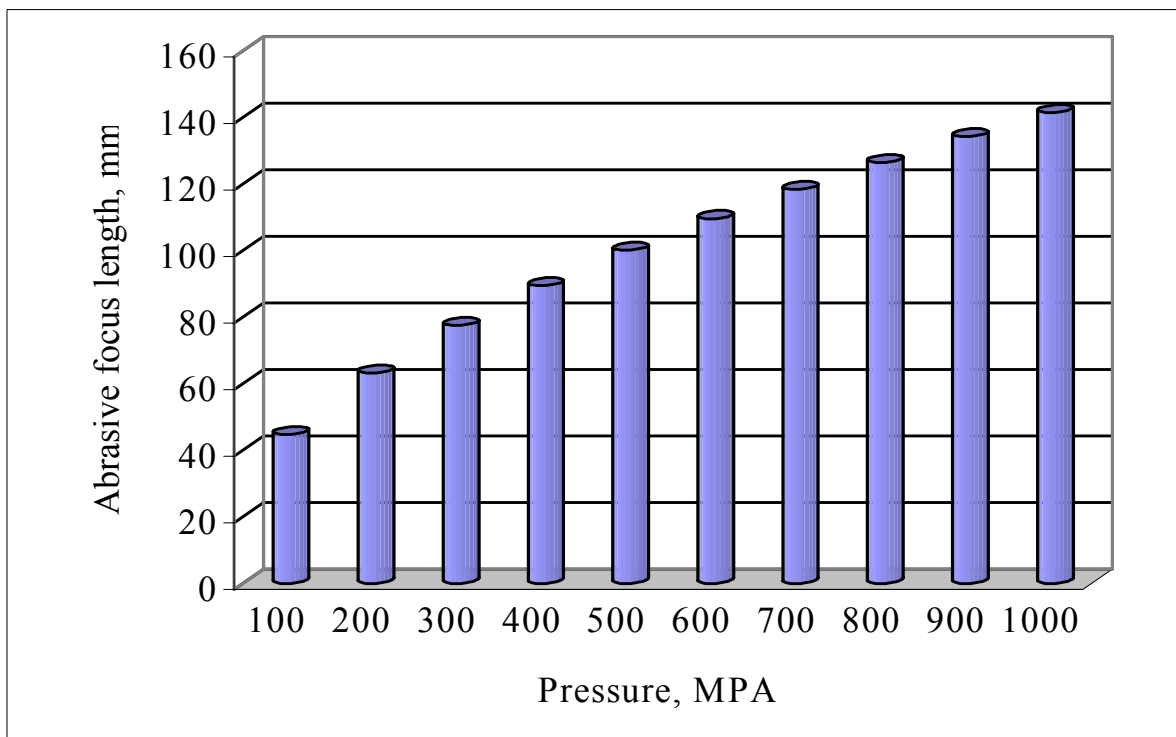


Fig. 2.13: Estimation of the abrasive focus length as function of pressure, [42].

On the basis of the impulse balance analytical model was developed [48] under consideration of the reduction of the waterjet speed during the acceleration procedure and under a variable waterjet density, which is affected by the amount of the sucked air to calculate an acceleration distance, which can be equal to the focus length, the final relation is

$$l_f = \frac{1}{k(1+R)^2} \left[ \frac{1}{1-\omega(1+R)} - + \ln(1-\omega(1+R)) \right] \rightarrow (2.9)$$

where  $R = \frac{m_a}{m_w}$ ;  $\omega = \frac{v_a}{v_w}$ ;  $k = c_f \frac{A_a \rho_{mix}}{2m_a}$  and  $\rho_{mix}$  is the carrier-fluid density

The final relation is calculated at the working conditions of 240 MPa pressure, 0.25 mm nozzle diameter, 1.2 mm abrasive focus diameter and 50 kg/m<sup>3</sup> carrier-fluid density. The minimum acceleration distance (focus length) is necessary to introduce the acceleration process. This length is between 20 mm to 40 mm. Beyond an acceleration distance of 100 mm no substantial improvement in the acceleration process occurs.

Based on the speed measurements, [49], a focus diameter of approximately the quadruple water nozzle diameter and an acceleration distance of 20 - 25 times the focus diameter are considered as favorable focus dimensions.

Blickwedel, [48] supposes an optimum ratio between the focus diameter and waterjet orifice diameter from 3 to 4 times the water nozzle diameter.

On advantages of high pump pressures will be the increase of efficiency of reduction of used abrasive materials. This also can be used at pressures for below 400 MPa. Figure 2.14 shows a comparison of abrasive consumption at a kerfing depth of 30 mm, where the experimental parameters are an orifice diameter of 0.25 mm, focus diameter of 1.2 mm, traverse rate of 100 mm/min and a standoff distance of 2 mm [50]. At this working condition the abrasive consumption goes down to 42% for pressure 300 MPa in comparison with 240 MPa.

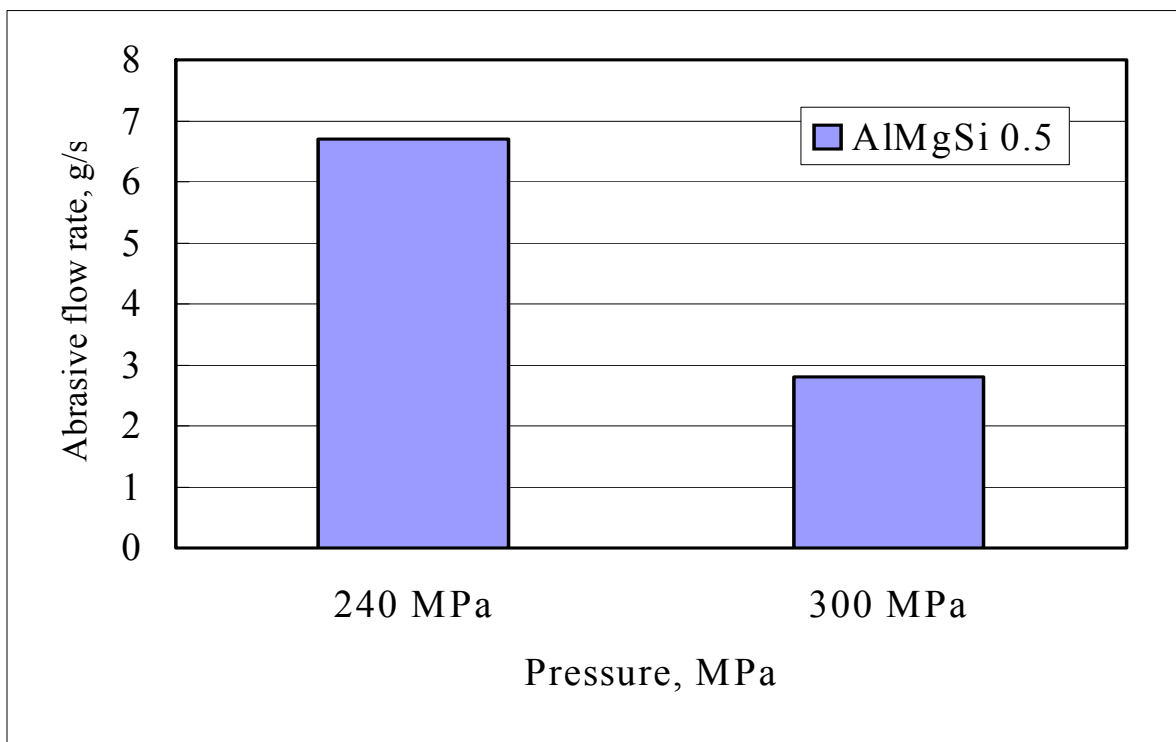


Fig. 2.14: Comparison of abrasive consumption of equal cutting depth, [50].

Tests conducted on aluminum and stainless steel with abrasive waterjet, [10] at working condition of operating pressure of 400 MPa, 600 MPa and 800 MPa, 0.10 mm orifice diameter, 0.60 mm abrasive focus diameter, 50 mm abrasive focus length, abrasive material Garnet of 120 mesh, 100 g/min abrasive flow rate and 100 mm/min traverse rate are shown in Figure 2.15. It is illustrated that the depth of cut increased with increasing the pressure for all the tested materials. The depth of cut increased from 7 to 15 mm at pressures of 400 and 800 MPa for stainless steel.

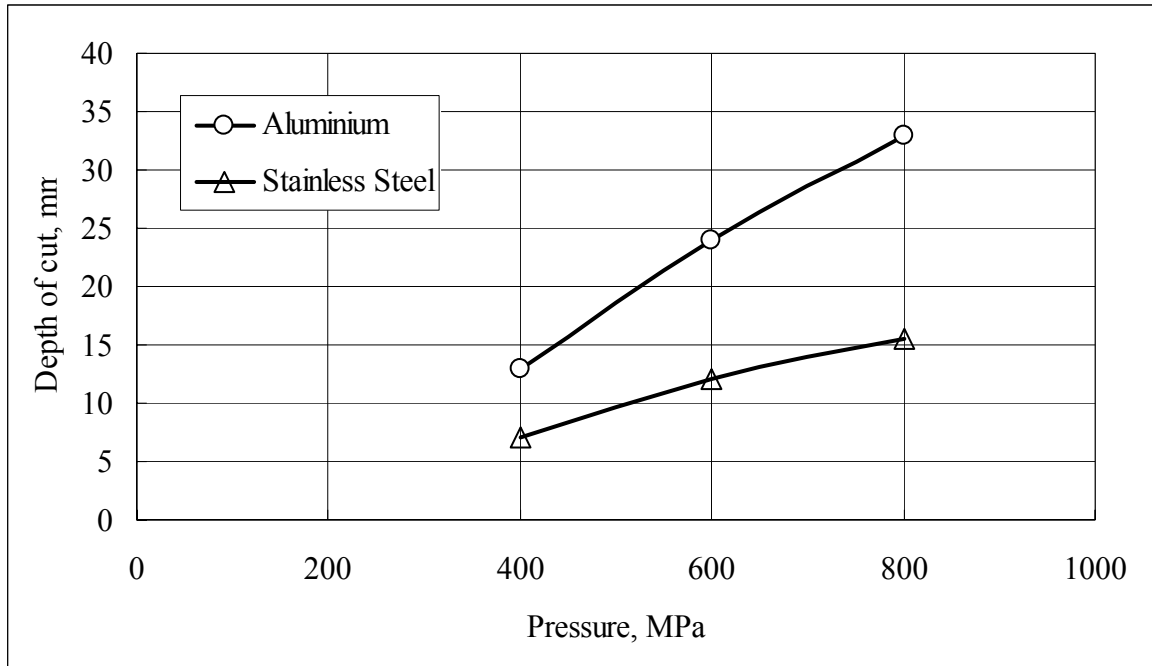


Fig. 2.15: Depth of cut as function of pressure, [10].

The effect of pressure up to 900 MPa on the depth of cut of aluminum at several orifice diameters is shown in Figure 2.16. The cutting depth increases with increasing both the pressure and the orifice diameter. This can be attributed to the increase of the hydraulic power of the waterjet, [12].

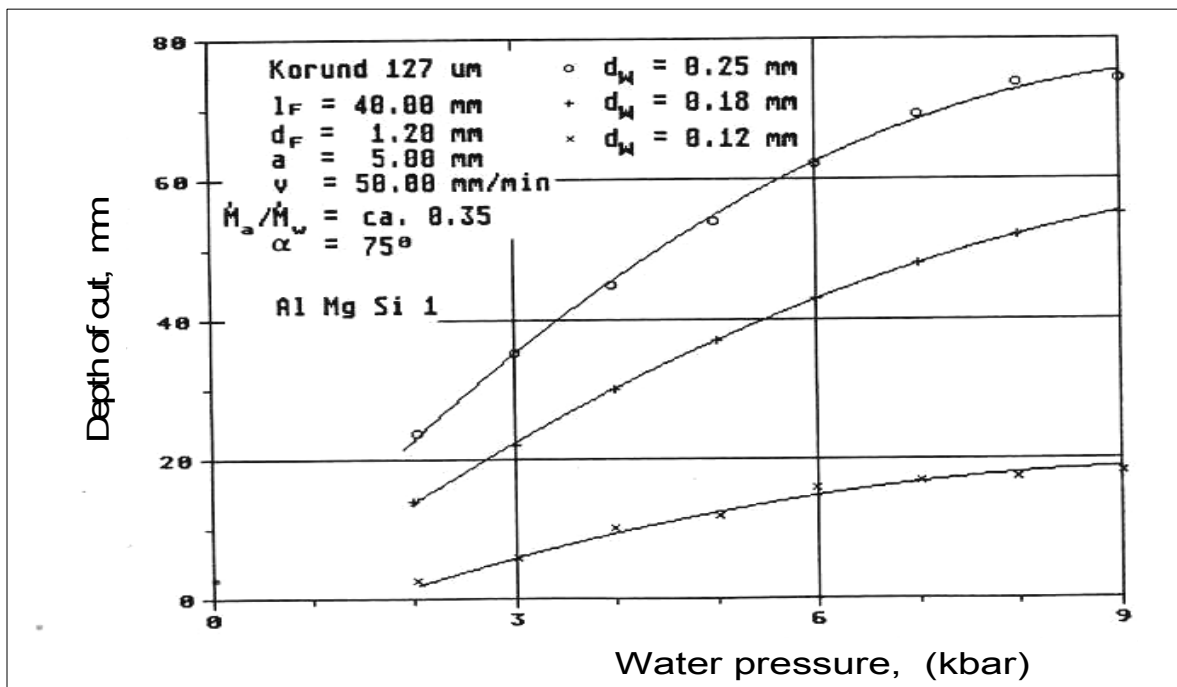


Fig. 2.16: Depth of cut as a function of water pressure, [12]

## 2.6 Cutting Quality and Material Removal Mechanisms

In this section the cutting quality and materials removal mechanism for both abrasive waterjet and plain waterjet so far is presented.

### 2.6.1 Mechanism in liquid impact erosion

The subject of material removal by liquid impact is not new, judging from the number of publications available in the open literature on the topic, [51-63]. Many aspects of the phenomena have been investigated in both ductile and brittle materials. The high velocity impact of a liquid drop against a plane solid surface produces two effects that result in damage to that surface: high contact pressure, which is generated in the area of the impact, and subsequent liquid “jetting” flow along the surface, radiating out from the impact area, [64]. A first approximation of the average impact pressure, before radial outflow initiates, is the one dimensional water-hammer pressure; that is, pressure generated in the impact of an infinite flat liquid surface against an infinite flat rigid surface. In this case a plane shock wave is formed at the instant of impact and travels into the liquid, bringing to rest one “layer” after another.

This impact or shock pressure, [65], can be defined as:”  $p = \rho C v_i$ ” where  $\rho$  the liquid density,  $C$  is the shock wave velocity in the liquid and  $v_i$  is the impact velocity. For water impacting at 500 m/s, this pressure is about 1250 MPa considerably above the yield strength of many alloys. The stagnation pressure of a continuous jet ( $\rho v^2/2$ ) at that speed is about one-tenth of the former. In ductile materials, a single intense impact may produce a central depression, with a ring of plastic deformation around it where the jetting outflow may remove material by a tearing action, Figure 2.17(a). With less intense but repeated impacts, there is no immediate material loss, but randomly disposed dimples gradually develop, and the surface undergoes gradual deformation. In brittle materials, circumferential cracks may be formed around the impact site that is caused by tensile stress waves propagating outward along the surface, Figure 2.17(b). In thin sheets subjected to

impacts, material can spall off the inside surface due to the compressive stress wave from the impact reflecting there as a tensile wave.

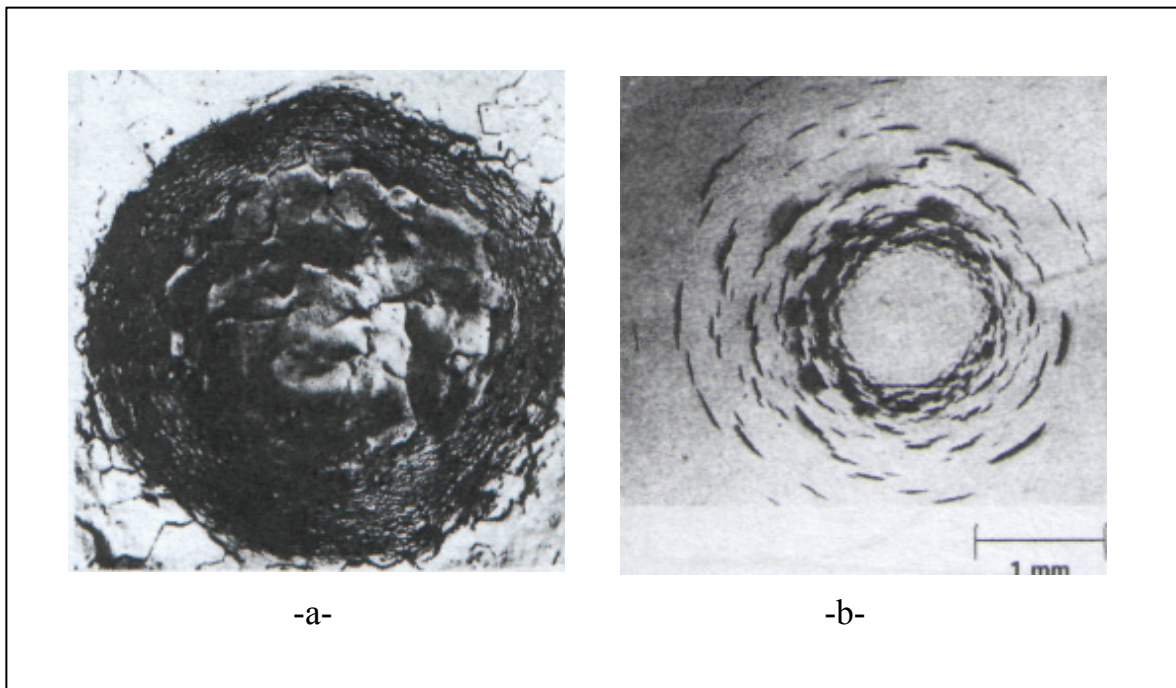


Fig. 2.17(a): Deformation due to a single impact on ductile materials (aluminum).  
Fig. 2.17(b): Damage due to a single impact on a brittle material (zinc), [65].

### 2.6.2 Mechanism in abrasive waterjet cutting

The role of the high speed water flow during the material removal by an abrasive waterjet is a phenomenon that is not yet completely understood but a plain waterjet causes a negligible low material removal rate of the work material when compared with an abrasive waterjet. Some authors, [66-67], consider the water to be a carrier and acceleration medium for the entrained abrasive particles. The cutting action can therefore be fully ascribed to the abrasive particles although the cutting action of the water-fraction of an abrasive waterjet can be neglected. Several authors present experimental and theoretical work on the material-removal process in ductile-behaving as well as in brittle-behaving materials to explain the basic cutting mechanism in abrasive waterjet cutting. The sides of the workpiece, produced by the jet are called the cutting surfaces. At these cutting surface two cutting zones is clearly visible, Figure 2.18. The upper zone is smooth and the lower zone shows a regularly striated pattern.

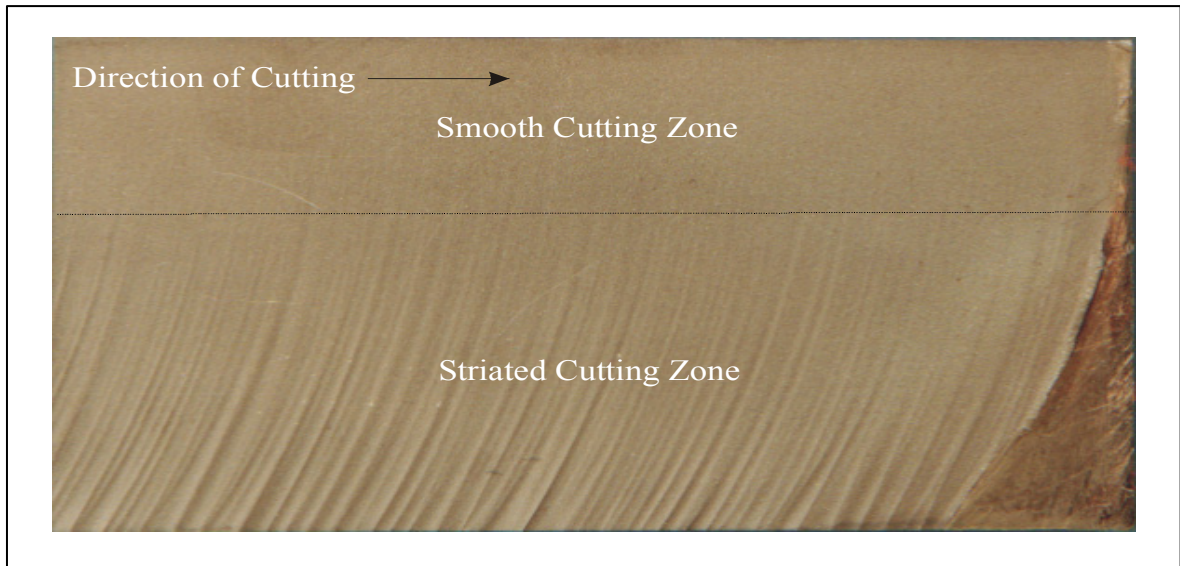


Fig. 2.18: A typical surface generated by AWJ cutting in 49 mm thick titan.

Study of the cutting action at the cutting front in transparent workpiece using a high-velocity video camera, [68], reveals that in cutting ductile materials two zones are cut with different cutting mechanisms, Figure 2.19. In the upper part of the cut towards the jet entrance side the work material is removed by cutting wear. This zone is denoted as cutting wear zone. In the lower part of the cut, towards the jet exit side the work material is removed by deformation wear. This zone is therefore denoted as deformation wear zone.

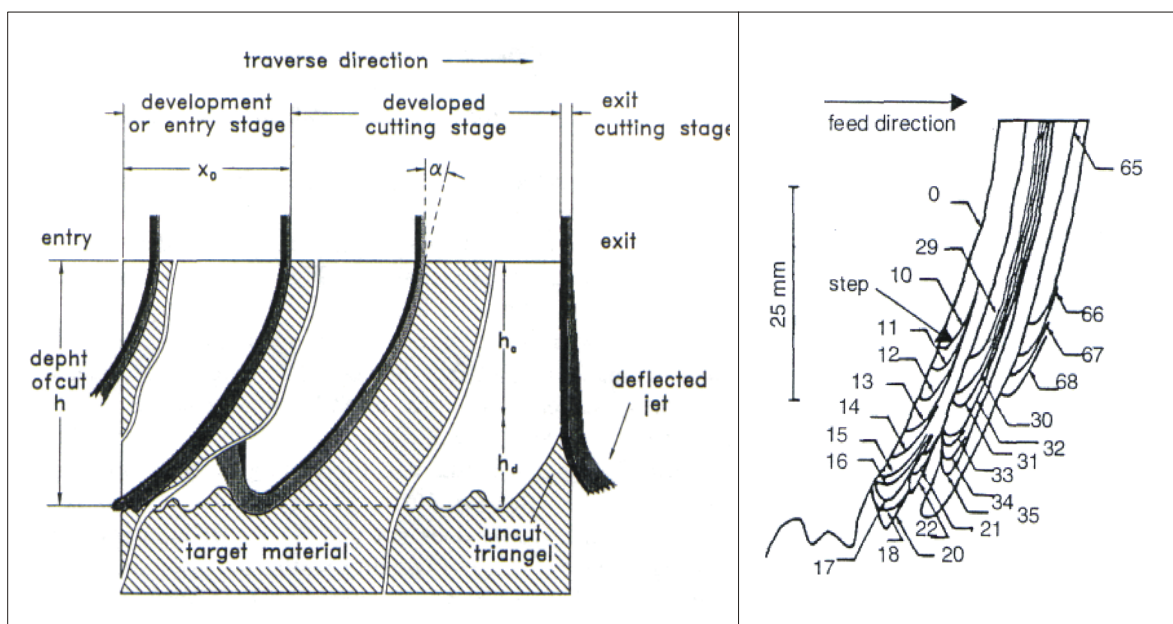


Fig. 2.19: Composition of the shape of the cutting front from high-speed video frames, [68].

Cutting wear is a low angle, glancing impact phenomenon, in which abrasive particle acts as a cutting tool with undefined cutting edges. Deformation wear is a high angle in which every particle impact causes plastic deformation of the workmaterial. After some impacts the deformation limit of the workmaterial is locally exceeded and a part of the workmaterial is removed. After the erosion of a step, new steps appear which are subsequently removed. The cutting process of brittle materials like stone differs on micro-scale from the cutting process of ductile material. The cutting mechanism for brittle materials is believed to be crack initiation and crack propagation [2]. Nevertheless, the appearance of the cutting surface on a macroscopic scale is identical to the cutting surface of a ductile material.

A three-dimensional integral abrasive waterjet cutting model was developed, [69-70]. The three-dimensional aspect of step formation consists of roughness formation due to individual abrasive particle impact, striation formation due to step formation in cutting direction and finally grooves formation due to Jet oscillation perpendicular to the cutting direction is shown in Figure 2.20.



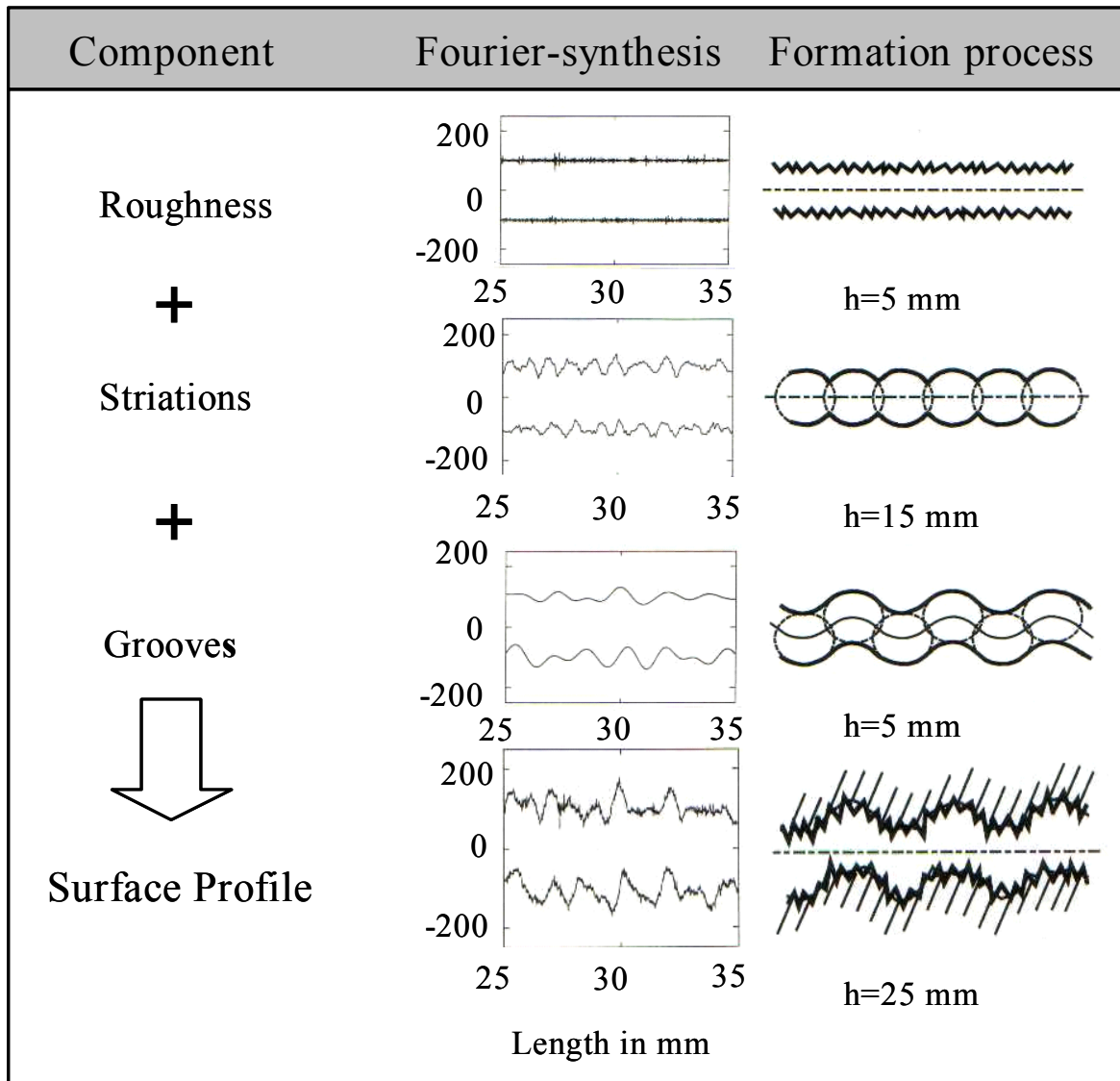


Fig. 2.20: Three dimensional model of the surface formation, [70].

### 2.6.3 Cutting quality

In comparison with plain waterjet at 800 MPa and abrasive waterjet at 300 MPa to studying surface roughness is shown in Figure 2.21, [10]. They explained that the plain waterjet was unable to achieve a so-called “quality cut” ( $R_a < 12 \mu\text{m}$ ). At 800 MPa and a traverse speed of 25 mm/min plain waterjet cutting generates nothing better than a “rough cut”. It can also be ascertained that the surface finish becomes worse with an increase in the depth cut, as it does for AWJ cutting. The mechanism of jet cutting process generally depends on the process parameters. In the case of AWJ is explained in section 2.6.2. In the case of WJ, the mechanism of waterjet cutting is erosion caused by localized failure which occurs by the localized fluid

pressure (impact pressure) [50]. This pressure exceeds the strength of the target material leading to a plastic deformation, flow and removal of the material.

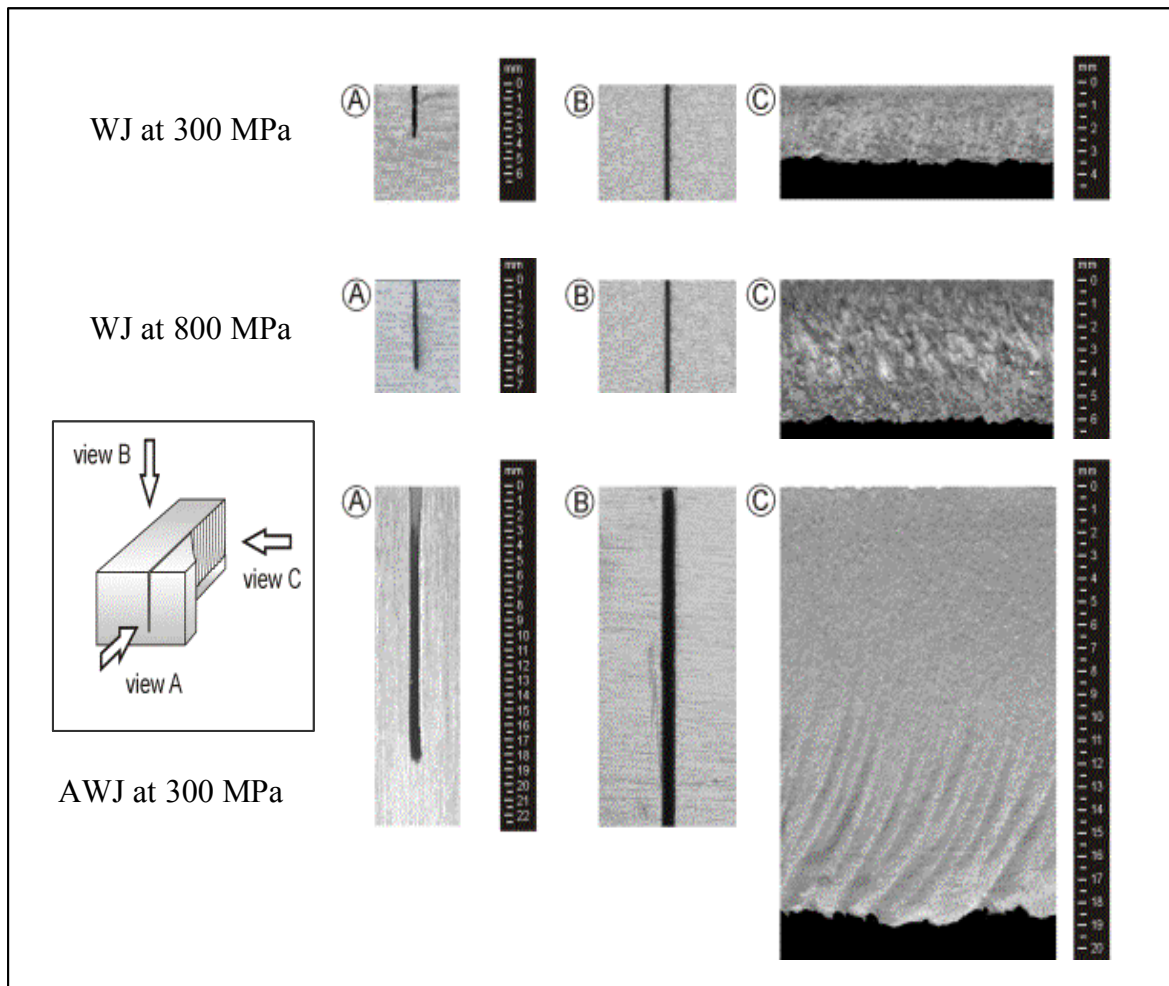


Fig. 2.21: Aluminium cutting quality by WJ and AWJ, [10].

## 2.7 Modelling of Waterjet Cutting Processes

Performance of any machining process is evaluated in terms of machining rate and surface finish produced. Higher machining rate and better surface finish are desirable for better performance of any machining process. Comprehensive qualitative and quantitative analysis of the material removal mechanism and subsequently the development of analytical model(s) of material removal are necessary for a better understanding and to achieve the optimum process performance. Analytical material removal models are also necessary for simulation, optimization and planning (i.e. operation and process planning) of the process

prediction of process performance indicators, verification and improvements of experimental results [71-72].

### 2.7.1 Modelling of plain waterjet cutting for metals

Erosion of materials by waterjet machining is still a complex phenomenon. The present section focuses on models for the calculation of the depth of cut especially for machining of metal. A first rough view of the models developed for this purpose so far shows that the models can be divided into at least two groups; volume-displacement models, and parameter-regression models

A Bingham plastic constitutive model was used, [73-75], to describe the time-dependent stress-strain relationship of the workpiece material when subjected to hydrodynamic forces, where the yield behavior is analogous to the jet cutting process, which starts only when the velocity exceeds a certain minimum value. The cutting mechanism of waterjet machining was suggested to be a complex series of phenomena which may involve compression, tension, shear, erosion, cracking and wear. The dominant mechanism depends on the type of material, type of cutting: (slotting or drilling) and traverse rate. The cutting mechanism was considered in this study to be governed by compression failure, where the stresses generated must be greater than the compressive fracture strength. As the kerf deepens, a critical velocity is reached where the compressive stress is insufficient to fracture the workpiece material and cutting stops. The dimensionless equation expressing penetration depth is

$$\frac{k}{d_n} = \frac{1 - \left( \frac{\sigma_y}{\rho v_j^2} \right)}{\left( \frac{2\mu_f}{\sqrt{\pi}} \right)} \left[ 1 - e^{-\left( \frac{2\mu_f}{\sqrt{\pi}} \right) \left( \frac{\rho v_j}{\eta} \right) \left( \frac{v_j}{u} \right)} \right] \rightarrow (2.10)$$

Mean values of the friction ( $\mu_f$ ) and damping coefficients ( $\eta$ ) which are used with the compressive yield strength ( $\sigma_y$ ) to characterize different materials which the coefficient of friction and damping coefficients can be determined experimentally.

The nondimensional regression models used to describe the depth of cut, [76], is represented by the following equation:

$$\frac{k}{d_n} = \left[ \frac{\rho_m (v_j^2 - v_c^2)}{\sigma} \right]^m \left[ \frac{v_j}{v_f} \right]^n \quad \rightarrow (2.11)$$

where  $\frac{k}{d_n}$  is a cutting depth number,  $\frac{v_j}{v_f}$  is a cutting speed number. The cutting stress number  $\frac{\rho_m (v_j^2 - v_c^2)}{\sigma}$  represents the ratio of the jet cutting stress above a certain critical value to the dominant strength property of the material. The equation satisfies the limiting conditions for all materials which no cutting occurs when  $v_j$  equal  $v_c$ . Three experimental constants are needed for each material but this model is derived without any physical explanation and not tested yet.

The cutting behaviour of a wide range of brittle material, [77], is described by an equation of the form:

$$\frac{k}{d_n} = A \left[ \frac{P}{\sigma_c} - 0.2 \right] \left[ \frac{v_j}{v_f} \right]^n \quad \rightarrow (2.12)$$

Two experimental constants are needed for each material.

An empirical equation, [78],

$$\frac{k}{d_n} = \left[ \frac{P}{1,131} \right]^{0.7} \left[ \frac{v_j}{v_f} \right]^{0.2} \quad \rightarrow (2.13)$$

was introduced for copper that did not contain a material property and its application is therefore limited to that material and the particular conditions of the experimental investigation.

Most of the previous models require characteristic coefficients which have to be determined experimentally. Table 2.2 describes the expected trend of the maximum

depth of kerf as a function of pressure, nozzle diameter and traverse speed by previous equations.

Table 2.2 Expected trend of the maximum depth of kerf for plain waterjet cutting

Eq. No.	$k = c_1 P^{n_1}$	$k = c_2 d_n^{n_2}$	$k = \frac{c_3}{V_f^{n_3}}$
(2.10)			
(2.12)			$n_3 = n, \text{ unknown}$

From Table 2.2 the following can be summarized

1. There is a threshold pressure to penetrate the materials which is different from model to another. The threshold pressure is equal to  $0.5 \sigma_y$  and  $0.2 \sigma_c$  from equations 2.10 and 2.12 respectively.
2. A linear relationship between the pressure and the depth of cut is given,
3. A linear relationship between the nozzle diameter and the depth of cut is given,
4. The relation between the traverse rate and the kerf depth is inversely proportional, as given in equations 2.10 but the exponential in equations 2.12 is unknown and must be determined from experimental work.

### 2.6.2 Modelling of abrasive waterjet cutting for metals

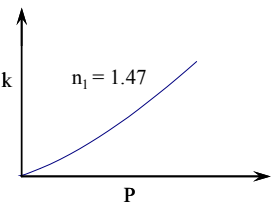
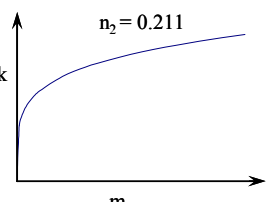
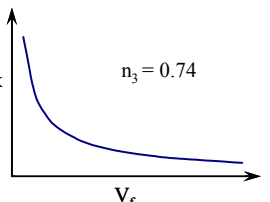
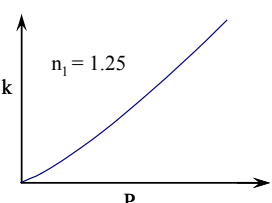
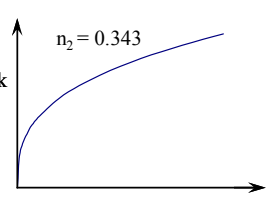
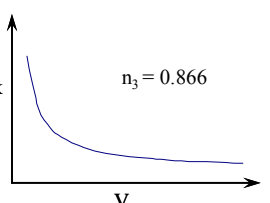
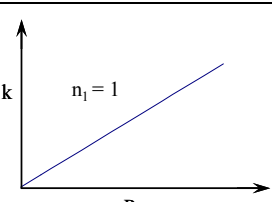
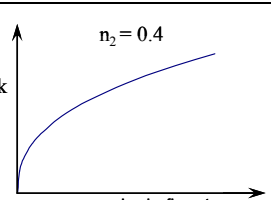
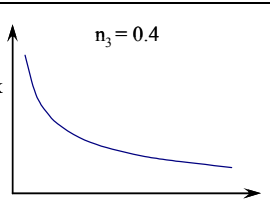
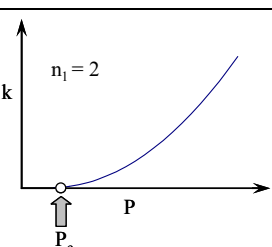
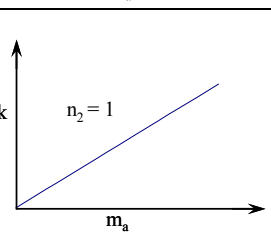
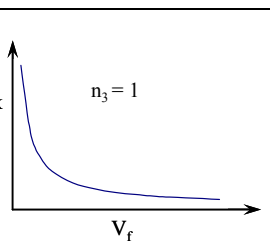
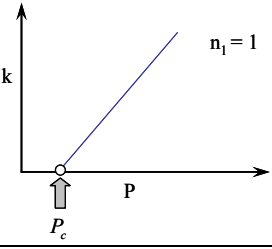
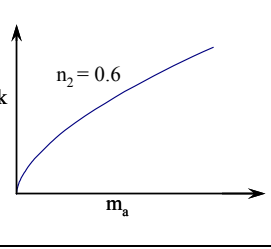
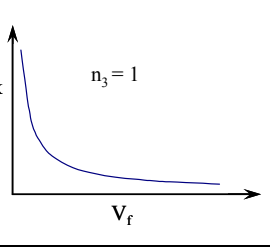
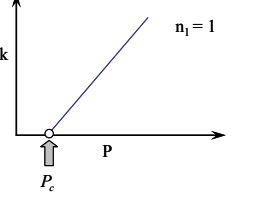
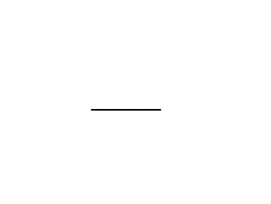
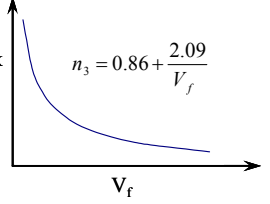
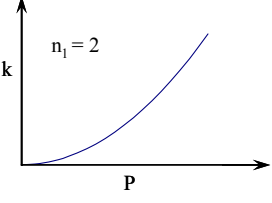
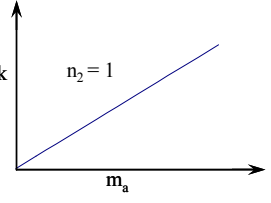
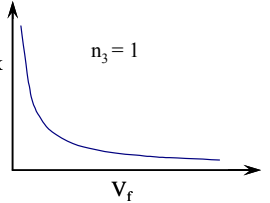
Many scientists have described the abrasive waterjet modelling from simple to complicated way. Table 2.3 describes only the most predictive models to determine the maximum depth of kerf as function of machining parameters.

Table 2.3: Abrasive waterjet modelling

Author	Basic Equations	Eq. No.	Descriptions
Matsui et al., [79]	$k = \frac{10^{4,74}}{V_f (H \cdot \varepsilon_s)^{0,67}}$	(2.14)	For ductile materials, where H hardness and $\varepsilon_s$ is the strain.
Kovacevic et al., [80]	$k = 0.00139 \frac{d_f^{0,765} m_a^{0,211} P^{1,47}}{S^{0,139} V_f^{0,74}}$	(2.15)	Regression Model refers to the theoretical model of Hashish
Zeng and Kim, [81-82]	$k = \frac{N_m \cdot P^{1,25} \cdot m_w^{0,687} \cdot m_a^{0,343}}{8800 \cdot d_f^{0,618} \cdot v_f^{0,866}}$	(2.16)	Regression Model where $N_m$ is the Machinability number of materials
Hashish, [83]	$k = \frac{cd_j v_a}{2.5C_k} \left( \frac{14 \cdot m_a}{\pi V_f d_j^2 \rho_a} \right)^{0,4}$	(2.17)	Cutting wear, modified Model of Finie, [84-85], where $C_k$ is constant (characteristic velocity)
Hashish, [83]	$k = \frac{2 \cdot (v_a - v_c)^2 \cdot m_a}{\pi d_j V_f \sigma_f}$	(2.18)	Deformation wear, modified model of Bitter, [86-87], where $\sigma_f$ is the materials flow stress
Chung et al., [88]	$k = \frac{(P - P_c) m_a^{0,6}}{V_f b_k}$	(2.19)	Regression model for ductile materials where $b_k$ is the width of cut
Blickwedel, [89]	$k = \frac{C \cdot (P - P_c)}{V_f^{0,86 + \frac{2,09}{V_f}}}$	(2.20)	Regression model test for aluminum and austenite
Oweinah, [12]	$k = \frac{v_a^2 \cdot \lambda \cdot m_a}{2V_f b_k \varepsilon}$	(2.21)	where $\lambda$ is regression parameter, $\varepsilon$ is the specific energy
Hlavac, [90]	$k = \frac{\sqrt{2} R_f \pi d_a^2 d_n \rho_a P H_a m_w^2 \sin \varphi}{12 N_d V_f \rho_w (\sigma_c + \sigma_s) H (m_w + m_a)^2}$	(2.22)	Energy balance model without a detailed deviation

The expected trend of the maximum depth of kerf as a function of pressure, nozzle diameter and traverse speed by previous equations is described in Table 2.4

Table 2.4: Expected trend of the maximum depth of kerf for AWJ.

Eq. No.	$k = c_1 P^{n_1}$	$k = c_2 m_a^{n_2}$	$k = \frac{c_3}{V_f^{n_3}}$
(2.15)			
(2.16)			
(2.17)			
(2.18)			
(2.19)			
(2.20)			
(2.21)			

From Table 2.4 the followings can be summarized

1. Some authors attempted that there is a threshold pressure required to penetrate the materials as proved in equations 2.18, 2.19 and 2.20, but the value of the unknown, must be determined from experimental works. Other authors did not determine the value of threshold pressure, as derived in equations 2.15, 2.16, 2.17 and 2.18.
2. The influence of the pressure in the depth of cut has a different reaction power parameter. In equation 2.17,  $n_1 = 1$ , which means that the influence is linear, but in equations 2.18 and 2.21 the reactions power,  $n_1 = 2$ , presents unexpected high value due to the rapid increase of the depth of cut with increasing the pressure.
3. The depth of cut increases with increasing the abrasive flow rate and has a different reaction power where the small value is 0.211, equation 2.15, and the maximum value is 1, equations 2.16 and 2.21. The experimental observations showed that the depth of cut increases up to certain value then decreases. No equation was found to describe this behaviour.
4. The relation between the traverse rate and the kerf depth is inversely proportional, but it has a different reaction power ranging from minimum value of 0.4 in equation 2.17 and maximum value of 1.0 in equation 2.18.



## **3. EXPERIMENTAL PROCEDURE**

This chapter describes the experimental setup, tested materials and measurements carried out in this study.

### **3.1 Experimental Setup**

This section described two systems were used in the experimental setup. The first system is 900 MPa cutting system. It consists of Autofrettage pump of 1000 MPa maximum pressure and 0.5 l/min flow rate, the CNC machine and the pressure gauge. The second alternative system was used in condition of using flow rate above the value delivered by Autofrettage pump and finally the abrasive waterjet cutting system.

#### **3.1.1 900 MPa Cutting systems**

The system used in these experiments consists of an inlet pressure pump feeding water from tapwater at maximum permissible pressure of 1.0 MPa at +20°C to the filtration system which contains two hydraulic filters, where the fineness of the filtering material for the first (coarse) and the second (fine), is 5 µm and 1.2 µm respectively. The filters are followed by the pressure intensifier that supplies a water flow rate up to 0.5 l/min with a maximum pressure of 900 MPa (Model CP 1000-0.5 Firma BÖHLER HOCHDRUCKTECHNIK). It is a double acting intensifier of 10 mm piston rod diameter and 120 mm stroke. The number of strokes per minute is 45 with intensification ratio of 1:63.

The pressure intensifier is operated by a hydraulic unit. The fluid media is mineral based hydraulic oil (ISO VG 46 DIN 51524 and 51525). The oil tank filling capacity is 60 Liter. The maximum permissible operating pressure is 21 MPa and flow rate of 0 - 130 l/min. The hydraulic pump is radial piston pump (BOSH RKP60) with proportional magnet control of synchronous cylinders. The piston diameter is 90 mm, while the piston rod diameter is 42 mm of 120 mm stroke. A

schematically diagram and photographically of the auttofrettage pump is shown respectively in Figure 3.1 and 3.2.

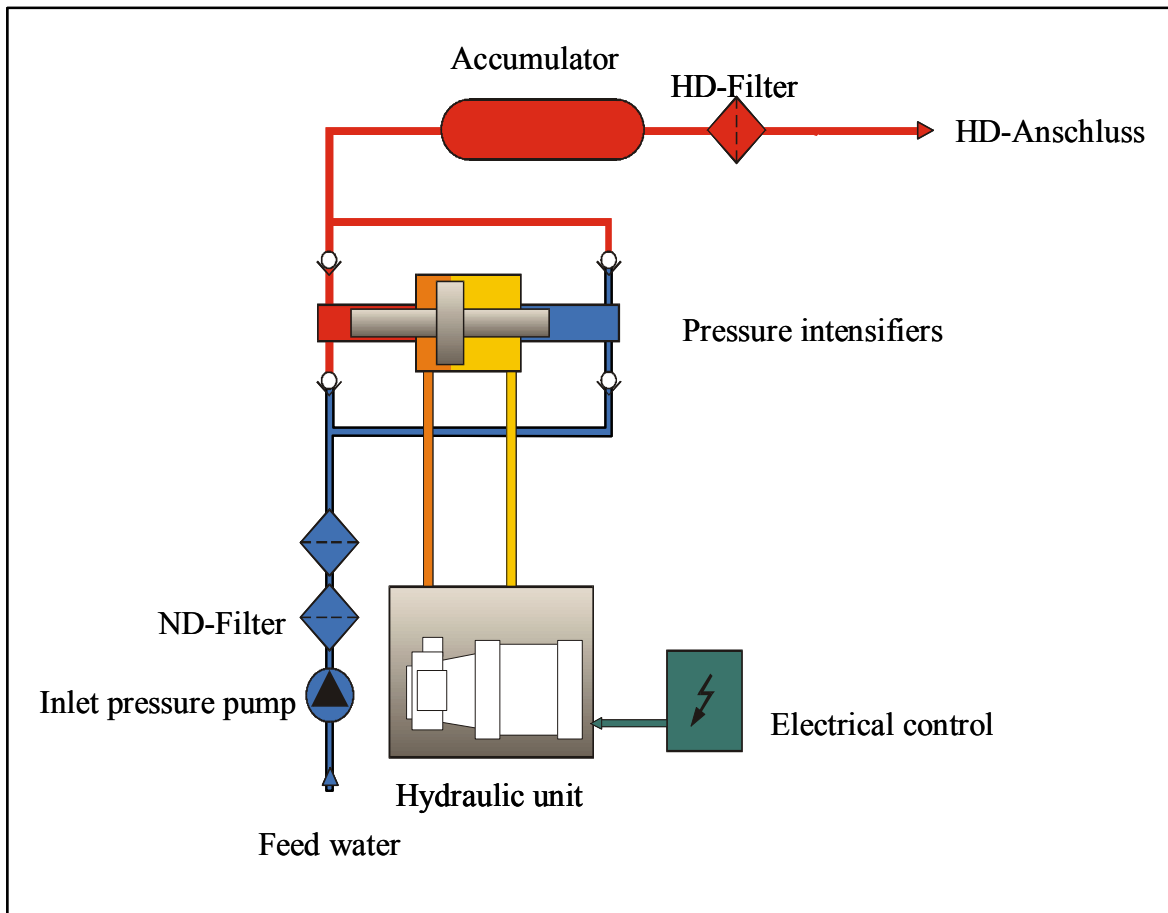


Fig. 3.1: A schematically diagram of the intensifier pump.

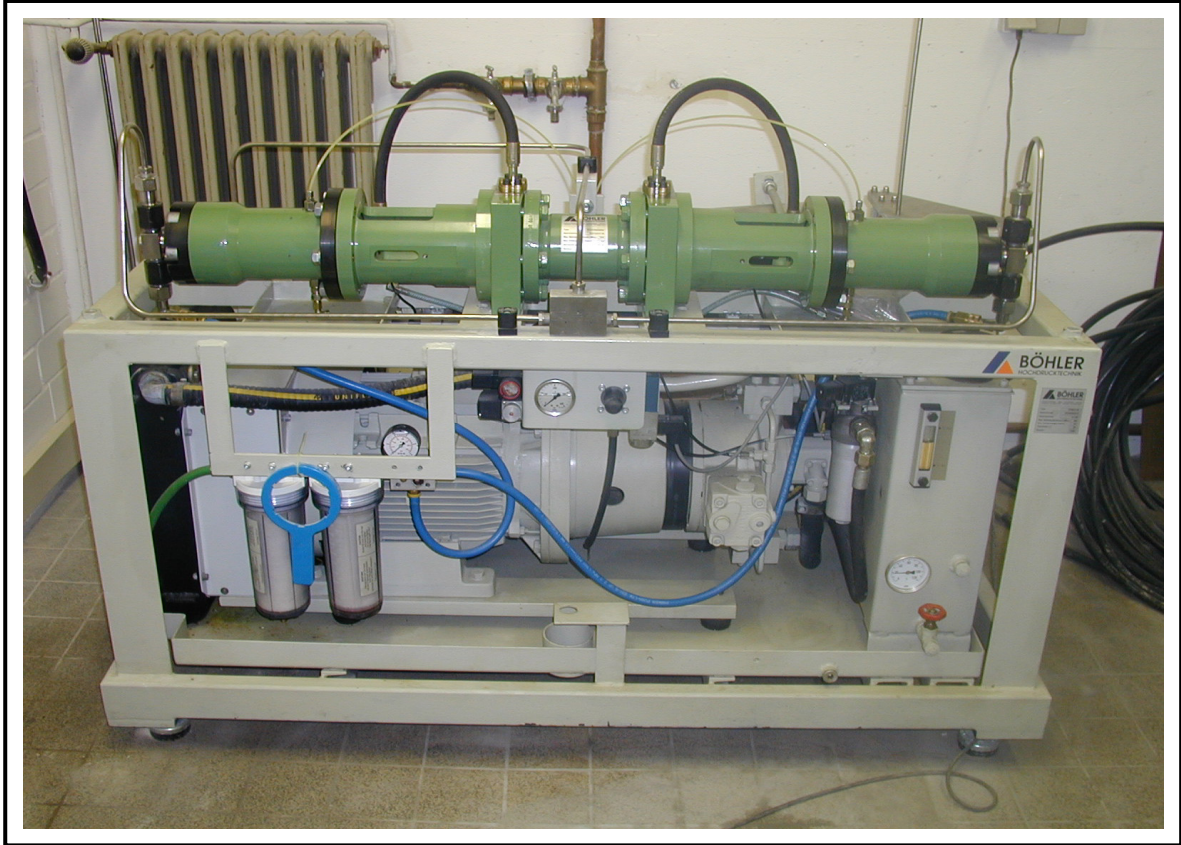


Fig. 3.2: Autofrettage pump.

It should be mentioned that in order to guarantee more safety, the high pressure pump was kept in a separate room, while the pump control unit was installed near to the CNC control unit in another room, where the experiments were carried out. A video-camera was used to monitor and record the cutting process. The movement of the workpiece is numerically controlled, where the guiding system consists of a two NC controlled axes, while the Z-axis is manually adjustable. The nozzle supply pressure was measured by pressure absorber with integrated measuring amplifier and digital indicators up to 1400 MPa (Firma Dustec Germany), of accuracy  $\pm 0.01$  MPa is shown in Figure 3.3. A schematically Layout and photographically for experimental setup are shown in Figure 3.4. The pump unit control, the CNC machine, the pressure gauge, the nozzle holder, the workpiece holder and the video camera to monitor the experimental setup is shown photographically in Figure 3.5

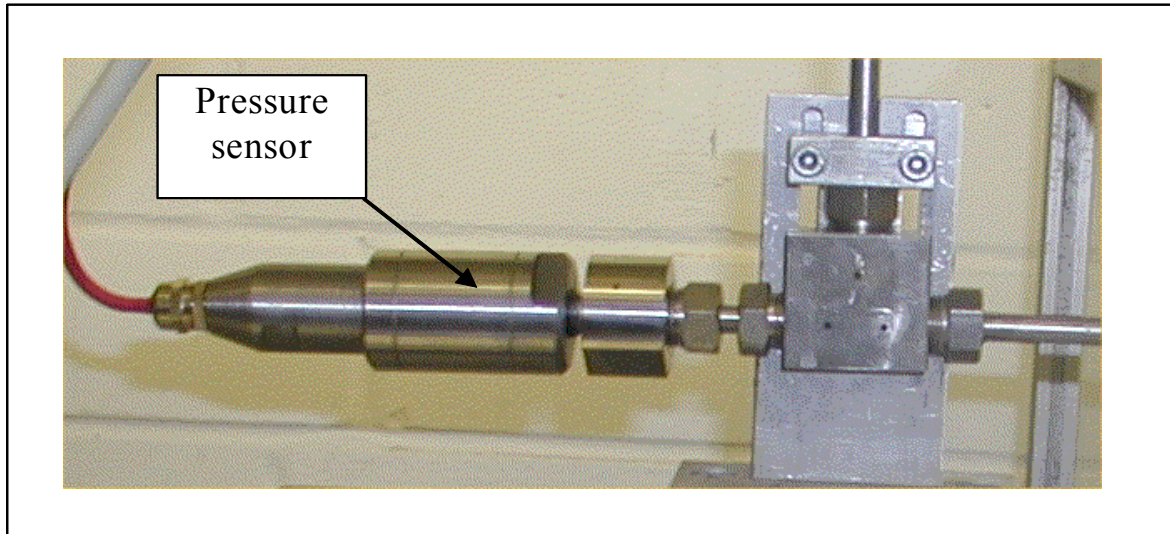


Fig. 3.3: Pressure gauge.

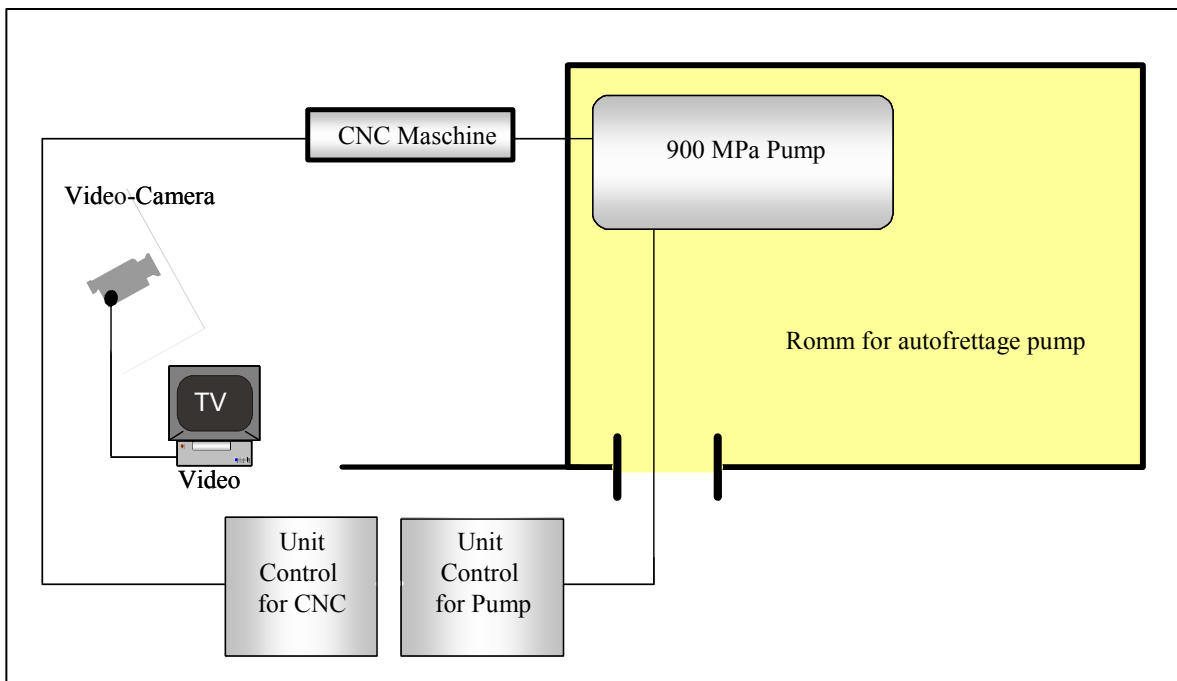


Fig. 3.4: A schematically layout for experimental setup.

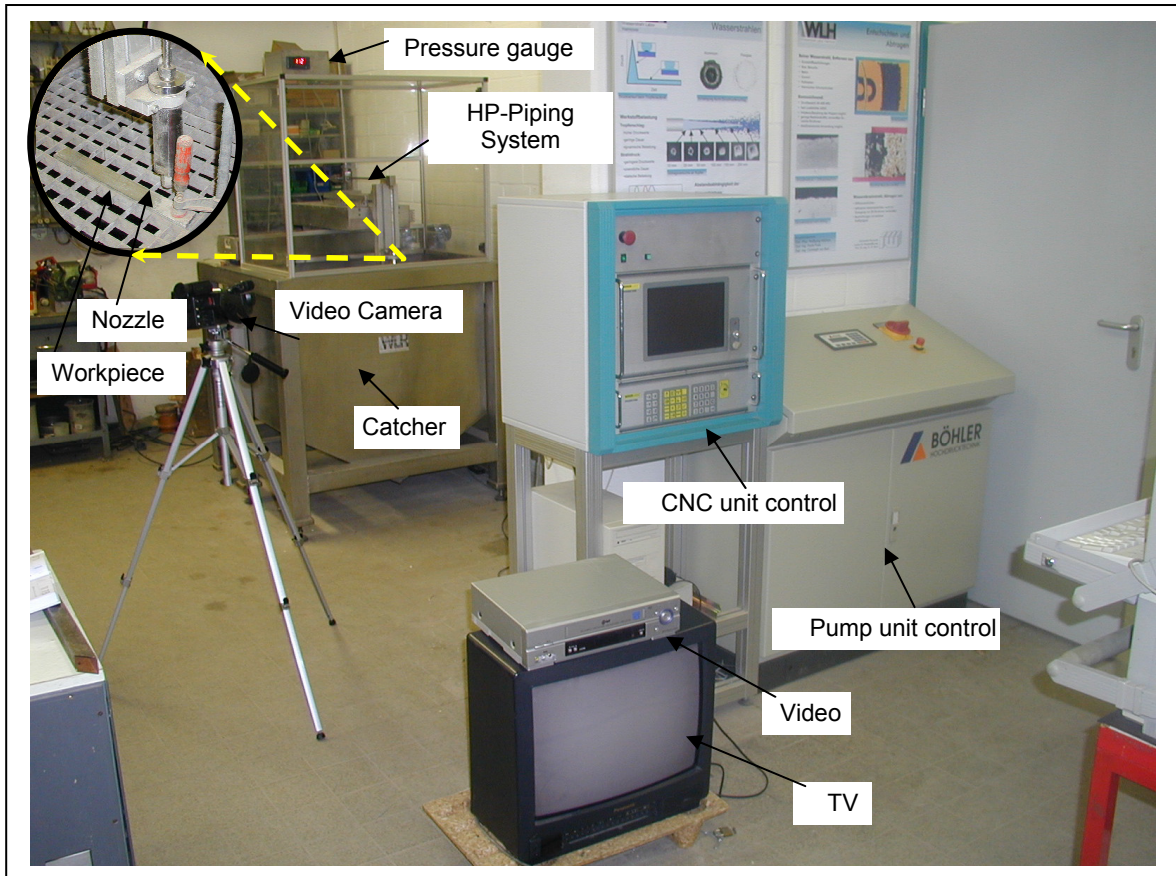


Fig. 3.5: Photographically experimental setup.

### 3.1.2 An alternative systems for fundamentals investigations

The selection of the nozzle diameter depends on both the flowrate and the pressure of the fluid. The relationship between the flow rate and pressure for different nozzle diameters and ideal efficiency coefficient, ( $\mu=1$ ), is shown in Figure 3.6. Based on the technical specifications of the pump described in section 3.1.1, an alternative pump systems for fundamental investigations was used in order to have flow rate above 0.5 l/min. A conventional cutting table, manufactured by Steiner-Moser Company in Austria, was used. The high pressure water was generated either by a plunger pump (WOMA, 150 MPa, 40 l/min) or intensifier pumps (UHDE 400 MPa, 3.8 l/min or FLOW 415 MPa, 7.6 l/min).

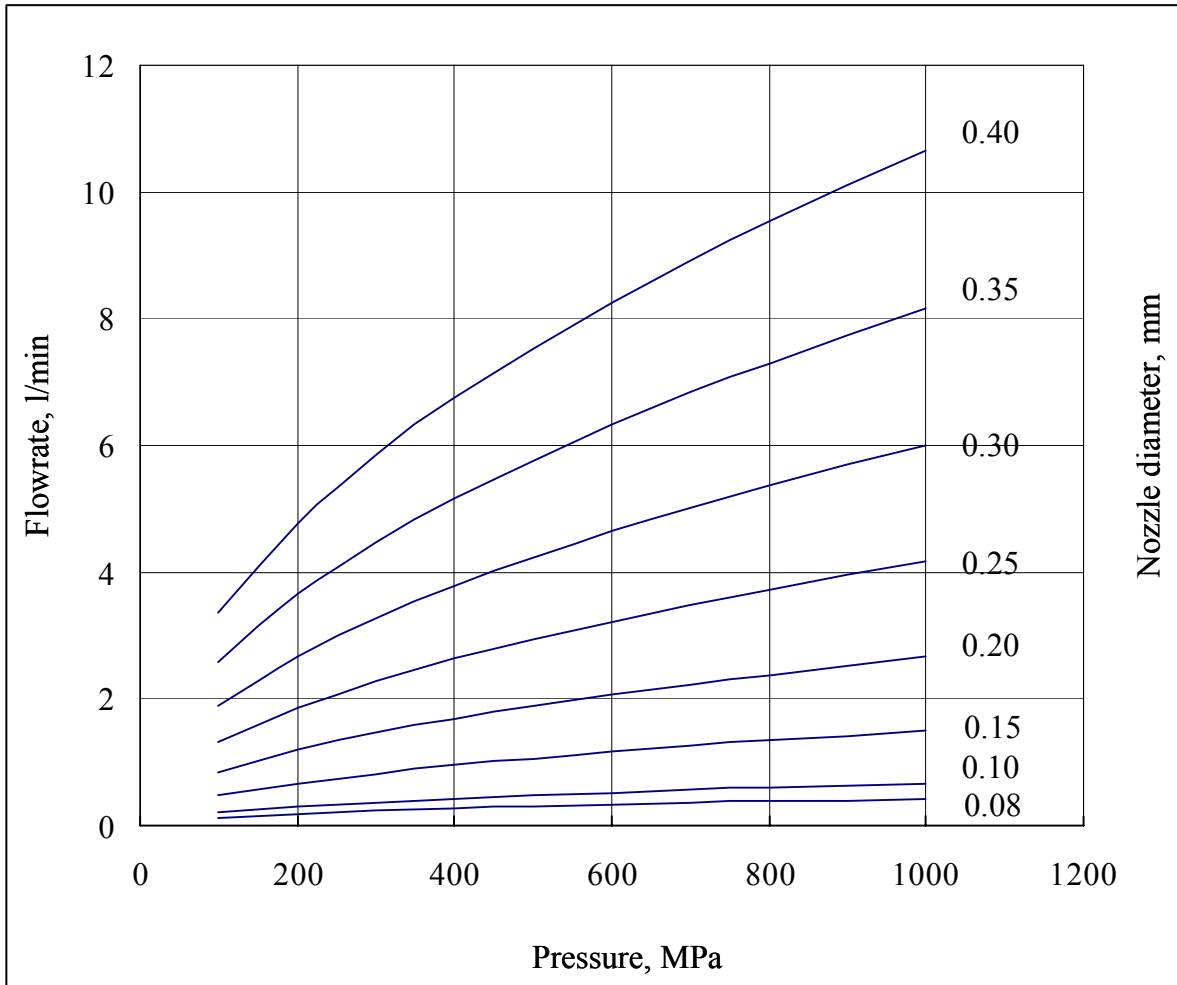


Fig. 3.6: Relationship between pressure and flowrate at different nozzle diameter.

### 3.1.3 Abrasive waterjet cutting system

The abrasive waterjet cutting consists of Böhler abrasive cutting head, 0.1 mm nozzle diameter, 0.4 mm focus diameter and 70 mm focus length as shown in Figure 3.7. Barton garnet 220 mesh was used as abrasive material.



Fig. 3.7: Abrasive cutting head.

### 3.2 Tested Materials

The tested materials were selected to represent the three types of crystal structure known for metals to study the cutting mechanism by plain waterjet. The tested materials were aluminium as ductile material of face centered cubic, (fcc), Armco-iron of body centered cubic, (bcc), representing the materials having less ductile and zinc of closed packed hexagonal structure, (hcp), representing brittle materials. To optimize parameters of the cutting process, aluminium, copper and austenite were tested. The properties of the tested materials are shown in Table 3.1.

Table 3.1 Materials test properties (data from manufacturer).

Materials	Tensile Strength, N/mm <sup>2</sup>	Yield Strength, N/mm <sup>2</sup>	Elongation A5 %	Hardness
Al 99.5	70-110	20-40	35-40	15-25 HB
AlMgSi0.5-3.3206	220	160	12	60 HV10
Armco-Iron-1.1003	270-350	190		90-110HB
Zinc	25-40			28-33HB
SF-Cu F25	250-300	150	20	80HB
X5CrNi 18 10-1.4031	500-700	195		130 -170HB

### 3.3 Measurements

In this section the measurements for tested parameters such as depth of cut, surface roughness and temperature rise are qualified.

#### 3.3.1 Depth of cut

Depth of cut depends on the waterjet diameter that is mainly affected by the nozzle diameter. In the present work, a nozzle diameter of 0.08 and 0.1 mm was used. Workpiece of tapered section were prepared to facilitate the measurement of the depth of cut, Figure 3.8. A calliper gauge was used to measure the depth of cut by an accuracy of  $\pm 0.01$  mm.

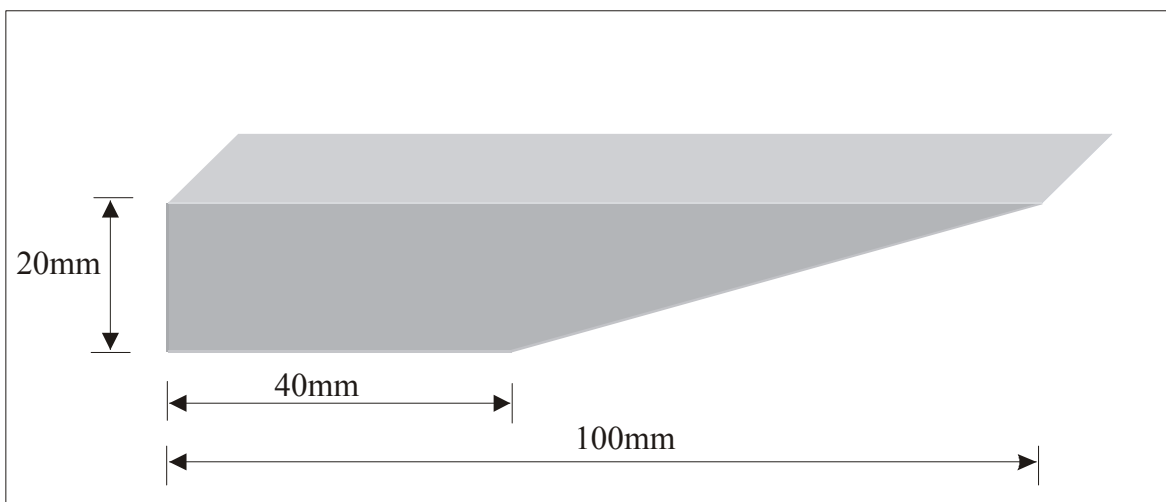


Fig. 3.8: Tapered workpiece preparations for plain waterjet.



Figure 3.9 shows the length of the cutting groove at the lower tapered workpiece face, however the depth of cut was measured at positions of continuous cutting groove.

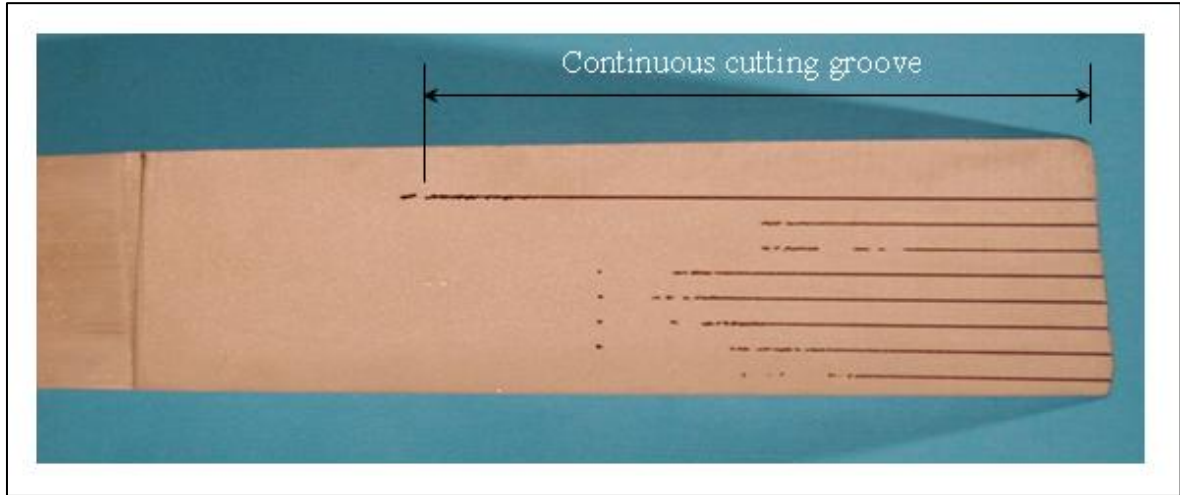


Fig. 3.9: Cutting groove length at bottom face.

### 3.3.2 Surface roughness

The roughness of the machined surface was measured by a laser scanning system, (RM-600, Fa. Rodenstock, Germany), of a measuring range up to  $\pm 300 \mu\text{m}$  and an accuracy of  $\pm 0.01 \mu\text{m}$ . The surface topography is traced by the laser beam which is focused by lens. The output signals are converted into profile height values through the attached computer, Figure 3.10.

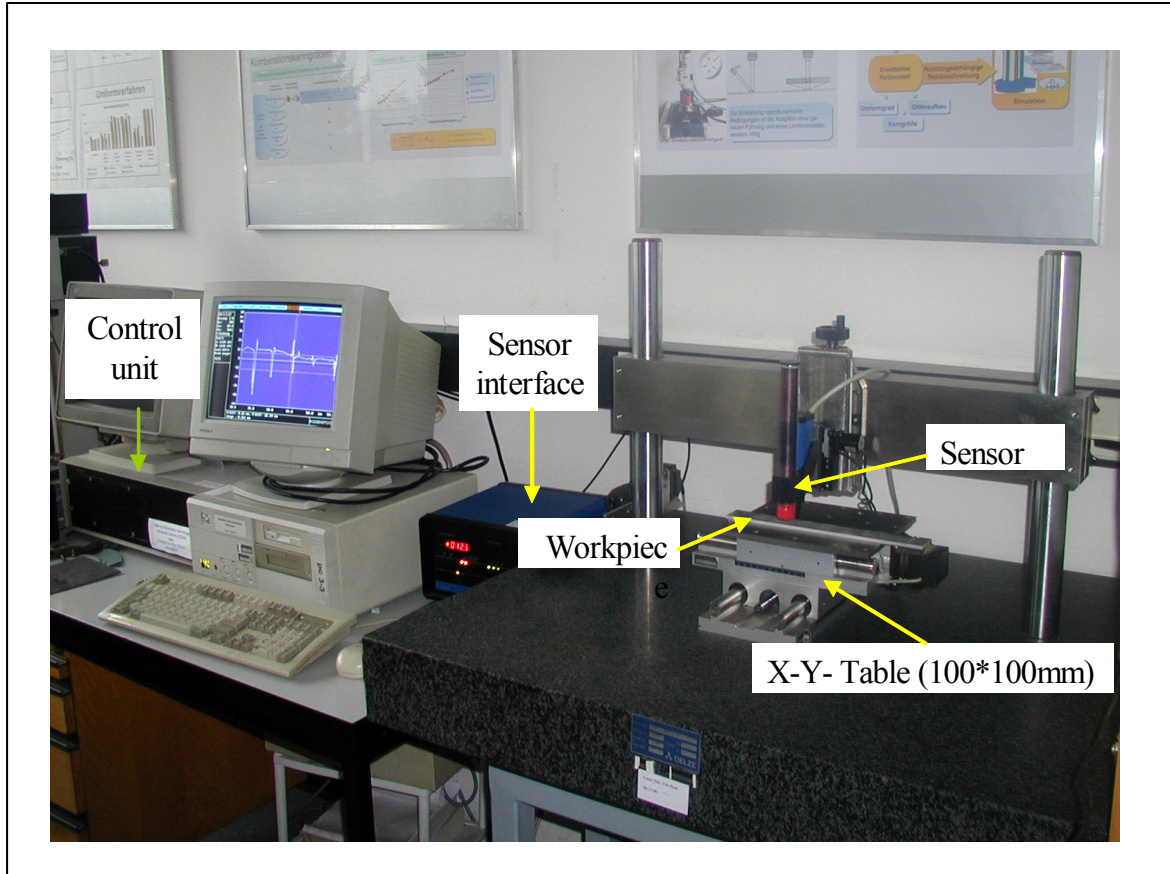


Fig. 3.10: Laser-optical topography measuring system.

### 3.3.3 Temperature

The temperature generated of the waterjet and abrasive waterjet process is measured during the cutting process. The measuring instrument used in this study is an infrared camera (type: FLIR ThermaCam SC 3000), Figure 3.11. It is placed at a distance of 1 meter from the workpiece for all tests, Figure 3.12. The infrared camera can scans the heat emitted by the machined surface. The function of the infrared camera is to display the temperature distribution of the followings:

1. The nozzle through the nut,
2. the abrasive waterjet head,
3. the surface of the workpiece across the depth of cut,
4. and the waterjet.



Fig. 3.11: FLIR ThermoCam SC 3000.

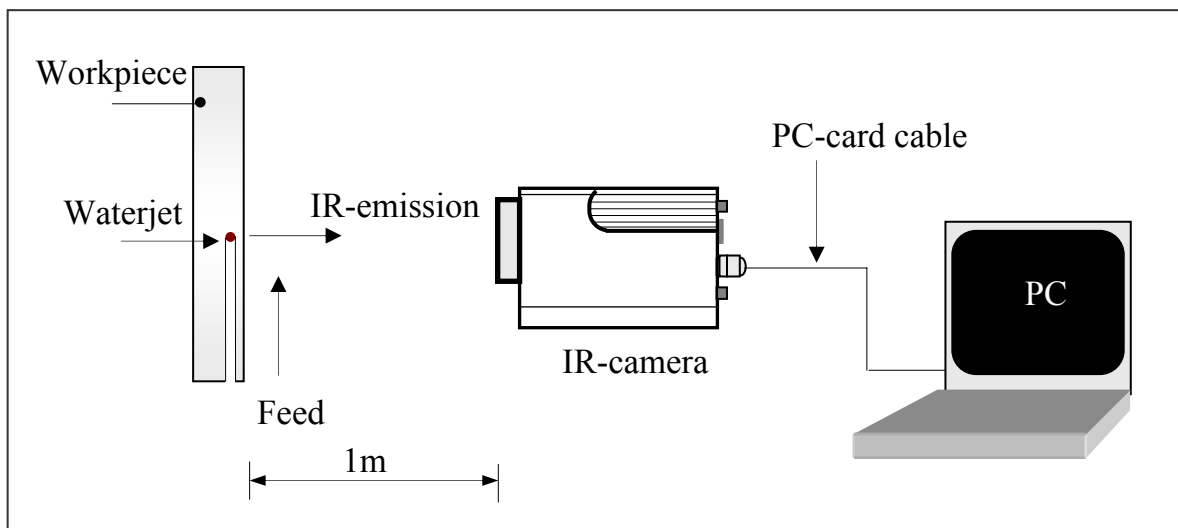


Fig. 3.12: Monitoring strategy for temperature measurements.

### 3.3.3.1 Plain waterjet

For plain waterjets, the effect of nozzle diameter and pressure on the temperature generations was investigated.

**a) The effect of the nozzle diameter**

The experimental setup is shown in Figure 3.13. It consists of Flow intensifier pump of 410 maximum pressure and 7 liter/min flow rate as well as, the pressure gauge, x-y cutting table, waterjet cutting head, workpiece holders and IR camera. The machining parameters are listed in table 3.2.

Table 3.2: Machining parameters at different nozzle diameter

Pump	Flow 410 MPa , 7 liter/min
Nozzle diameter	0.08, 0.1, 0.2 and 0.3 mm
Pressure	300 MPa
Traverse rate	10 mm/min
Workpiece material	Al 99,5
Cutting length	10 mm
Cutting depth (through cut)	2 mm

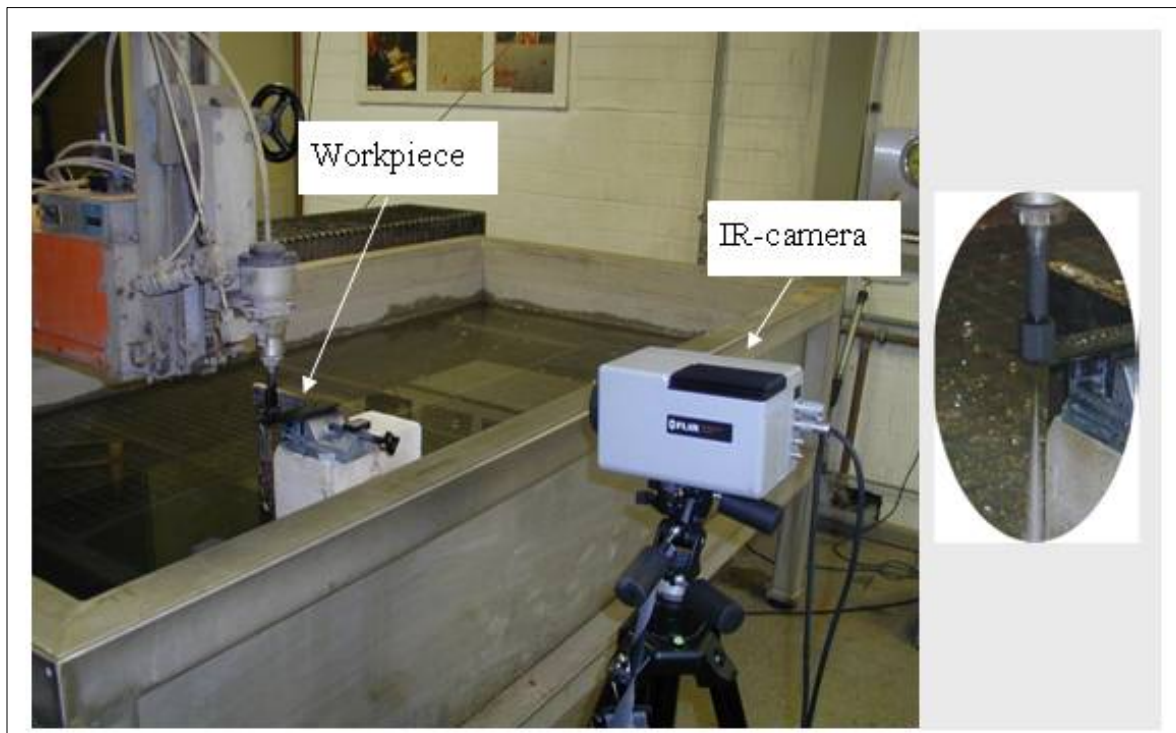


Fig. 3.13: Arrangements of studying the effect of the nozzle diameter.

**b) The effect of the pressure**

The arrangements of studying the effect of the pressure on the temperature are shown in Figure 3.14. It consists of Autofrettage pump of 1000 MPa maximum pressure and 0.5 l/min flow rate, the CNC machine, the pressure gauge, waterjet

cutting head, workpiece holder and IR camera. The machining parameters are listed in Table 3.3.

Table 3.3: Machining parameters at different pressure

Pump	Böhler 1000 MPa , 0.5 liter/min
Pressure	from 100 to 900 MPa
Nozzle diameter	0.1 mm
Traverse rate	10 mm/min
Workpiece material	Al 99,5
Cutting length	10 mm
Cutting depth (through cut)	3 mm

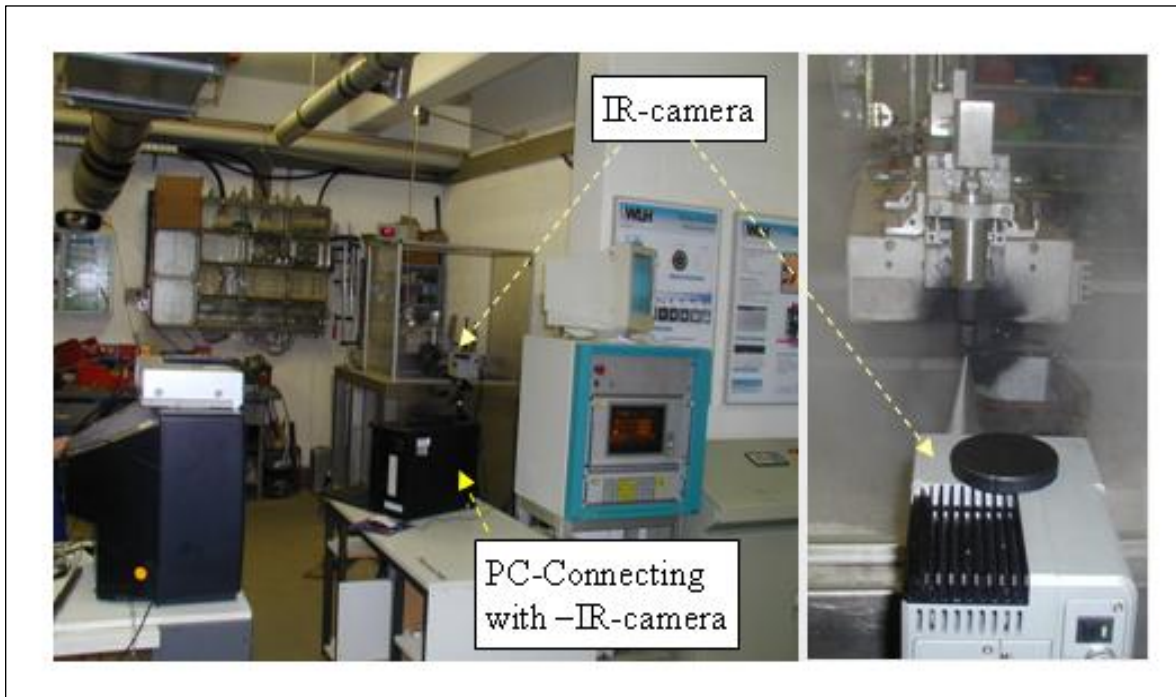


Fig. 3.14: Arrangements of studying the effect of the pressure.

### 3.3.3.2 Abrasive waterjet

For abrasive waterjet, the experimental setup of studying the effect of the pressure on the temperature is shown in Figure 3.15. It consists of Autofrettage pump of 1000 MPa maximum pressure and 0.5 l/min flow rate, the CNC machine, the pressure gauge, abrasive waterjet cutting head, abrasive feeding system, workpiece holder and IR camera. The machining parameters are listed in Table 3.4.

Table 3.4: Machining parameters

Pressure	from 300 to 800 MPa
Pump	Böhler 1000 MPa , 0.5 liter/min
Pressure	from 300 to 800 MPa
Traverse rate	30 mm/min
Nozzle diameter	0.1 mm
Focus Diameter	0.4 mm
Abrasive	Barton garnet, 220-mesh
Abrasive flow rate	0.5 g/s
Workpiece material	AlMgSi0,5
Cutting length	40 mm
Cutting width	0.5 mm
Cutting depth (through cut)	10 mm

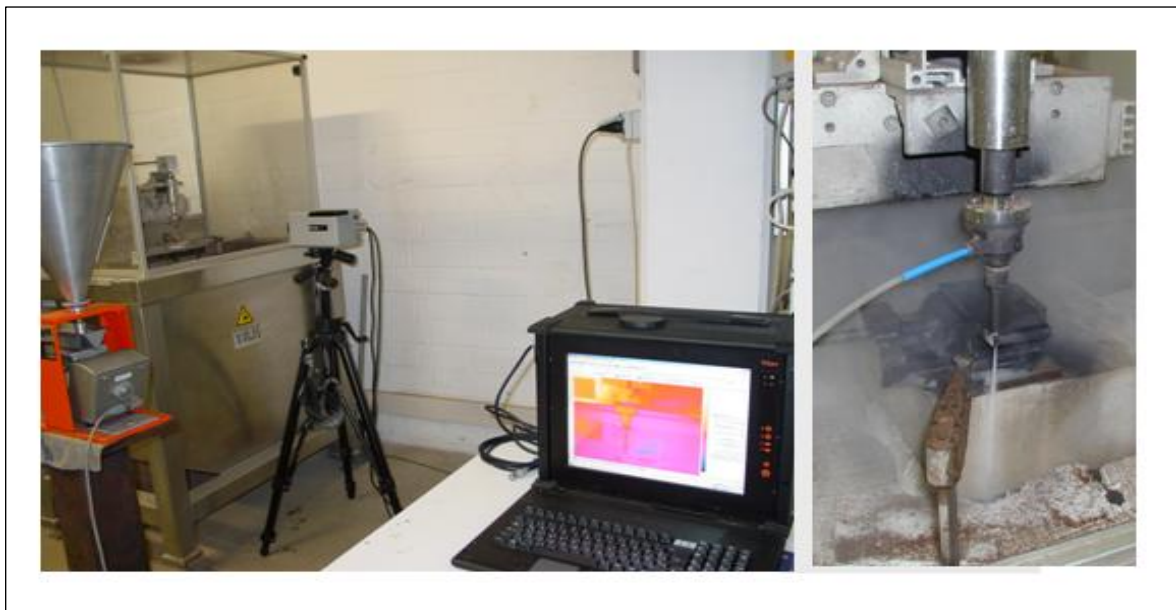


Fig. 3.15: Experimental setup for AWJ.

### 3.4 Surface and Wear Particle Examination

In this section the inspection of both the generated surface and wear particle produced by waterjet cutting are described.

#### 3.4.1 Surface examination

After cutting process the machined surface was examined by scanning electron microscope (SEM) to have specific information about the mechanism of wear, to

make detailed observation of the workpiece surface and to note the micro-structural changes that waterjet had made by its impact on the machined surface.

### 3. 4. 2 Wear particle examinations

A plastic tube (filled with water to prevent the wear of the tube wall caused by the waterjet), positioned under the workpiece, of 100 mm diameter was used to collect water containing wear particles removed from the wear track during cutting process, Figure 3.16. The collected water was filtered by a membrane of 3.0  $\mu\text{m}$  fineness. The deposited wear particles on the membrane were inspected by SEM.

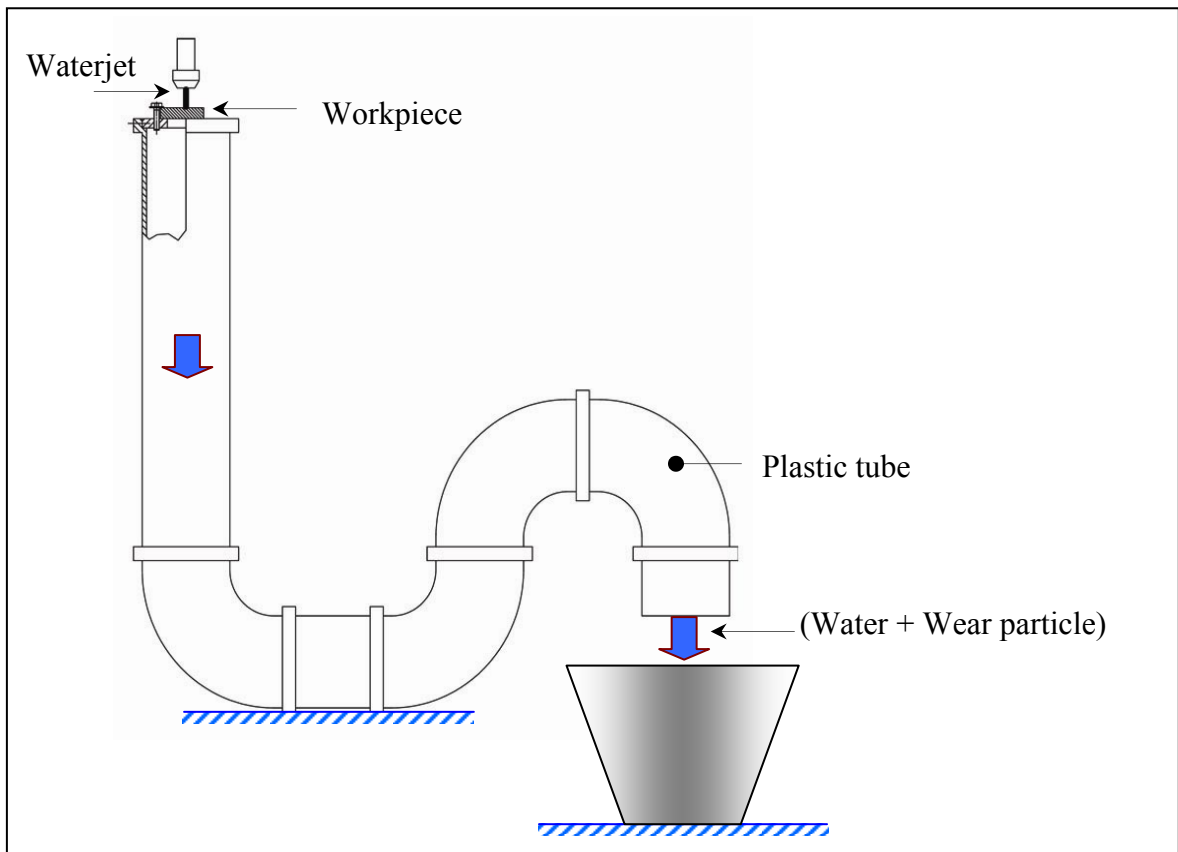


Fig. 3.16: Wear particle collected.

## 4. MATERIAL BEHAVIOUR

In the present chapter, the effect of loading art and the tested metallic materials types on the mechanism of material removal in the waterjet cutting is discussed through examining the topography of the generated of cutting surface and erosion wear debris.

### 4.1 Effect of Standoff Distance

A special workpiece holder was used to study the effect of the standoff distance on the cutting mechanism of the waterjet, Figure 4.1. This procedure was developed to qualify water nozzles in respect of their jet disintegration behaviour and the resulting damage at ductile materials (aluminium), [34]. The workpiece was assembled on an inclined position relative to the moving table allowing a variable standoff distance and controlled distance between the workpiece and nozzle.

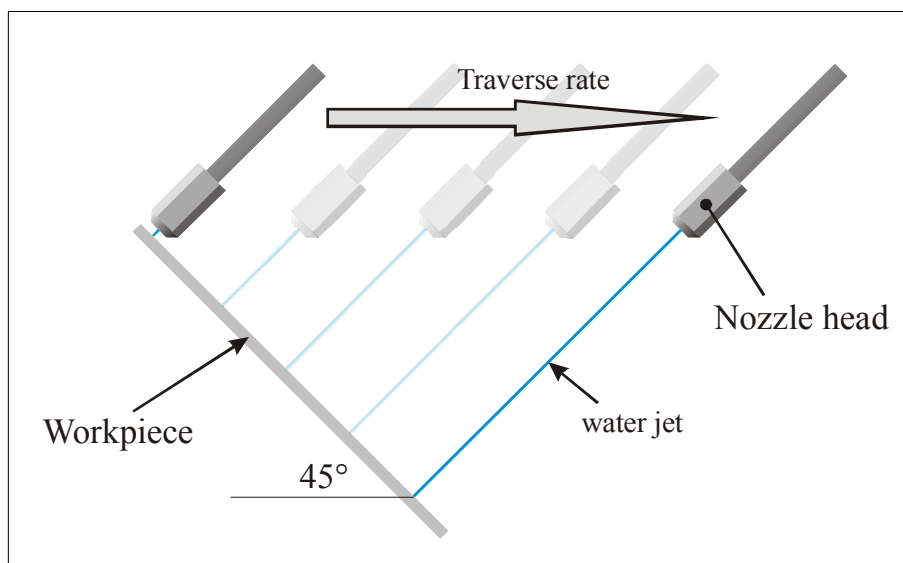


Fig. 4.1: Continuous standoff distance variation.

We notes that if we have the system as shown in Figure 4.1 to study the effect of the standoff distance, we should determine the effective traverse rate as shown in



Figure 4.2. Where the effective traverse rate equal to the traverse rate multiple by,  $\cos(\theta)$ , in our case,  $\theta$ , equal to  $45^\circ$ .

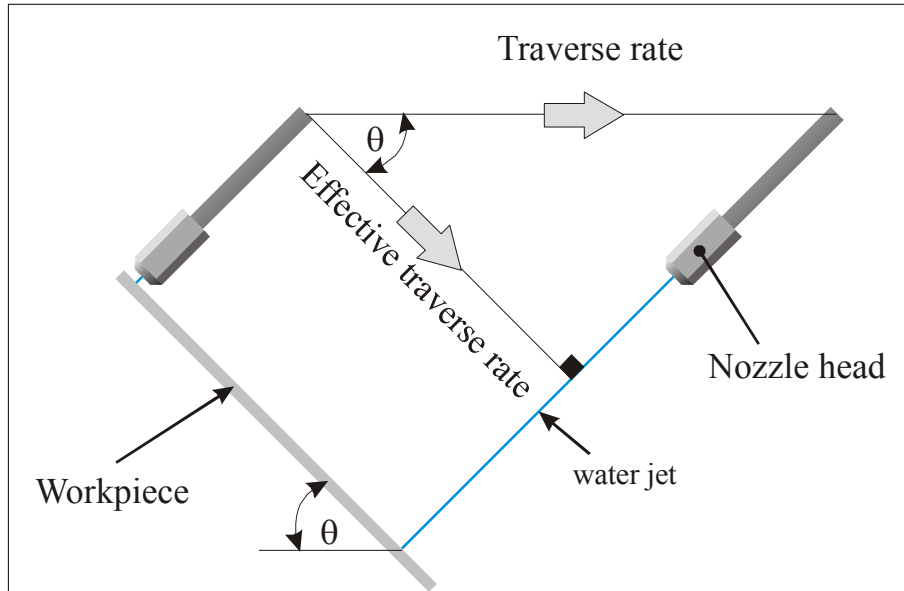


Fig. 4.2: Effective traverse rate for continuous standoff distance variation

Figure 4.3 shows the influence of standoff distance on the depth of cut in aluminium using 200 mm/min traverse rate, 0.3 mm nozzle diameter and 300 MPa pressure. It is clear from the Figure that the standoff distance represents a fairly effective cutting tool depending on the type of loading by waterjet. Interpolation of this Figure indicates that there is an optimum standoff distance, where the depth of cut is maximum value. This optimum is related to the properties of the material, pressure, nozzle type and size. The depth of cut was increased by increasing the standoff distance to a certain value due to the change of loading from mainly stagnation to impact pressure and was decreased by increasing the standoff distance due to the increased jet diversion and reduction of energy by friction with the surrounding medium (air) as discussion in chapter 2 section 2.4. The photomicrographs at different standoff distances for polished aluminium using a traverse rate of 300 mm/min, a nozzle diameter of 0.2 mm and a pressure 50 MPa is shown in Figure 4.4. At distances lower than  $100 d_n$ , scarcely plastic deformation near the grain boundaries is observed. At the distance  $100 d_n$ , deformation and

pitting of the surface as it is exposed to start the liquid impact is generated, where pitting is inhomogeneous and concentrated in areas near the grain boundaries than in the interior of the grain. As the standoff distance increased to  $200 d_n$ , the water trapped in the depressions, formed by pitting, began to cause tunnelling effect. The deformed surface, the raised rims and the irregularities produced by the formation of depressions will be subjected to severe shear forces from the outward flow of water across the surface. At standoff distance of  $350 d_n$ , the number of water drops in the waterjet increased, wear severity increased and consequently, a significant increase in the number of craters as well their sizes ( $20 \mu\text{m}$ ) was observed. The craters are looking like small pits with well-built-up platelets in and around it, plowing craters of deformed platelet ridges surrounding the circumference of the central depressions as a result the shear stress caused by tangential water flow. At distance of  $500 d_n$  the diameter of craters decreased (about  $10 \mu\text{m}$ ) and looking like the pitting observed at the beginning in the water impact, at standoff distance  $100 d_n$ , and concentrated near the grain boundaries too. At distance of above  $500 d_n$ , scarcely deformation of the grain boundaries.

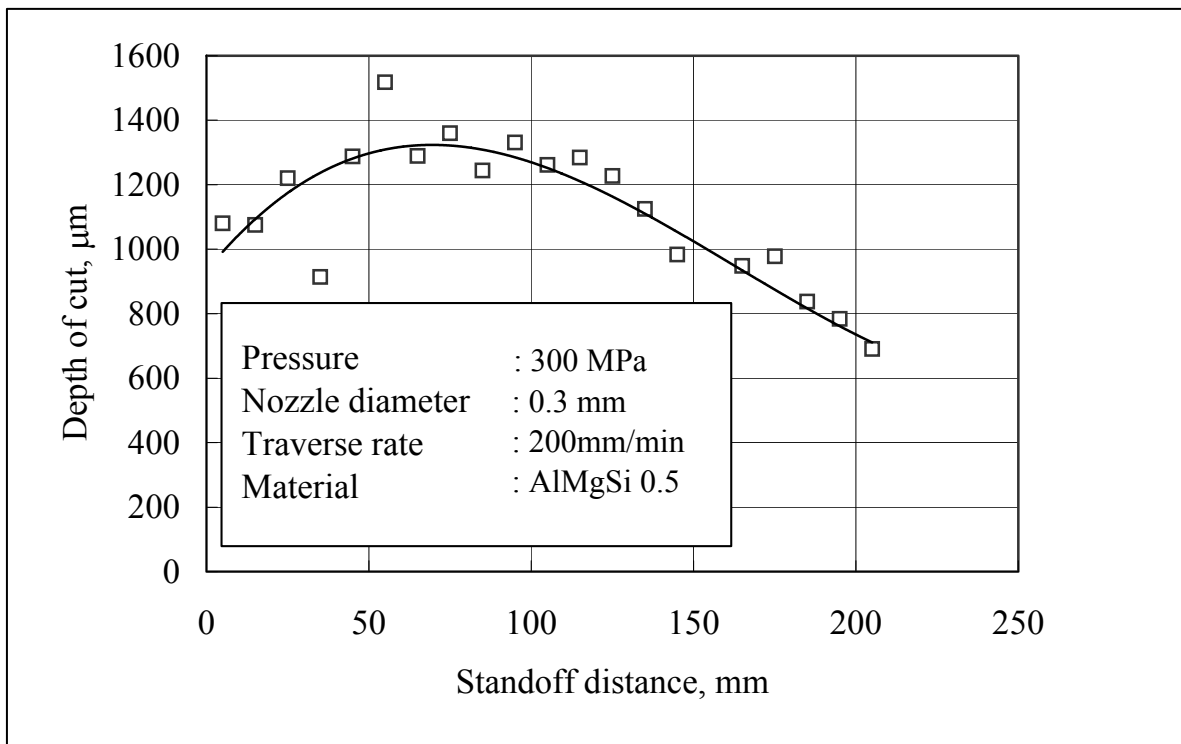


Fig. 4.3: Effect of the standoff distance on the depth of cut.

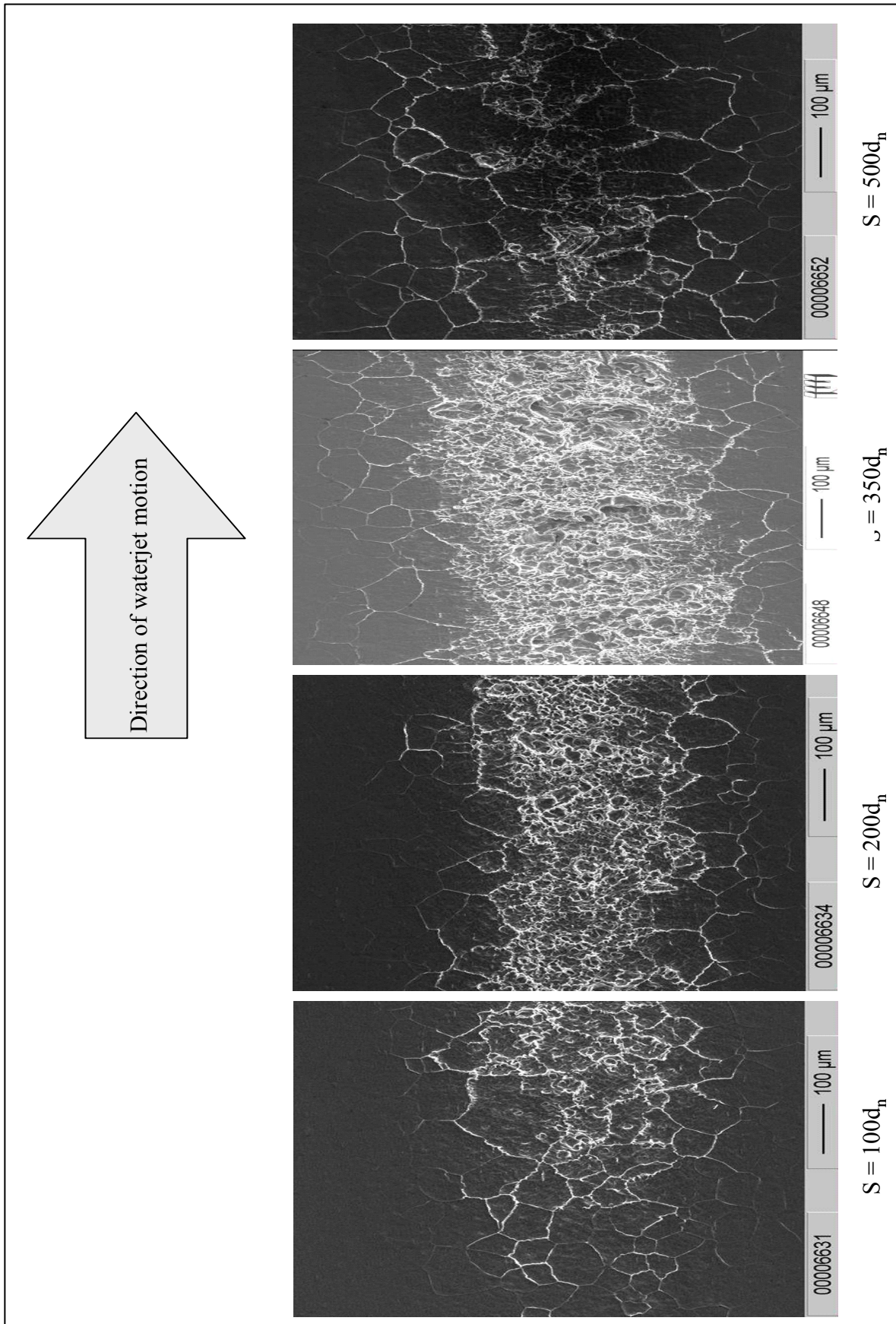
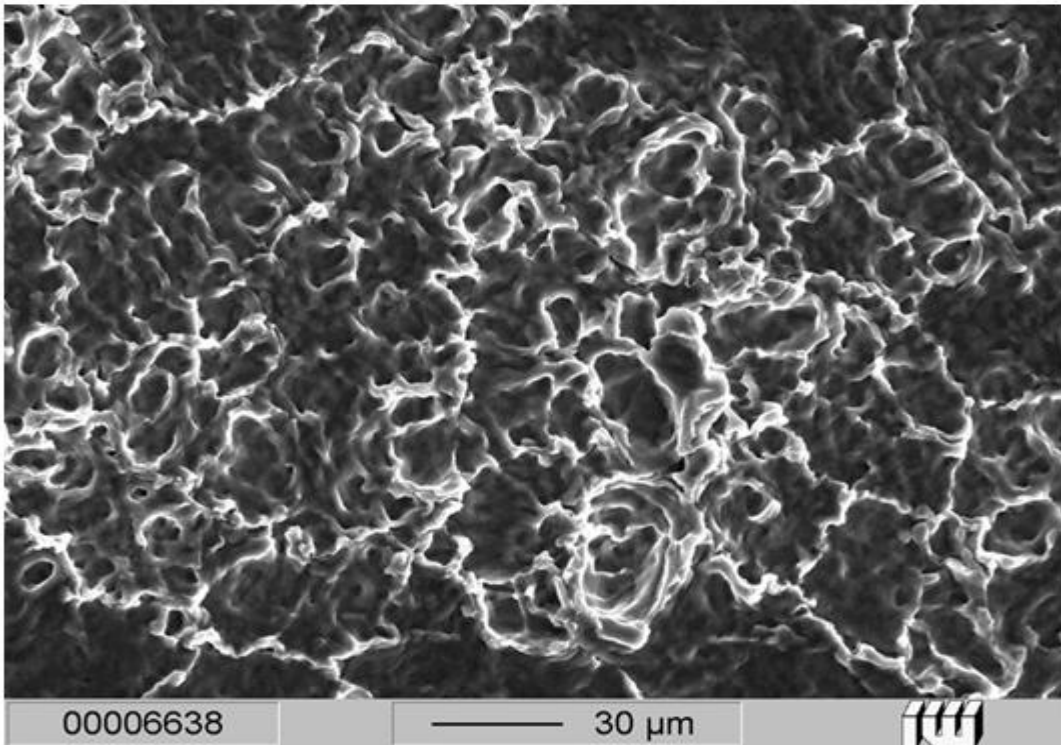
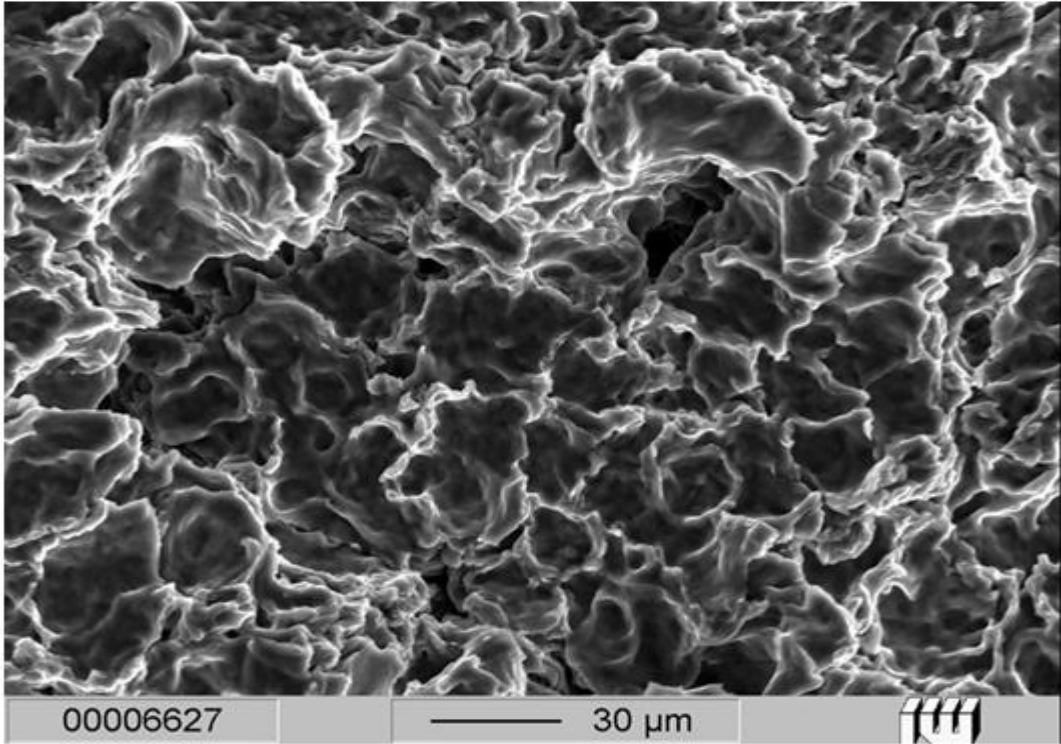


Fig. 4.4: The photomicrographs at different standoff distance.

## 4.2 Effect of Traverse rate (Loadings Time)

The effect of traverse rate (the loading time) on the material removed from the tested aluminium was investigated in the present work by changing the traverse rate (300, 500, 800 and 1000 mm/min). The photomicrographs of the wear tracks at a pressure of 50 MPa and a standoff distance of 50 mm, 70 mm and 100 mm, are shown in Figure 4.5-4.7. It can be seen (Figure 4.5) that at a traverse rate of 300 mm/min the degree of plastic deformation is relatively high where the details of the formed craters are clearly shown. The water droplets impact the stress free surface and form indentation craters looking like small pits of 15 – 20  $\mu\text{m}$ , plowing craters of deformed ridges surrounding the circumference of the central depression, which is a result of the shear stress caused by tangential water flow. As the traverse rate is increased to 500 mm/min, the plastic deformation of the deformed craters decreased and the diameter of the indentation craters decreased to be 10 – 15  $\mu\text{m}$ . The reduction of the diameter of the indentation craters may be attributed to the decrease of the loading time causing significant decrease in the craters formation. At 800 mm/min, the cavities vanished and the grain boundaries became delineated, where coarse slip bands developed across the width of the grains and the grains became increasingly undulated. At 1000 mm/min, only grain boundaries were observed without cavities. The same trend was observed, Figure 4.6, accompanied by a lower degree of plastic deformation at standoff distance 70 mm. The depressions of the surface in form of small pits are shown in Figure 4.7, indicating that the water jet was not able to penetrate the surface and the craters began to disappear with further decrease of the grain formation at standoff distance of 100 mm. At 1000 mm/min traverse rate, surface depressions began to vanish.



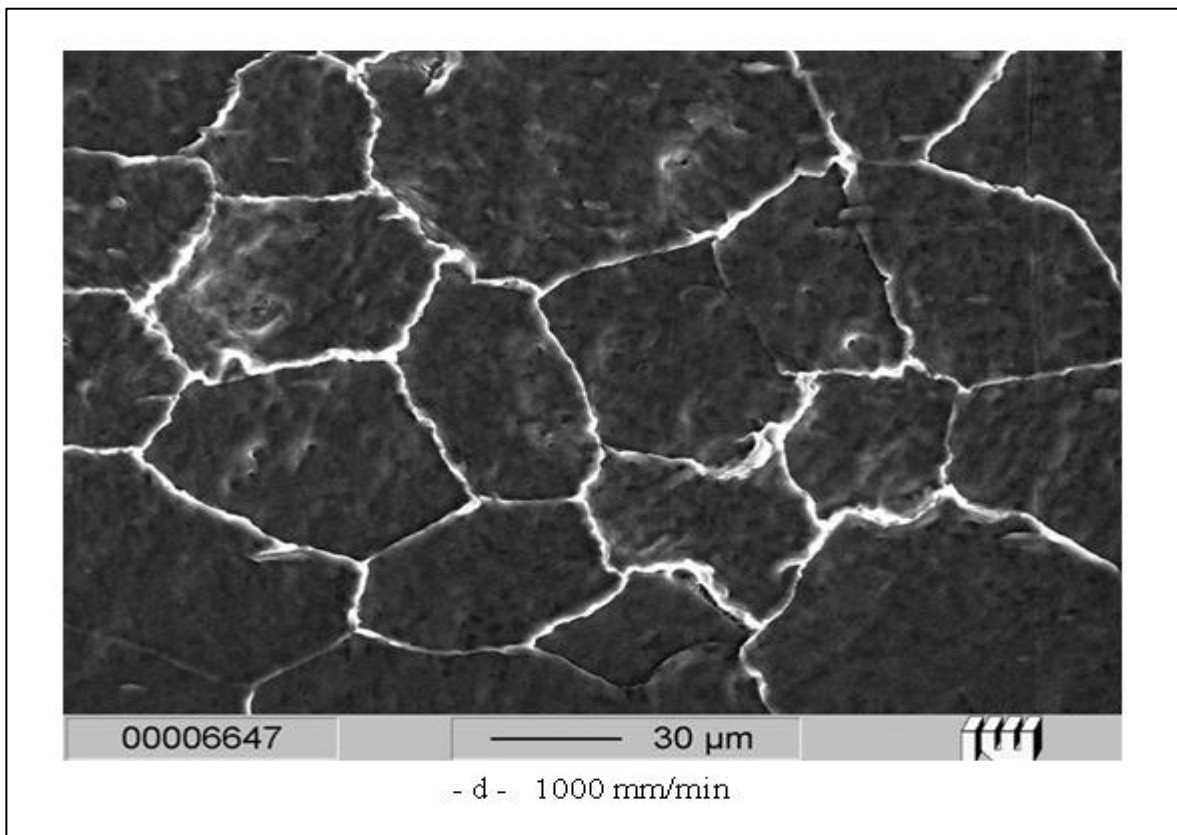
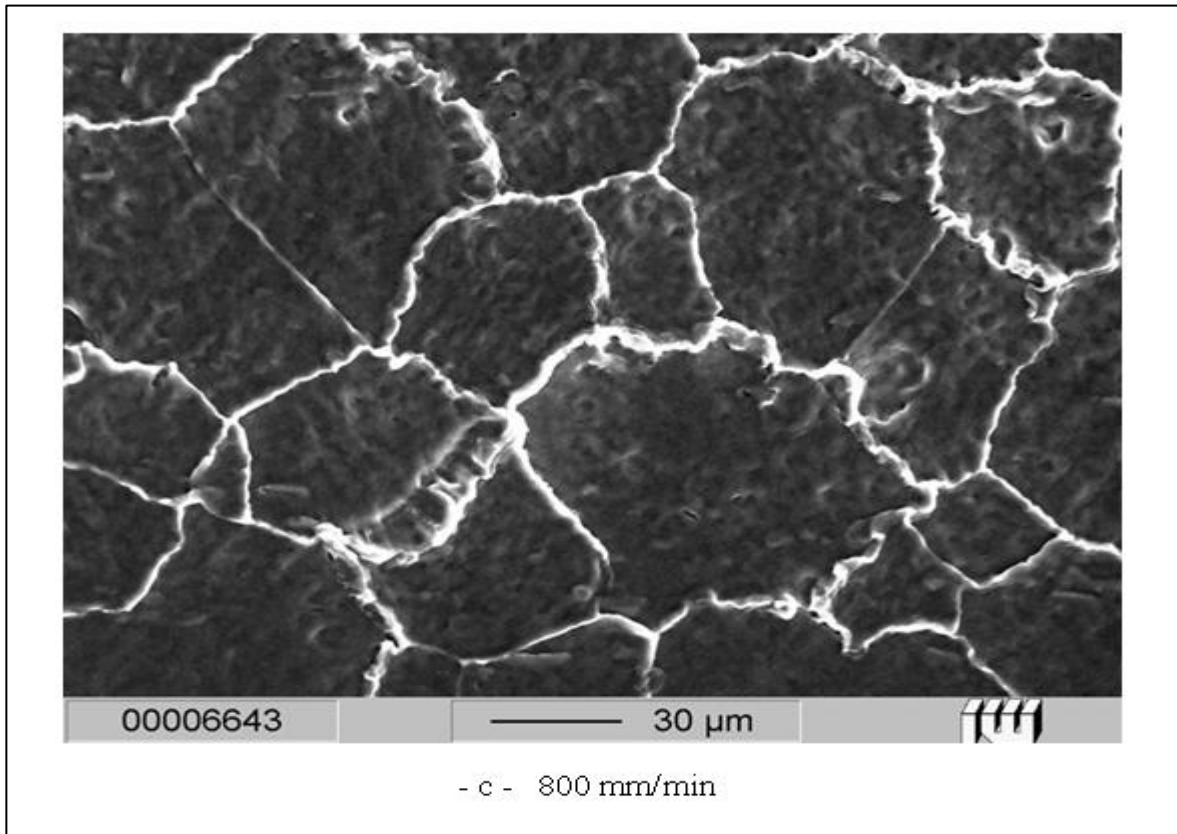
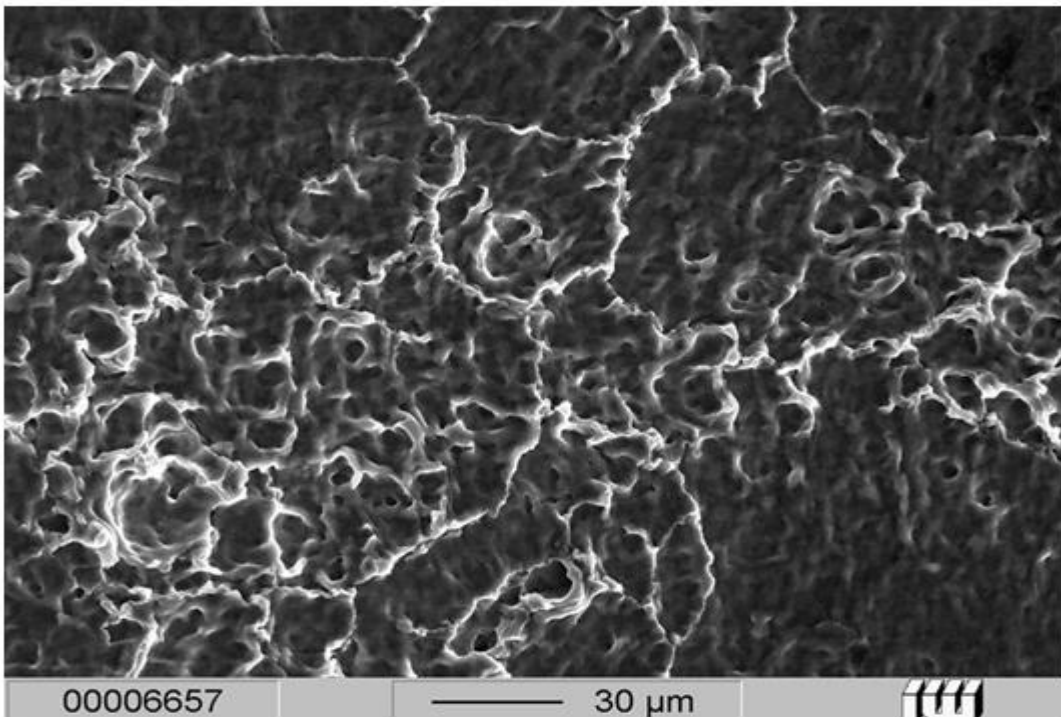
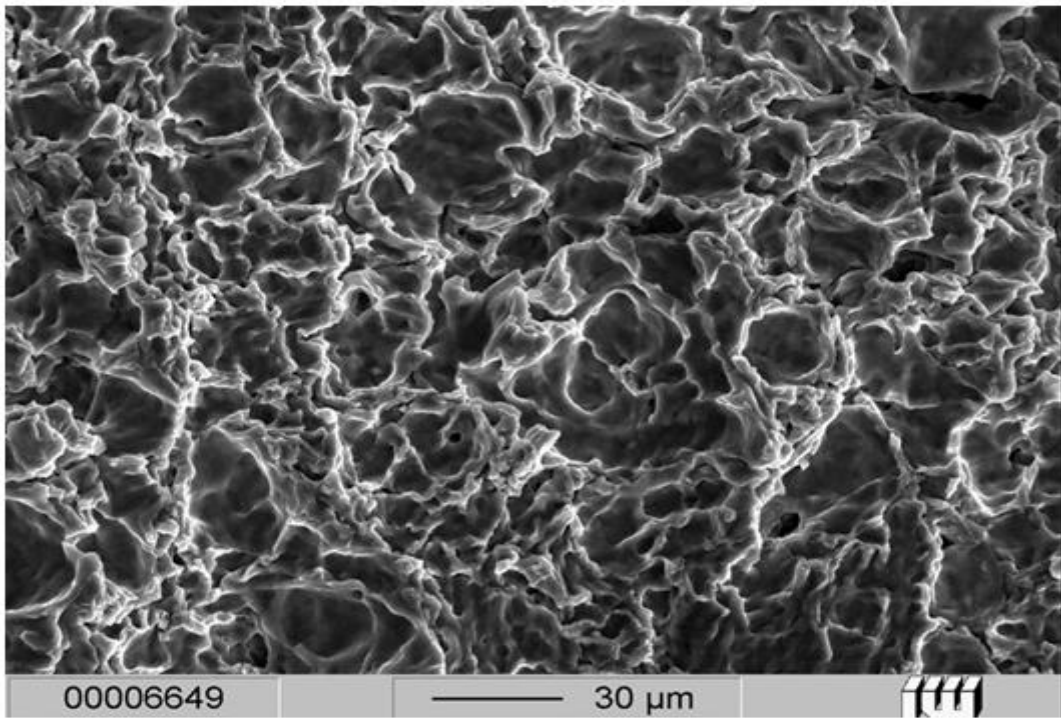


Fig. 4.5 (a, b, c and d): The effect of traverse rate (the loading time) on aluminium at standoff distance 50 mm.



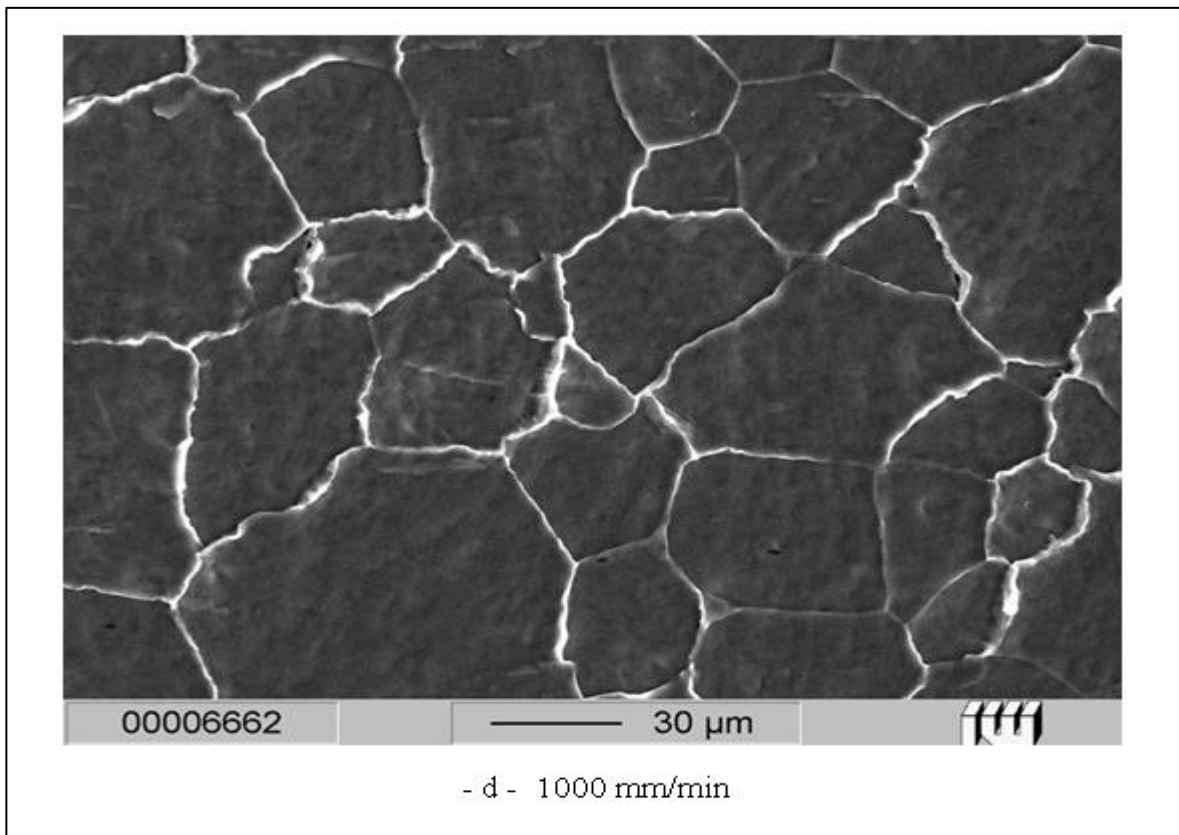
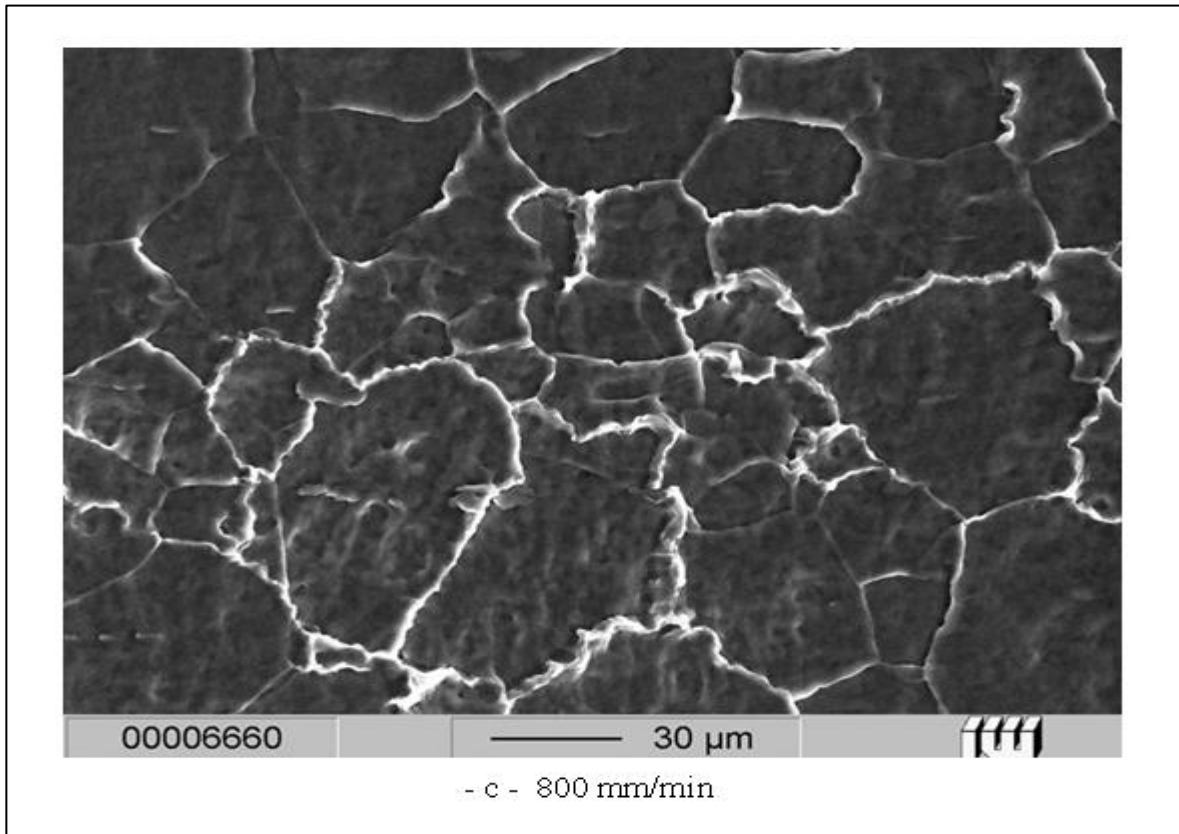
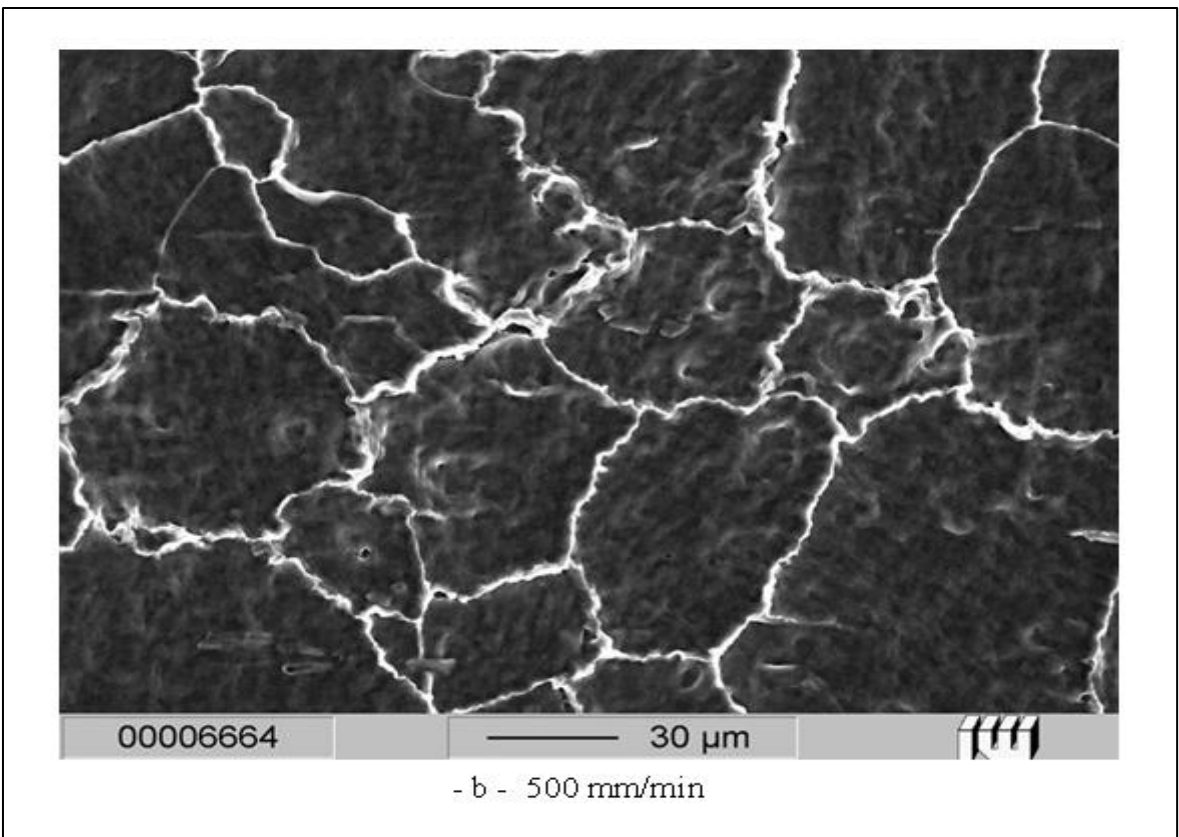
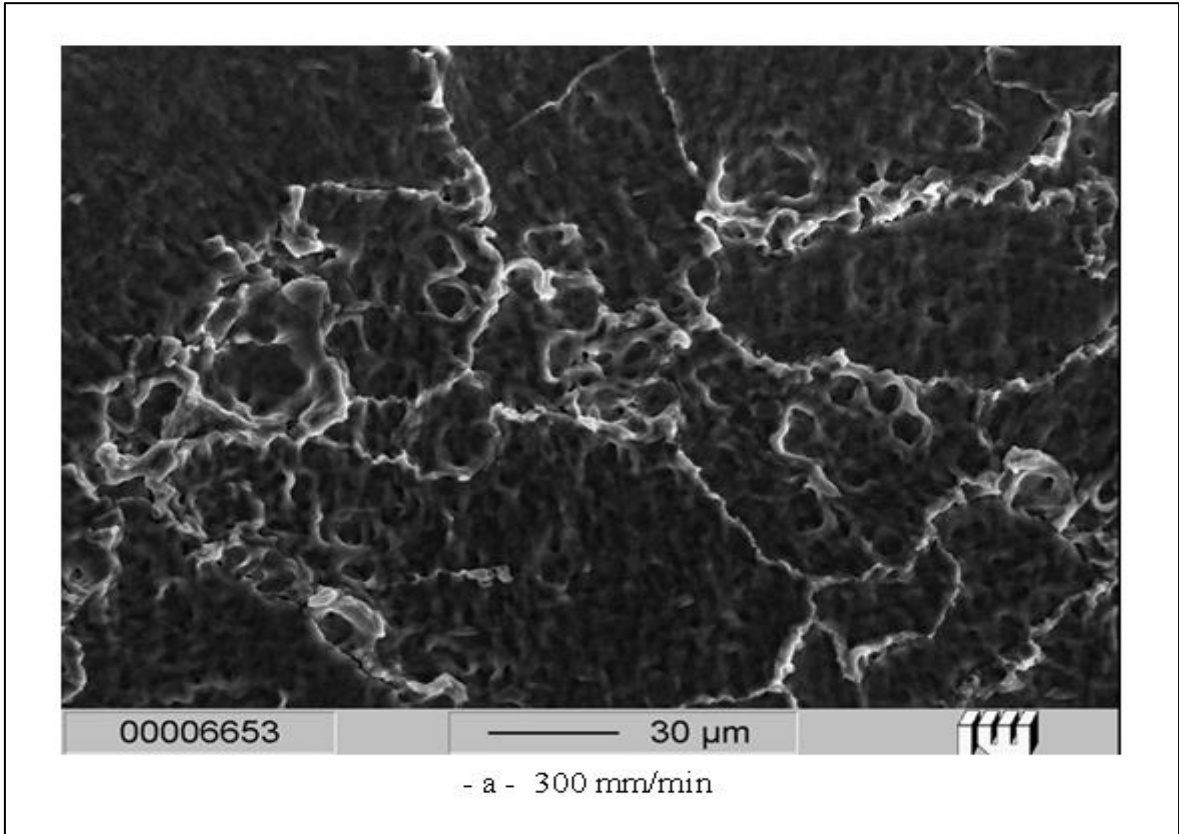


Fig. 4.5 (a, b, c and d): The effect of traverse rate (the loading time) on aluminium at standoff distance 70 mm.





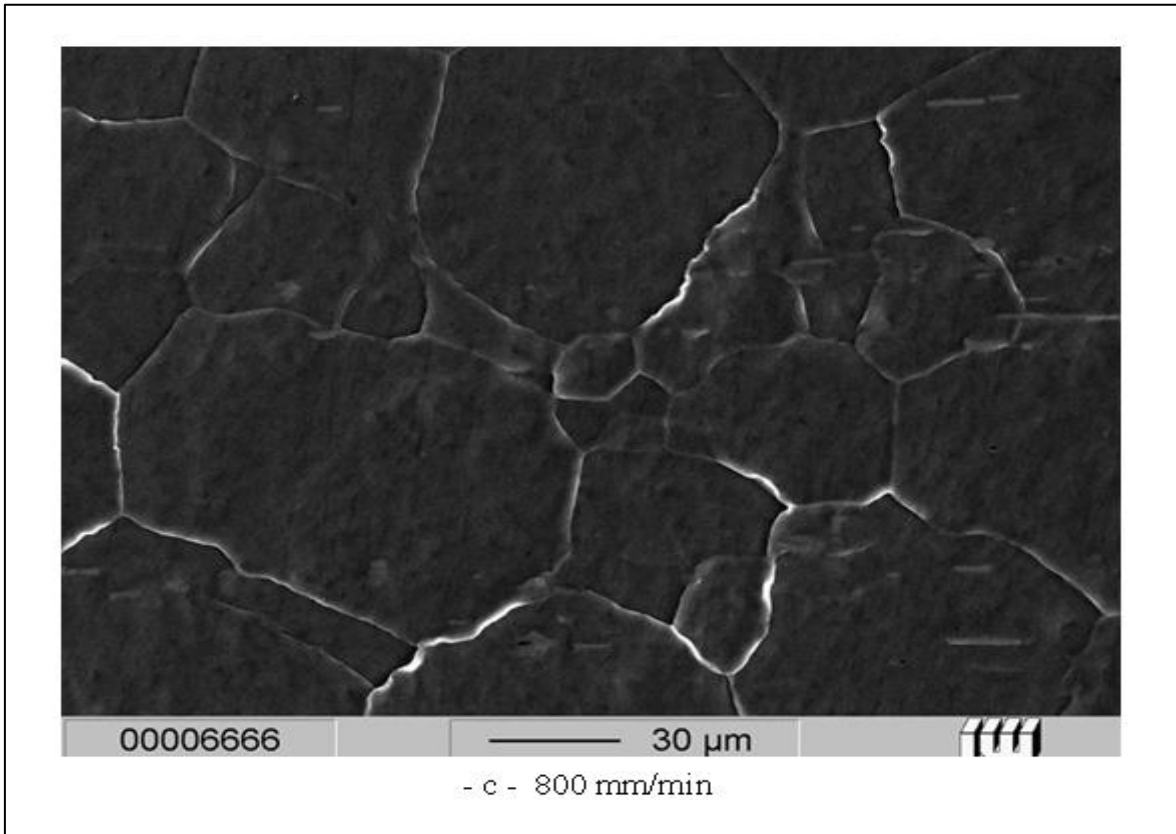


Fig. 4.7 (a, b and c): The effect of the loading time on aluminium at standoff distance 100 mm.

### 4.3 Effect of loading Pressure

The effect of the pressure on the material removed from the tested aluminium was investigated in the present work by changing the pressure (200, 400, 600 and 800 MPa). The photomicrographs of the wear tracks at a traverse rate 100 mm/min, a standoff distance  $300d_n$  and nozzle diameter 0.1 mm is shown in Figure 4.8. It is clear that with increasing the working pressure increasing the wear depth crack and the lateral ridge of the wear track, while the width of the lateral ridge shown in shiny colour can be measured in a direction perpendicular to the wear direction. For example the width of the lateral ridge increased from 140  $\mu\text{m}$  at 400 MPa pressure to 240  $\mu\text{m}$  at 800 MPa pressure. But increasing the working pressure has no significant effect to the surface topography.

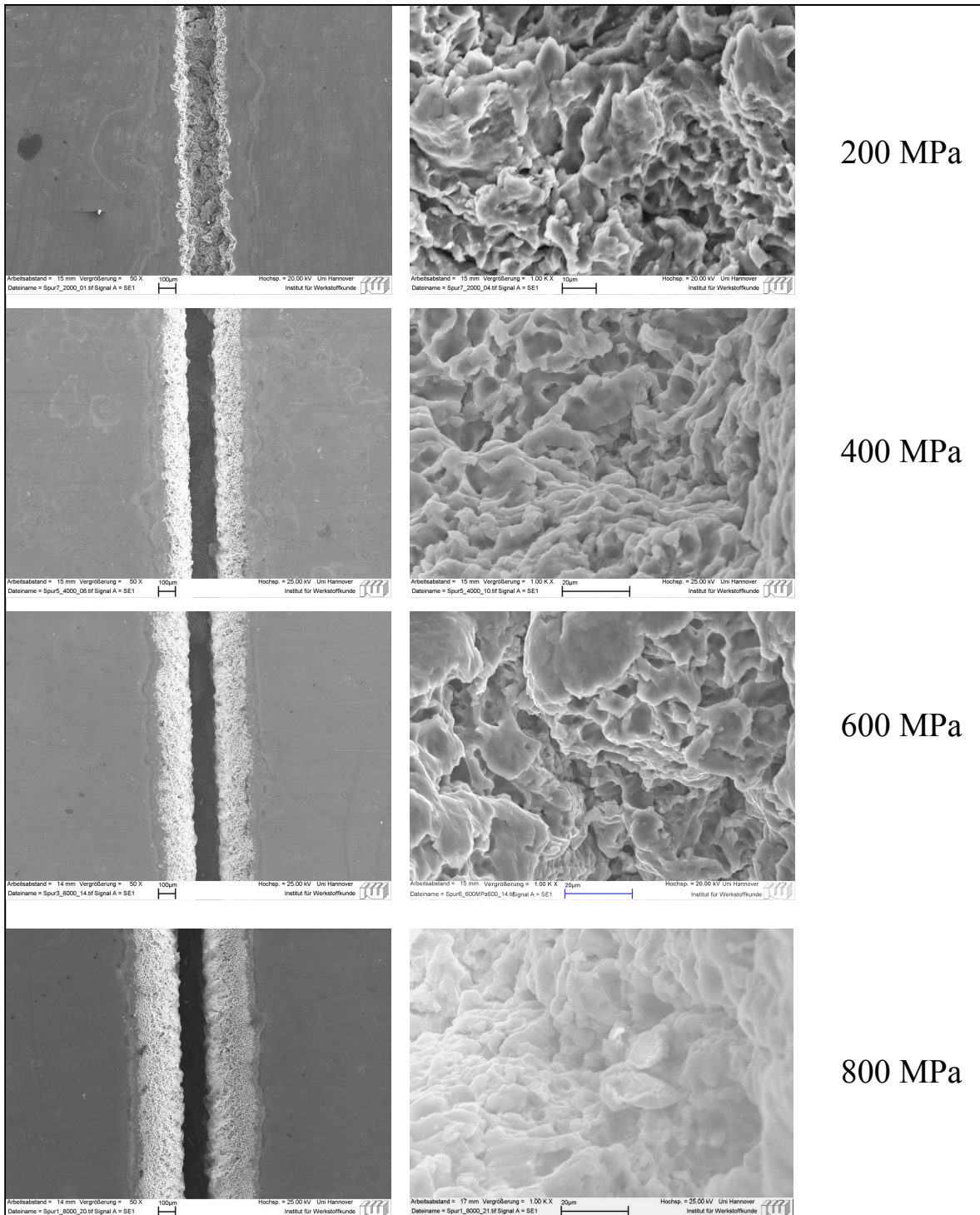


Fig. 4.8: The photomicrographs at different working pressure.

#### 4.4 Effect of Nozzle Diameter

The effect of the nozzle diameter on the material removed from the tested aluminium was investigated in the present work by changing the nozzle diameter (0.1, 0.125, 2 and 3 mm). The photomicrographs of the wear tracks at a traverse rate

100 mm/min, a standoff distance  $300d_n$  and pressure 150 MPa is shown in Figure 4.9. It is clear that with increasing the nozzle diameter the width of wear track increased but increasing the nozzle diameter had no significant effect to the surface topography. At nozzle diameter of 0.3 mm, the width of wear track represented relatively high value indicating the improper performance of the nozzle.

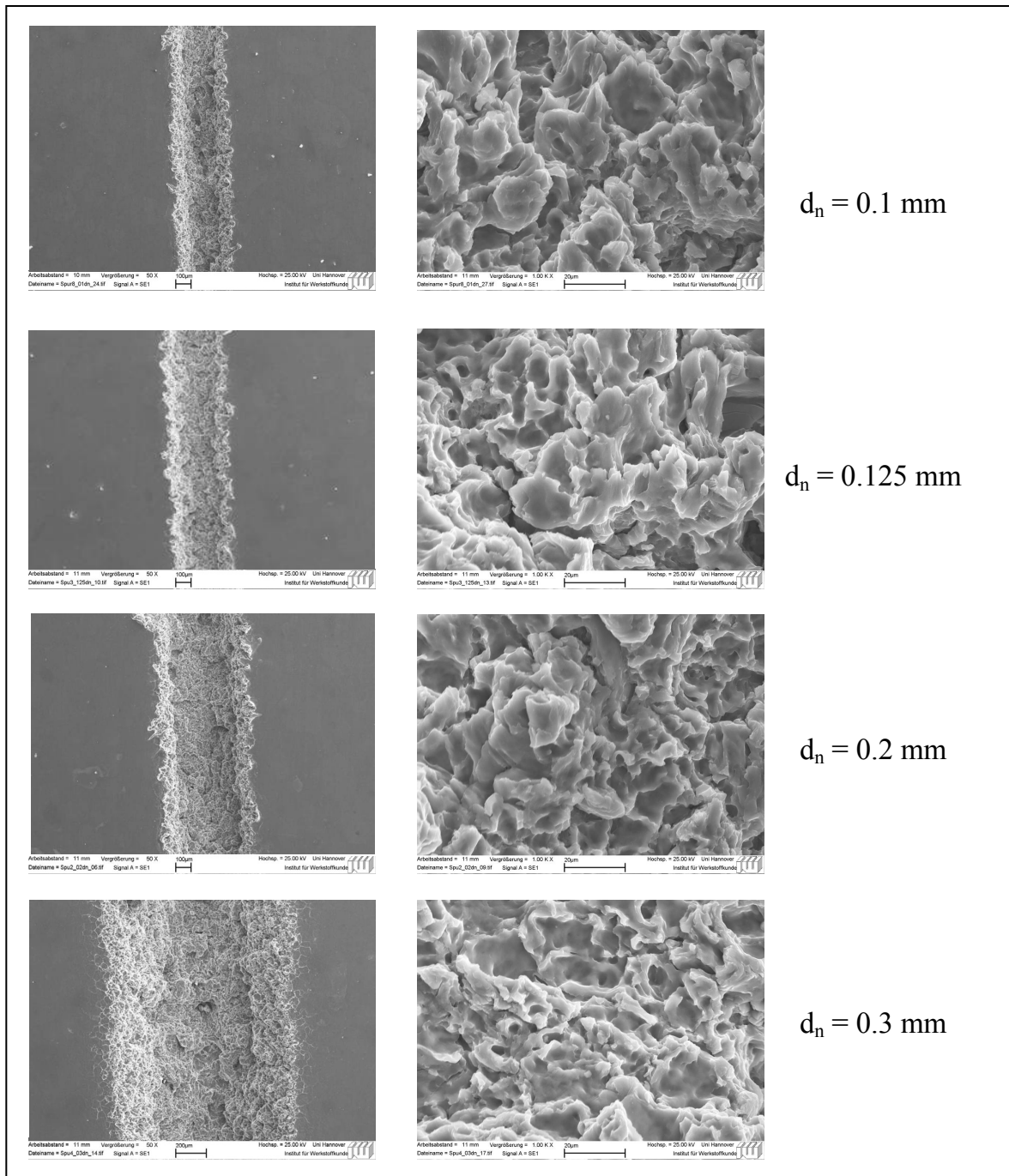


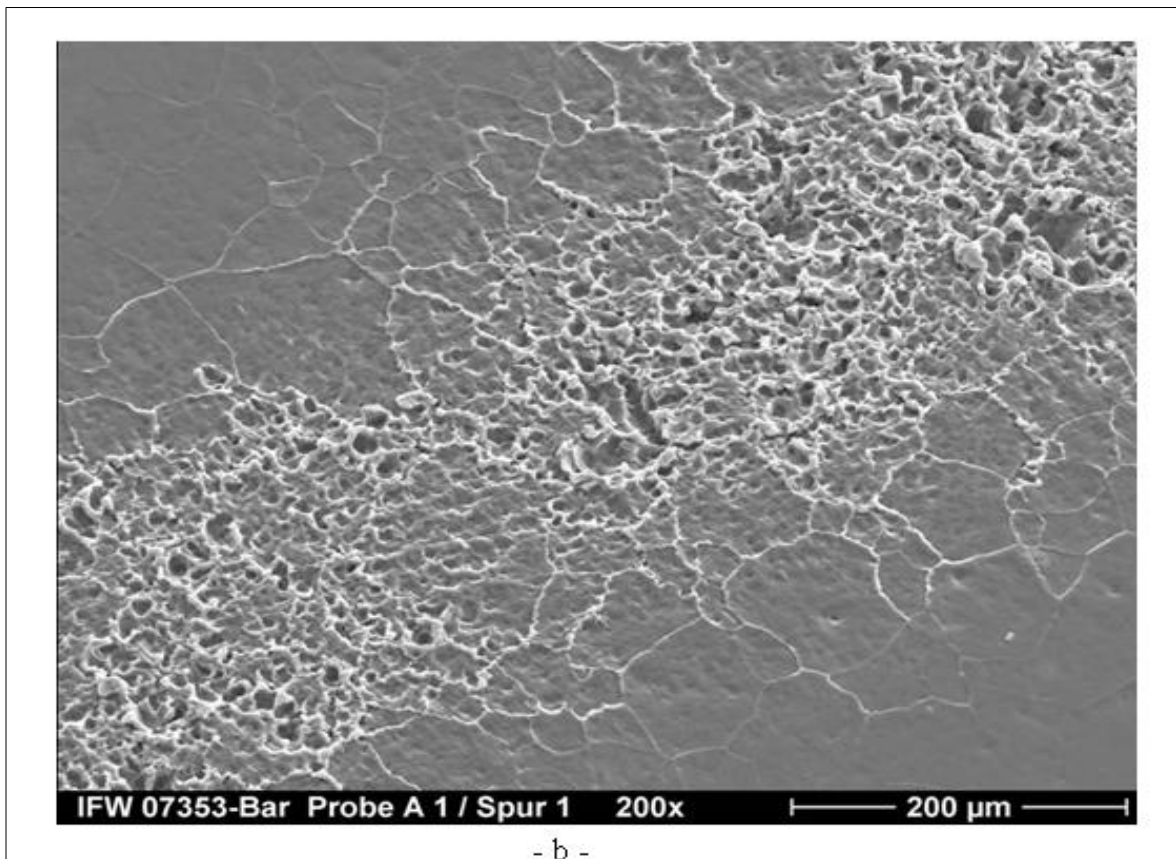
Fig. 4.9: The photomicrographs at different nozzle diameter.

## 4.5 Effect of Types of Materials

The inspection of the worn surface can reveal the mechanism of the action of waterjet. So in this section we investigate both the behaviour of the metal surface and the wear debris generations by the waterjet impact.

### 4.5.1 Behaviour of Aluminium

The wear track caused by the waterjet for aluminium using (a pressure of 100 MPa, traverse rate of 40 mm/min, a standoff distance  $300d_n$  and nozzle diameter 0.2 mm) is shown in Figure 4.10 (a, b, c and d). Where Figure 4.10 (a), (b) shows the wear track, Figure 4.10 (c) shows the lateral ridge of the wear track and Figure 4.10 (d) shows the centre of the wear track. In Figure 4.10(a), the width of wear track reached 350  $\mu\text{m}$ . In Figure 4.10 (b), it can be seen that the severity of wear is maximum in the centre of the wear track and decreases towards the sides. The distortion occurred in the surface depends on the diameter of the water drops, not on the grain size of the worn surface, Figure 4.10(c). Plastic deformation is clearly shown on the worn surface. The erosive action of water drops is clearly shown forming a lot of holes and cavities. The diameter of the holes and cavities is relatively fine (ranging from 5 to 10  $\mu\text{m}$ ). The direction of the striking of the water drops is varying due to the irregularity of the severely deformed surface. The material deformed around the holes shows relatively higher magnitude due to the ductility of the material tested. The deformation of the grains shows significant irregularities due to the behaviour of the metals



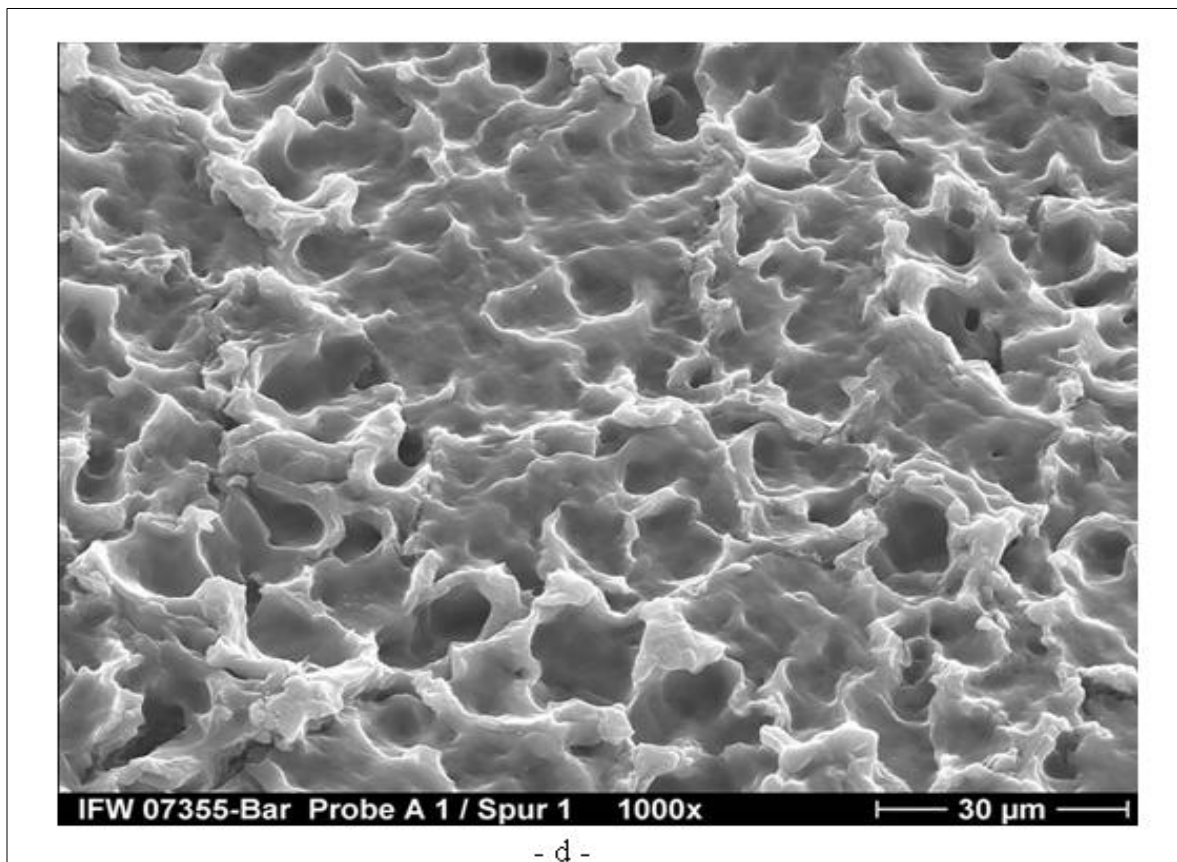
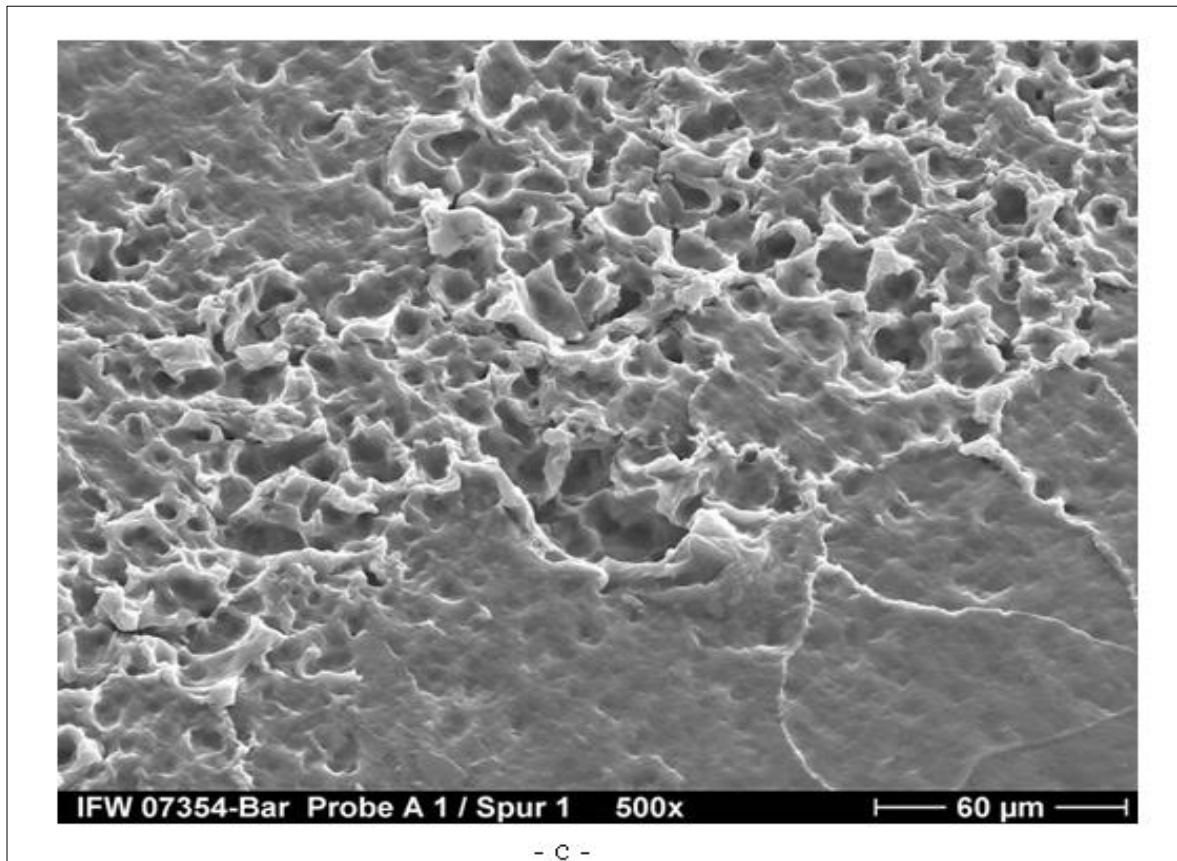


Fig. 4.10 (a, b, c and d): Wear track caused by waterjet for aluminium.

The wear particles removed during erosion process are shown in Figure 4.11. The mechanism of the formation of wear particles can be summarized as the water drops impact the surface and cause three types of craters; indentation, ploughing and smear ones.

The waterjet impact causes microscopic roughening of the surface because of the plastic deformation experienced by the large localized stresses in the immediate areas of the waterjet impacts. In the process of forming craters, platelets of aluminium that are locally attached to the crater rim are forged-extruded. As the water drops impact craters and their attendant platelets, a gradual increase in frequency of smear-type craters with platelet formation starts and measurable erosion begins. The appearance of the wear particles confirms the mechanism mentioned above. All wear particles are formed from the platelets deformed around the craters then subjected to the repetitive impacts of water drops.

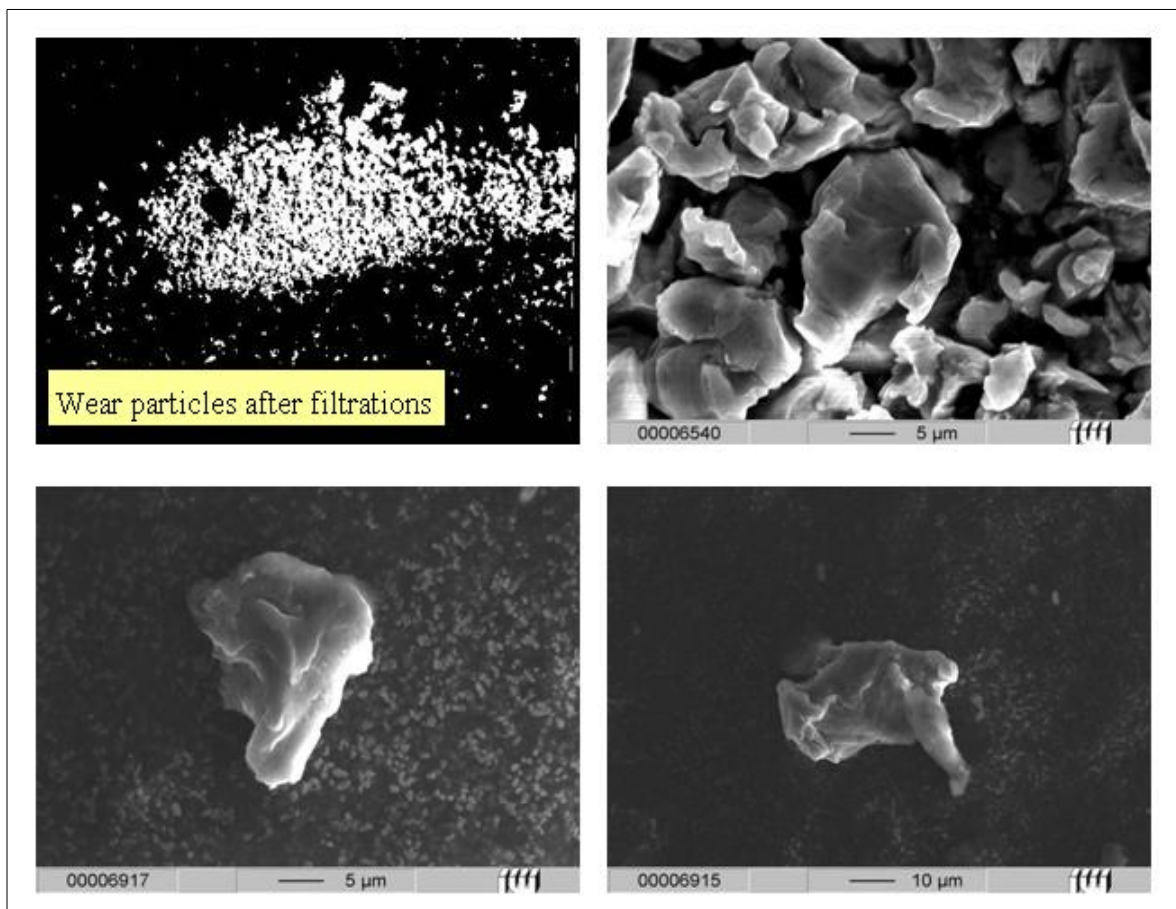


Fig. 4.11: Wear particle of aluminium.



#### 4.5.2 Behaviour of Armco-Iron

The wear track of steel test specimens is illustrated in Figure 4.12, at 300d<sub>n</sub> standoff distance 40 mm/min traverse rate and 150 MPa pressure to study the changes in surface morphology and to gain additional insight into the erosion process. The water drops impact the tested iron surface and form indentation, plowing and smear craters. Erosion occurred by ductile removal of the material constituting smearing craters that raised sharp ridge lines. It should be noted that some indentation occurred, as evidenced by the impressed surface flaws, but that the smearing mode is dominant. The sharp ridge lines and the different contour profile of smearing craters were not observed in aluminium test specimens thus due to the fact that the steel is less ductility. Wear particles collected during the erosion of steel test specimens were inspected by scanning electron microscope fitted by an energy-dispersive X-ray emission spectrum (SEM EDS) analysis, Figure 4.13. The energy-dispersive X-ray emission spectrum (SEM EDS) analysis was used to check the kind and source of the material of the wear particles.

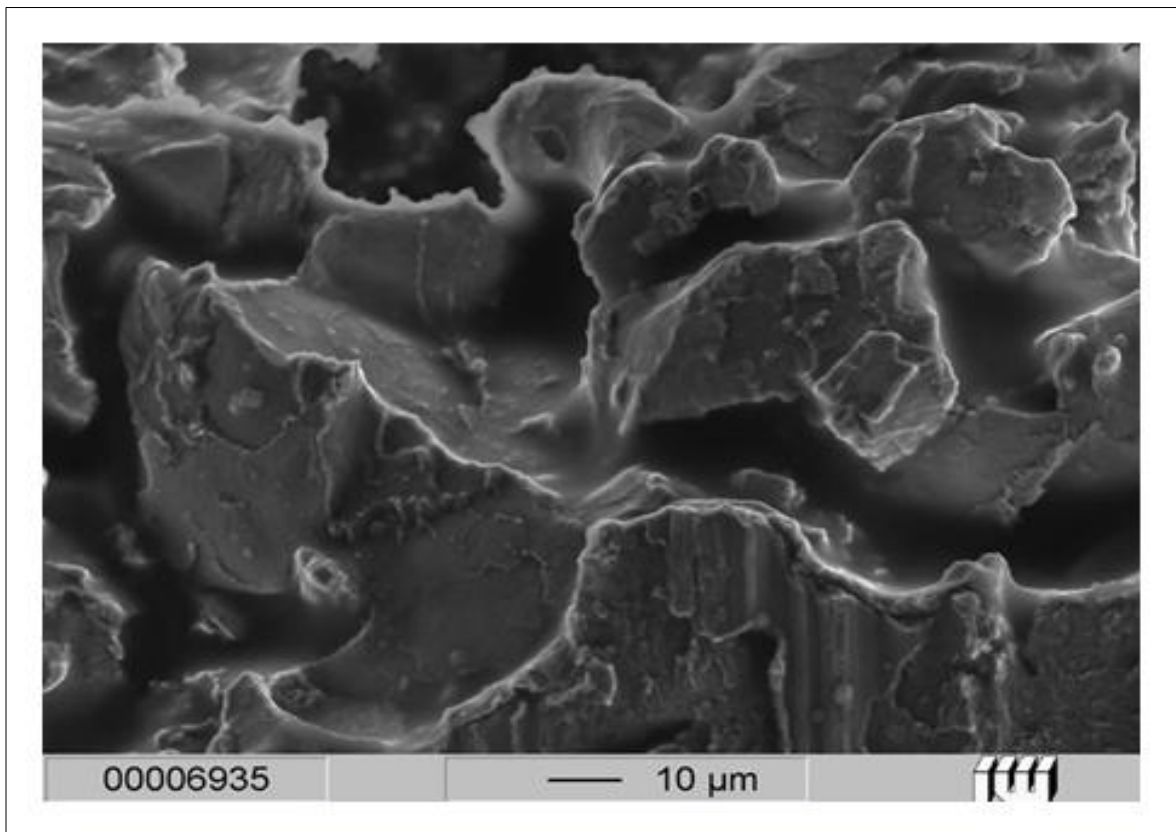


Fig. 4.12: Wear track caused by waterjet for Armco-iron.

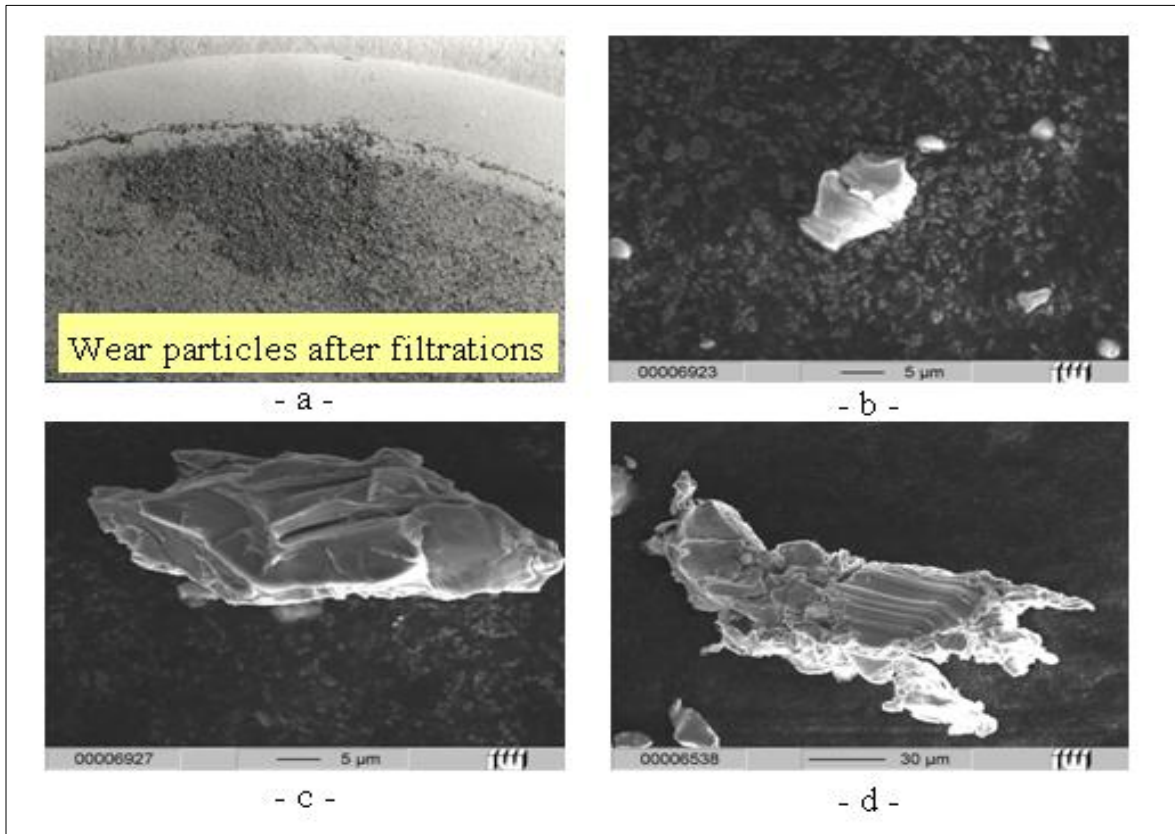


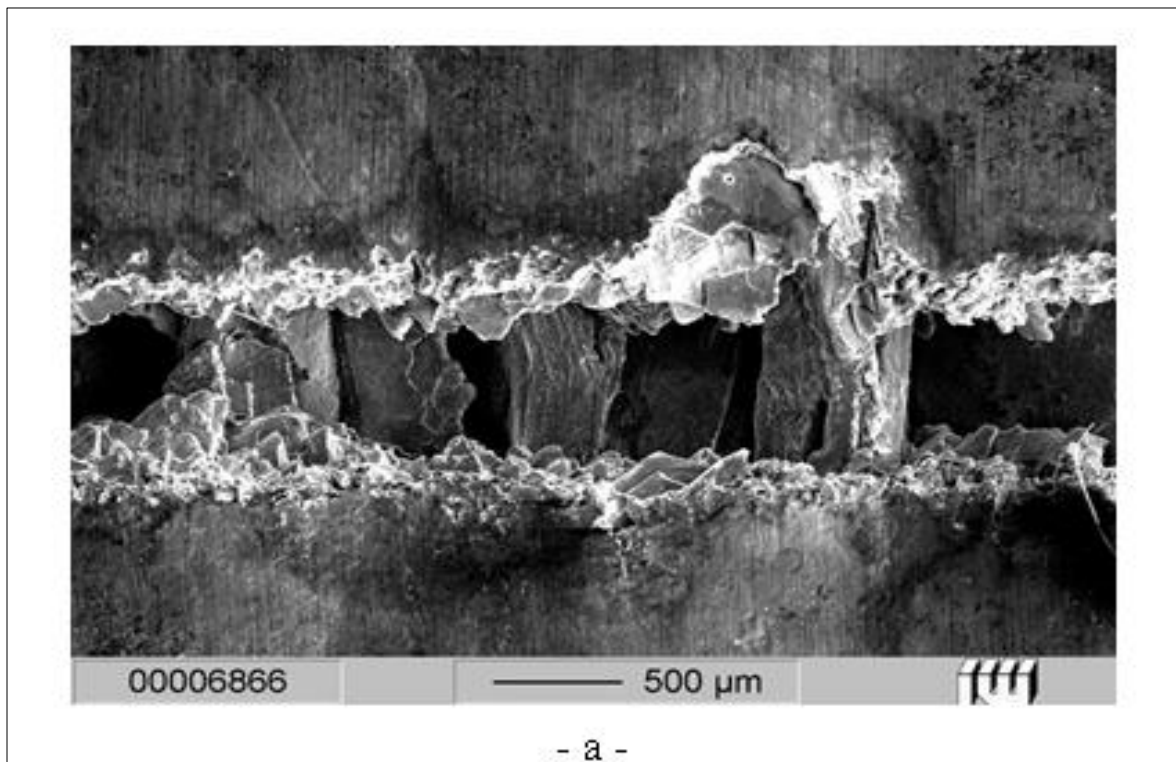
Fig. 4.13: Wear particle of Armco-iron.

Figure 4.13 (b) shows steel wear particle of  $20\ \mu\text{m}$  size. This particle may be formed from the removal of the plowing crater and suffered from excessive impacts of the water drops. A wear particle of  $50\ \mu\text{m}$  length and  $20\ \mu\text{m}$  width is shown in Figure 4.13 (c). This particle was formed from few plowing as well as smearing craters and contains two smearing craters of sharp edges. The both sides of the ridge show the start of small platelet formation. A relatively big particle of  $150\ \mu\text{m}$  long is shown in Figure 4.13 (d). This particle consists of the deformed craters. The middle part is of interest due to the presence of the slip bands of regular-spaced ripples with hills and valleys. The wavelength between ripples varies between  $4$  and  $7\ \mu\text{m}$ . The slip bands generally occur along the walls of already formed craters where a fresh crater has been formed immediately adjacent to them. The waterjet impact forces act on the unsupported surface of the already existing crater, resulting in slip band formation, [91-92]. The outflow of waterjet is considered to

be responsible for the initiation of small ripples away from the pit, which is probably associated with shear. As the exposure time increases the pits deepen and cause outflowing water to go away from the surface in a tangential direction.

#### 4.5.3 Behaviour of Zinc

Wear groove caused by the erosion of zinc test specimens by waterjet 100 MPa pressure, a traverse rate of 40 mm/min, standoff distance  $300d_n$  and a nozzle diameter of 0.2 mm is shown in Figure 4.14. Zinc exhibits crack initiation and growth rather than simply ductile shearing of small particles where deformation and crack growth can be facilitated. The initial depressions grow and do not develop into craters, but the material is lost by removal of the big parts of the grains by transcrystalline fracture. The edge of the wear groove is corrugated indicating brittle failure of zinc. Wear particles were removed from the surface in form of platelets, Figure 4.14 (b). Material deformed on the sides of wear groove showed platelet forms indicating that severe shear stress caused by outgoing water flow removed the platelets parallel to their slip planes.



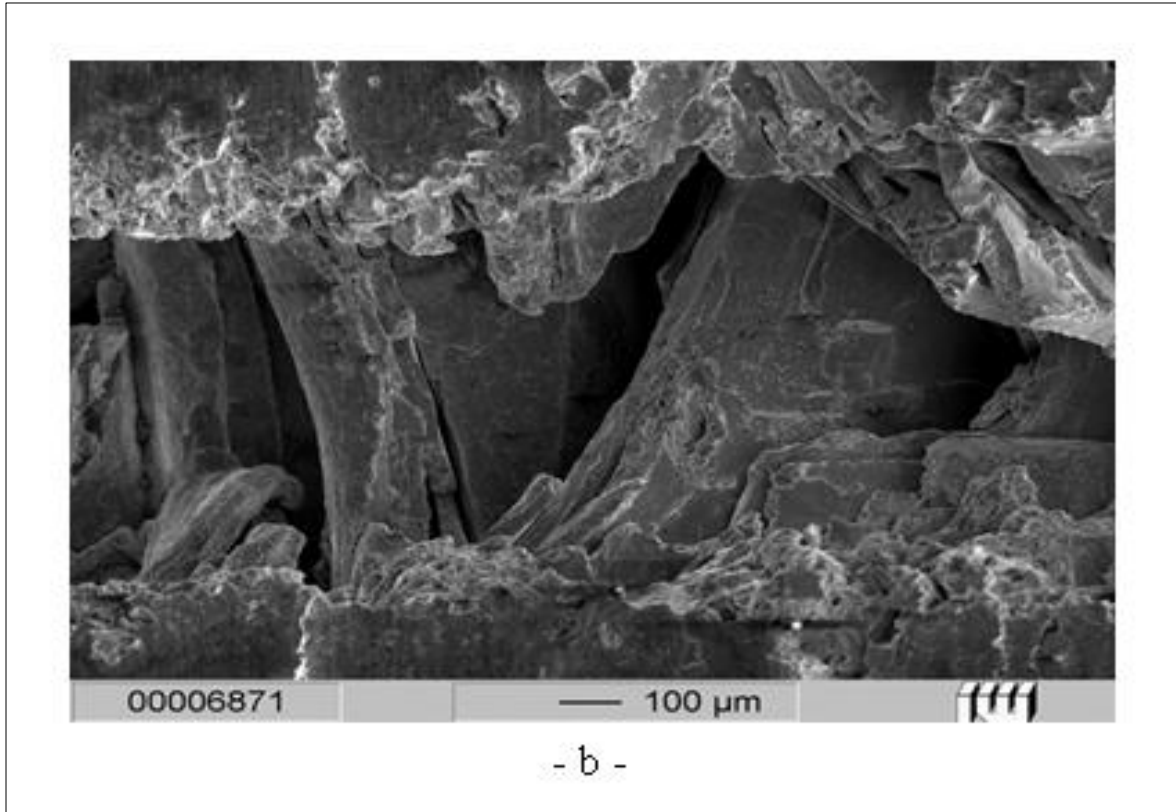


Fig. 4.14 (a and b): Wear track caused by waterjet for zinc.

Wear particles removed from the zinc surface are shown in Figure 4.15. A relatively big wear particle of 500  $\mu\text{m}$  size is shown, Figure 4.15 (a), where the edges are approximately straight and have a shiny appearance. This particle was removed under the action of severe shear indicated by surface striations showing the direction of shear. Figure 4.15 (b) shows relatively big particle of 160  $\mu\text{m}$  length and 60  $\mu\text{m}$  width. Bent wear particles of about 300  $\mu\text{m}$  size is shown in Figure 4.15 (c). This particle may be removed from the material deformed on the sides of the wear groove. Very big wear particle is shown in Figure 4.15 (c) of 800  $\mu\text{m}$  length, 500  $\mu\text{m}$  width and 40  $\mu\text{m}$  thickness. Few cracks are shown on the surface of the wear particles indicating the action of the fatigue stress.

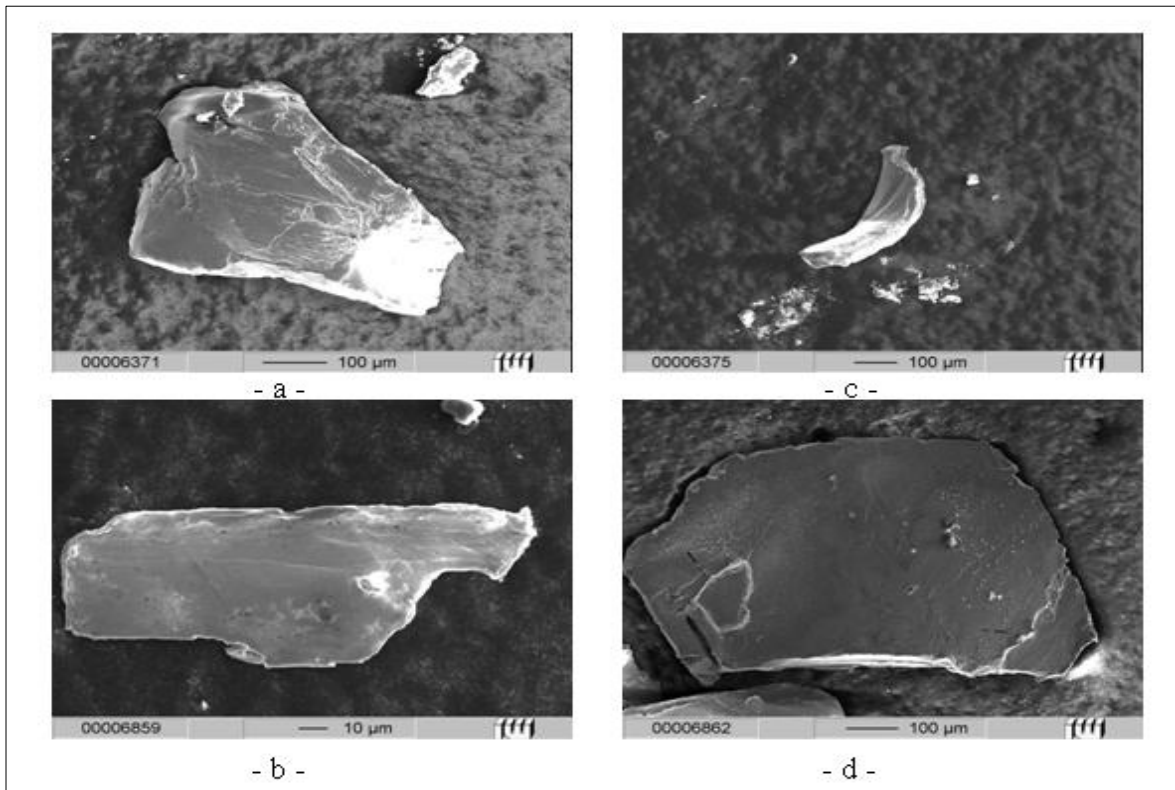


Fig. 4.15: Wear particle of zinc.

## 4.6 Surface Inspection and Cutting Mechanisms

In this section the inspection of the surface generated by waterjet and abrasive waterjet as well as the cutting wear mechanisms are described.

### 4.6.1 Surface inspection

The generated cutting surface of aluminium (Al 99.5) by waterjet under working conditions 0.5 mm nozzle diameter, 300 MPa working pressures, 2 mm standoff distance and 10 mm/min traverse rate is shown in Figure 4.16. Two cutting zones are clearly visible, the first zone (upper zone) is called the quality (smooth) cut and the second zone (lower zone) is called the striated cut. The first inspection of the surface generated by plain waterjet reveals that it is similar to the surface produced by abrasive waterjet cutting but the cutting mechanism is different.

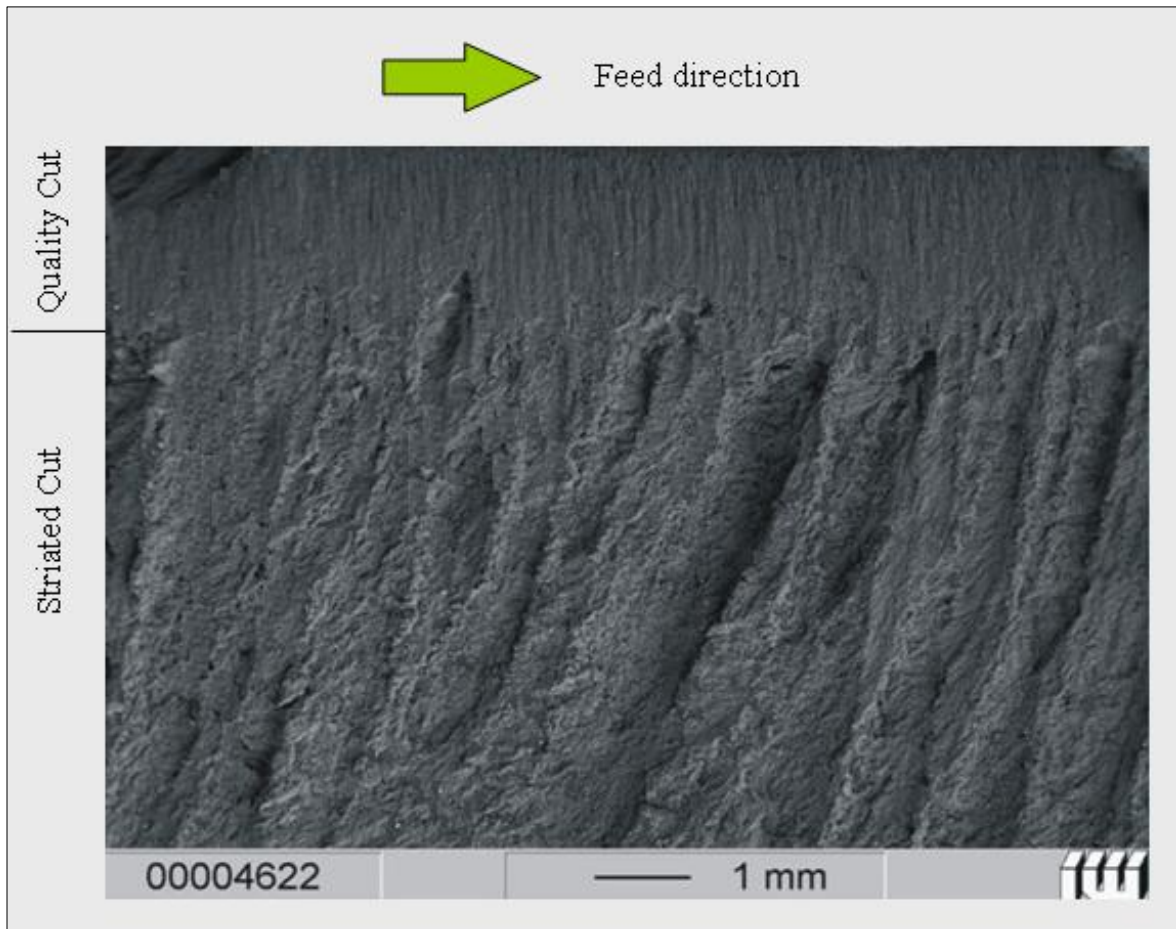


Fig. 4.16: The surface generations by plain waterjet in Al 99.5.

The photomicrographs of cutting surface of aluminium test specimen at 2 mm standoff distance, 10 mm/min traverse rate, 0.5 mm nozzle diameter and 300 MPa working pressure are shown in Figures 4.17 and 4.18. The high magnification of the surface, Figure 4.17 (b), reveals that the majority of the craters are smearing type as a result the shear stress caused by tangential water flow accompanied by few indentation craters. The lateral flow of water across the surface causes extremely high shear stresses and smears the deformed ridges of the plowing craters surrounding the circumference of the central depression because the lateral flow velocity is approximately three times the impact velocity, [93]. The surface, Figure 4.17 (d), shows three parallel rows of indentation craters in the form of small (about 5  $\mu\text{m}$ ) depressions in the same direction of the waterjet motion. The presence of such craters in that form indicates that the waterjet acts as hard indenter

that abrades the surface of the tested aluminium, where the removed materials are formed in the front ridge. The deformed materials as raised side ridges are sheared by the out flowing water. In this condition erosion occurred by ductile removal of the material constituting the front and side ridges. Erosion may not continue by tunneling through the thickness of the sample. Instead the edges of the eroded area are peeled back. Figure 4.17 (c) shows the lower end of the tested aluminium full of smearing craters as well as a portion of the highly distressed platelet about to break off. The eroded area is full of the smearing craters which confirm that the waterjet acts on the surface at small impingement angle as the out flowing water shears the surface at the lower end. Figure 4.18 shows that the waterjet penetrates the materials and makes tunneling way in the inlet position of the jet.

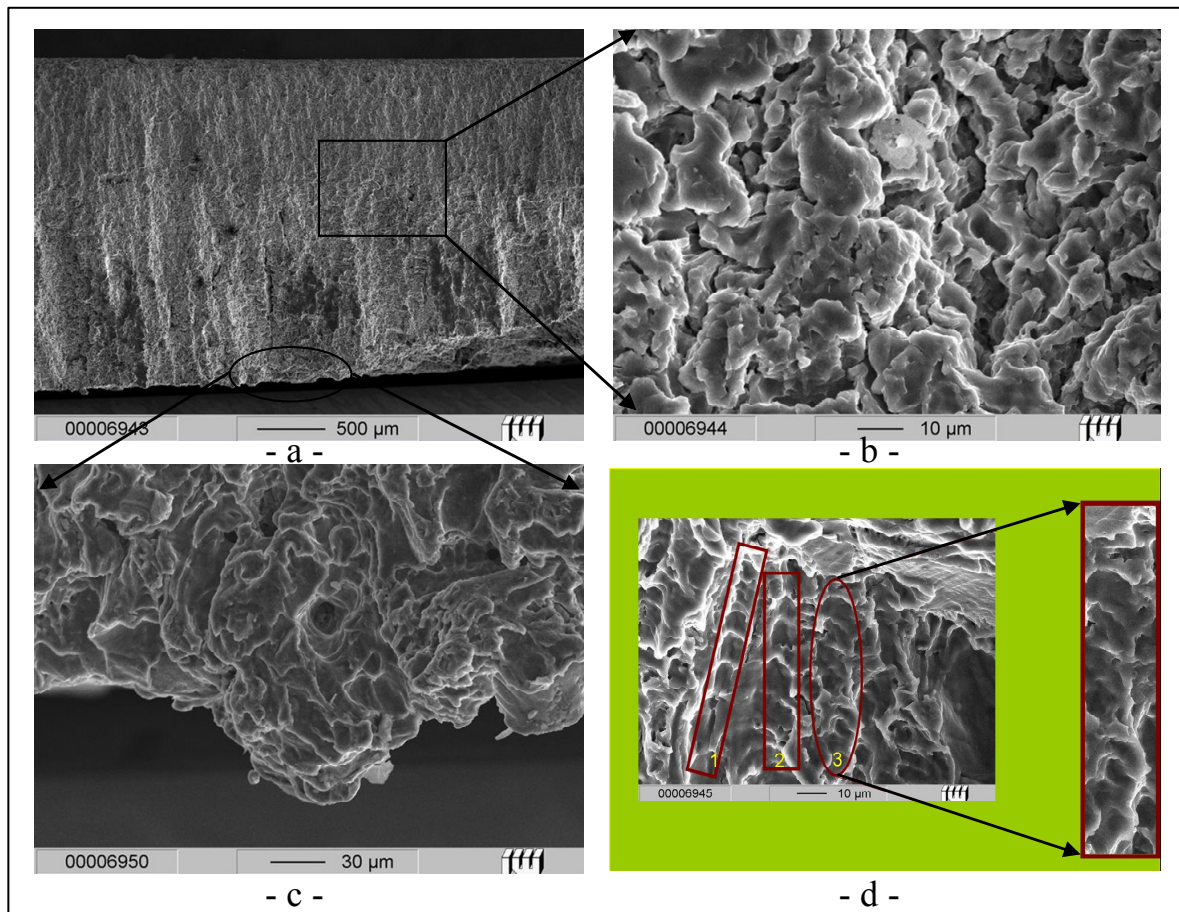


Fig. 4.17: The photomicrographs of cutting surface of aluminium.

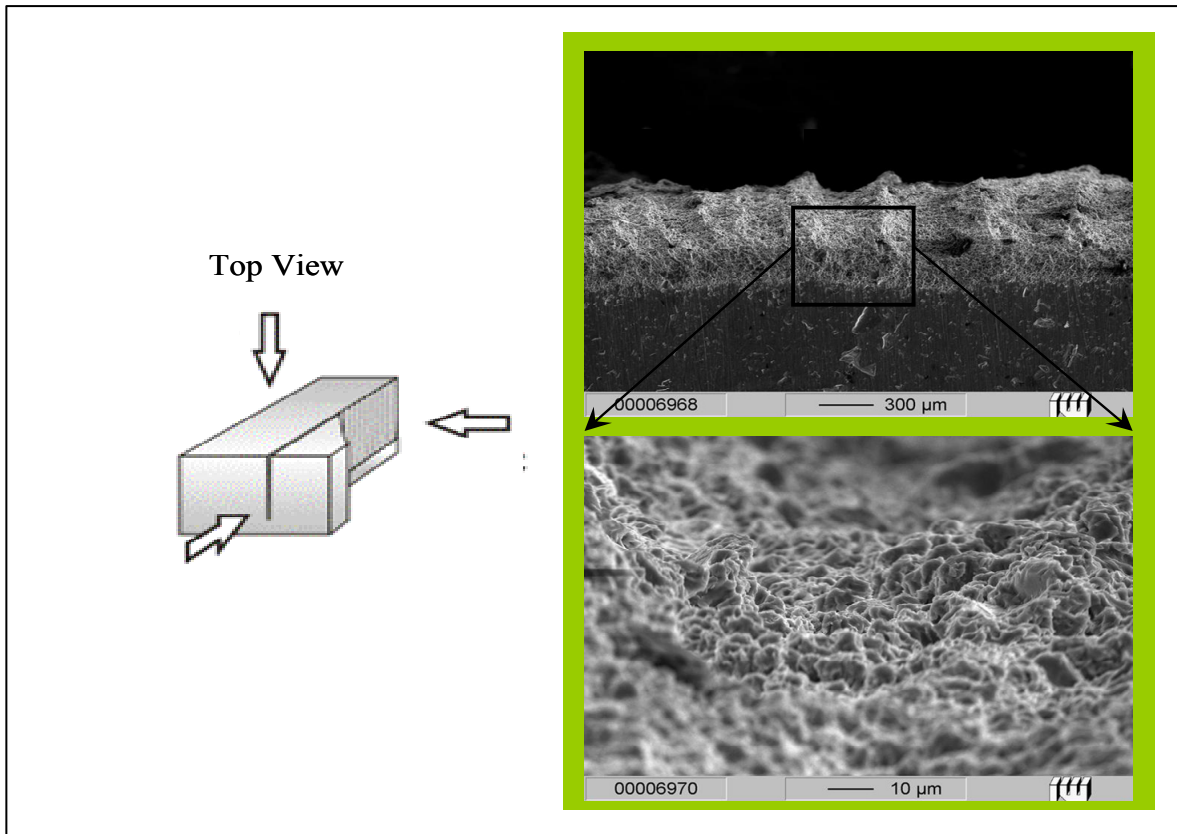


Fig. 4.18: Top view of the waterjet penetrations the materials.

### 6.6.2 Cutting Mechanism for WJ and AWJ

Figure 4.19 shows the microstructure variation of the cutting area with abrasive waterjet (AWJ) for AlZnMgCu1.5 with the machining parameters (nozzle diameter 0.25 mm, abrasive focus diameter 0.9 mm, pressure 240 MPa, traverse rate 100 mm/min, abrasive flow rate 8 g/s). The microstructure of the cutting area with plain waterjet (WJ) for AlMgSi0.5 with the machining parameters (sapphire nozzle diameter 0.08 mm, pressure 900 MPa, traverse rate 10 mm/min, standoff distance 10 mm). The microstructure differs due to the material removal mechanism of waterjet and abrasive waterjet. It can also be ascertained that the surface finish becomes worse with an increase in the depth cut, as it does for abrasive waterjet cutting. The mechanism of jet cutting process generally depends on the process parameters. In the case of abrasive waterjet cutting, in the first stage of cutting the abrasive particles strike the surface at a shallow angle producing a relatively smooth surface. The material removal phenomenon associated with this process of cutting



is called the cutting wear mechanism. The secondary region, displaying unsteady cutting with striation marks is called the deformation cutting zone. The trace of the micro-grinding as the basic mechanism can be seen on the whole cutting area. In the case of plain waterjet, the mechanism of waterjet cutting is erosion caused by localized failure which occurs by the localized fluid pressure (impact pressure). This pressure exceeds the strength of the target material leading to a plastic deformation (depending on the types of materials), material flow and material removal. The dynamic loading by waterjet leads in principle to the same structure as can be seen in section 4.1, 4.2, 4.5 and 4.6.1.

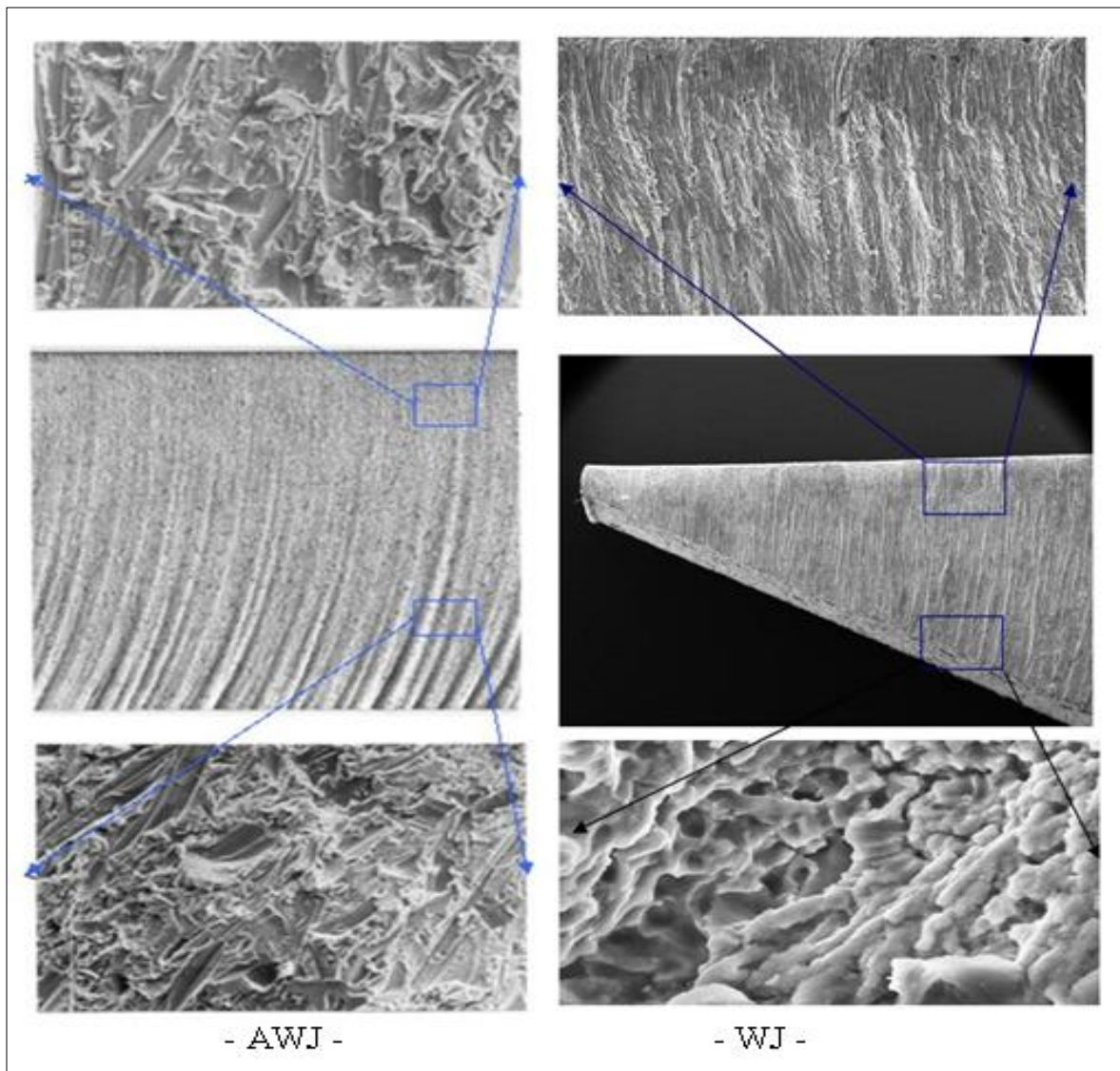


Fig. 4.19: Surface topography sample cutting with AWJ and WJ.

## **5. TEST RESULTS**

This chapter gives the results of waterjet (WJ) and abrasive waterjet (AWJ) cutting at ultra high pressure up to 900 MPa. The effects of cutting parameters especially the pressure, nozzle diameter, traverse rate and abrasive mass flow rate on the tested materials are discussed.

### **5.1 Plain Waterjet**

This section discusses the experimental results of cutting by plain waterjet at ultra high pressure up to 900 MPa.

#### **5.1.1 Effect of pressure in the depth of cut**

The effect of pressure in the depth of cut for pressure up to 800 MPa, a traverse rate of 10 mm/min, a sapphire nozzle of 0.1 mm diameter and standoff distance of 2 mm to cut workpiece of different materials such as zinc, copper, Armco-iron and austenite is shown in Figure 5.1. It is clear that, with increasing pressure the depth of cut increases due to the increased hydraulic power. The mathematical relationship between the pressure and the depth of cut is linear. The depth of cut increased from 0.4 mm at pressure of 500 MPa to 1.3 mm at pressure of 800 MPa for austenite, from 0.6 mm at pressure of 300 MPa to 2.6 mm at pressure of 800 MPa for Armco-Iron, from 1 mm at pressure of 300 MPa to 4.2 for copper and from 1.2 mm at pressure of 300 MPa to 6.1 mm at pressure of 800 MPa for zinc. The depth of cut as a function of pressure up to 900 MPa for a diamond nozzle of 0.1 mm diameter are shown graphically in Figure 5.2 and photographical in Figure 5.3. The relationship between the pressure and the maximum depth of cut at aluminium is linear as previous and the depth of cut increased from 1.4 mm at pressure 300 MPa to 8.2 mm at 900 MPa pressure

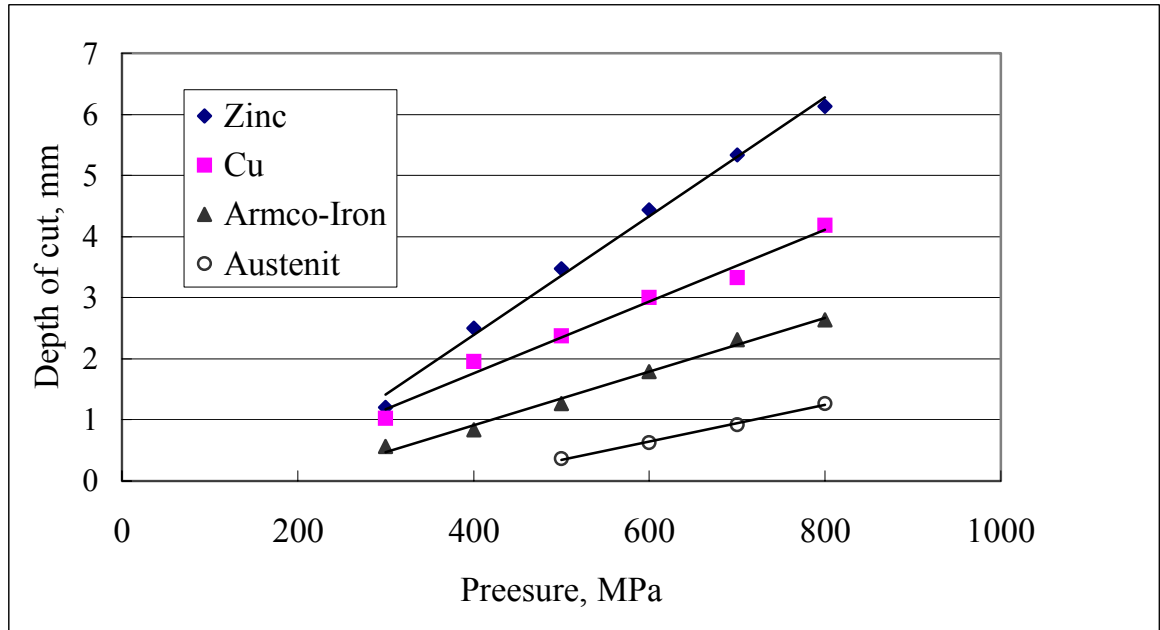


Fig. 5.1: The depth of cut as a function of pressure for different materials.

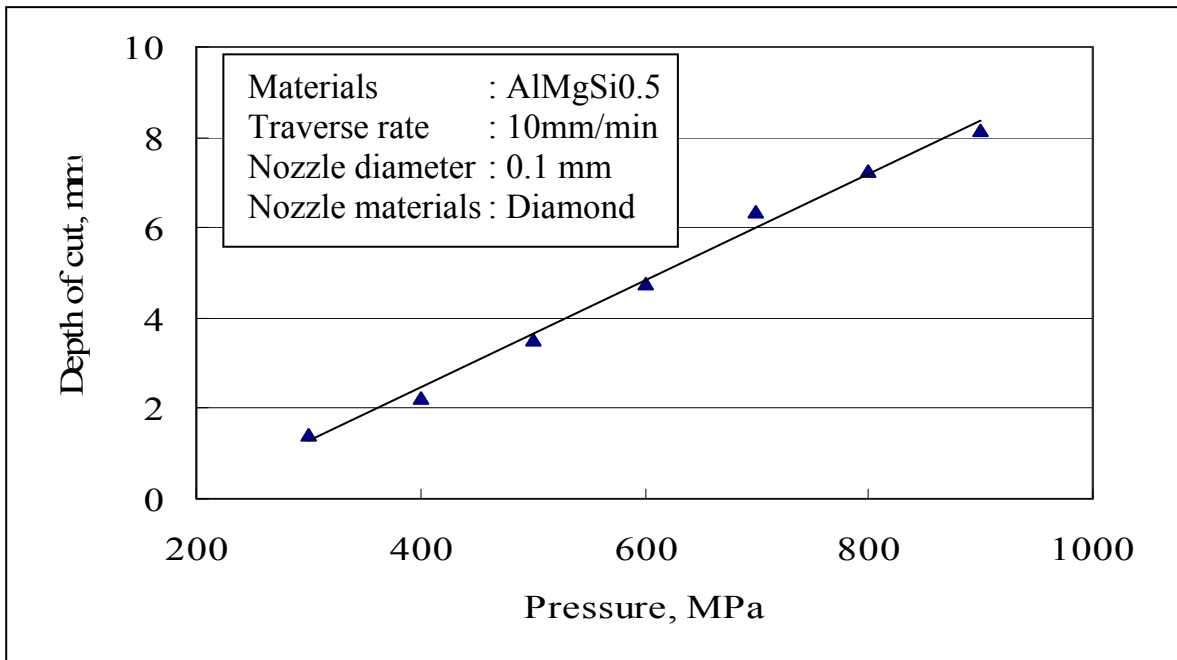


Fig. 5.2: The effect of pressure on the depth of cut for aluminium.

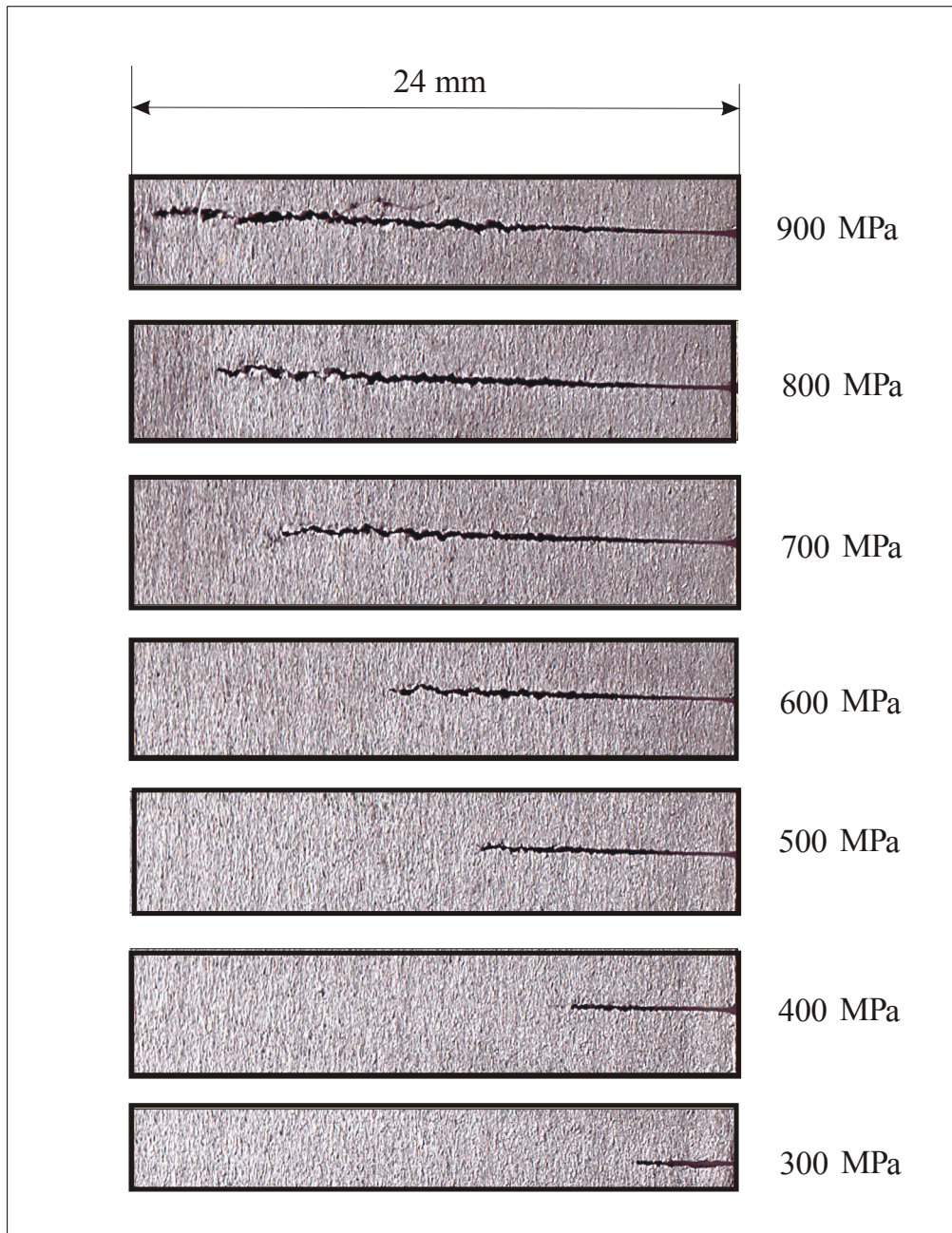


Fig. 5.3: Photographically bottom face cutting aluminium with WJ up to 900 MPa.

### 5.1.2 Effect of nozzle diameter in the depth of cut

The effect of nozzle diameter on the depth of cut at pressure of 300 MPa, a traverse rate of 10 mm/min and standoff distance of 2 mm to cut different workpiece of Al99.5, AlMgSi0.5 and copper are shown graphically in Figure 5.4 and photographical in Figure 5.5. The depth of cut increased with increasing the nozzle diameter for all the tested materials. This can be attributed to the increase of the hydraulic power. The depth of cut increased from 2 mm at nozzle diameter of 0.08 mm to 10 mm at nozzle diameter of 0.3 mm for AlMgSi0.5. The increase in the depth of cut was 5 times, while the hydraulic power increase at this condition was about 14 times. It was observed that the increase of the depth of cut is a function of the increase of the hydraulic power.

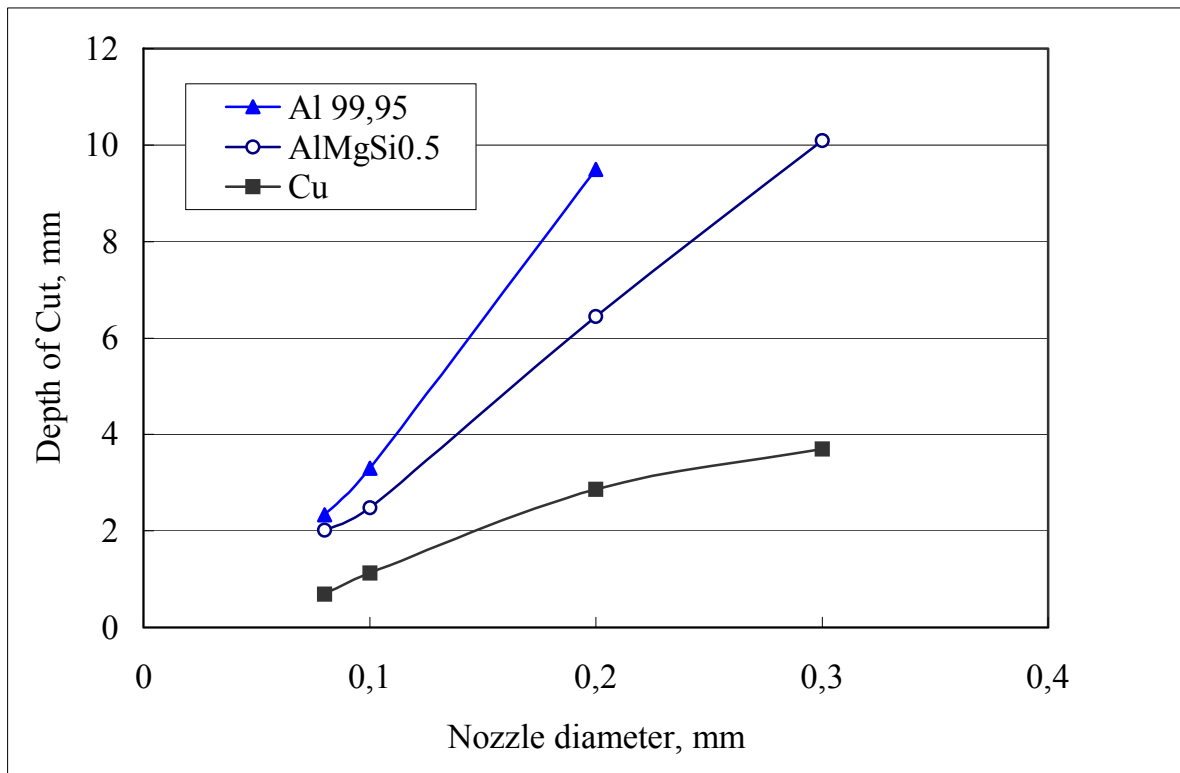


Fig. 5.4: Effect of nozzle diameter in the depth of cut at pressures 300 MPa.

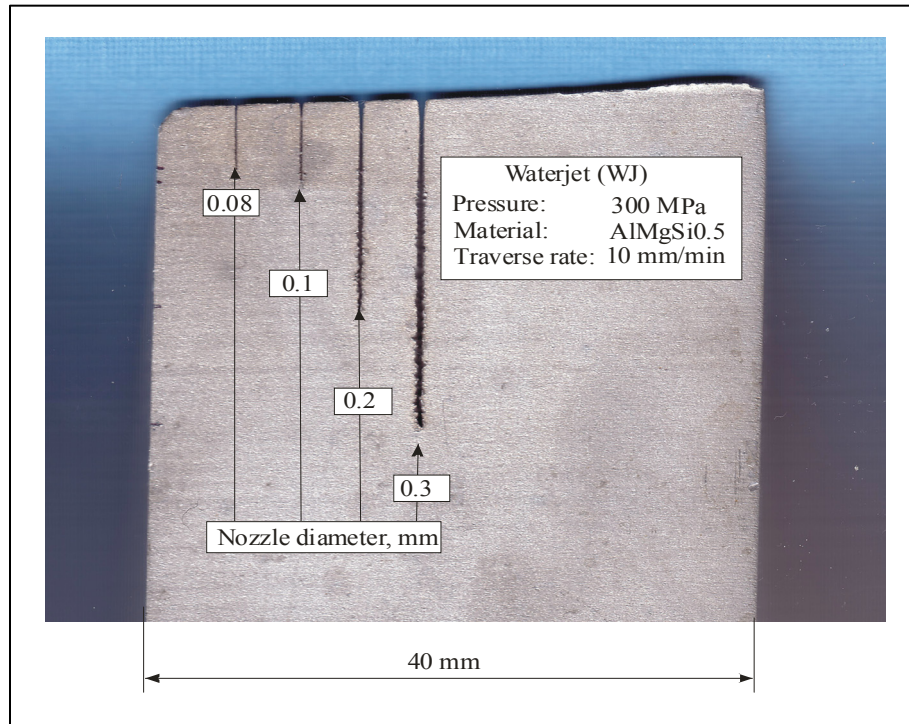


Fig. 5.5: Bottom face cutting of Al at different nozzle diameter.

The effect of nozzle diameter on the depth of cut at Pressure of 800 MPa is shown in Figure 5.6. It is clear that with increasing the nozzle diameter from 0.08 mm to 0.1 mm the depth of cut, for all materials were tested, increased.

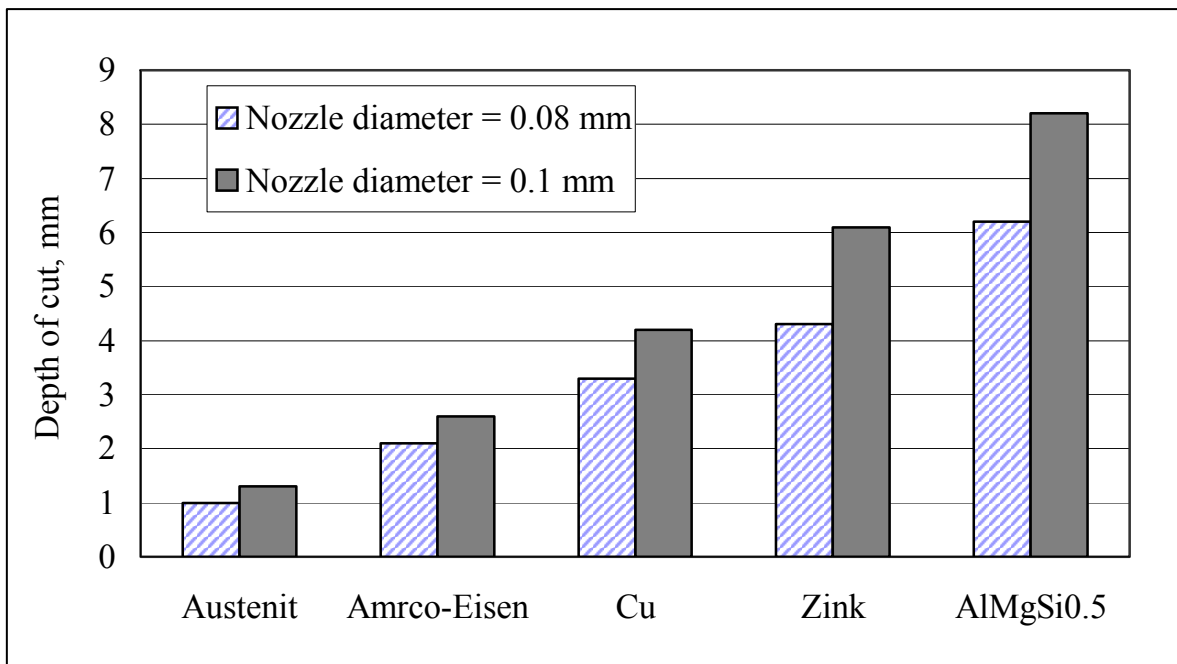


Fig. 5.6: Effect of nozzle diameter in the depth of cut for pressures 800 MPa.

### 5.1.3 Effect of traverse rate in the depth of cut

The effect of the traverse rate on the depth of cut at working conditions, (pressure 900 MPa, sapphire nozzle diameter 0.08 mm, standoff distance 2 mm and workpiece materials aluminium) is shown in Figure 5.7. It is clear that with increase the traverse rate decrease the depth of cut. The depth of cut increased from 4.7 mm at traverse rate 20 m/min to 8.3 at 5 mm/min.

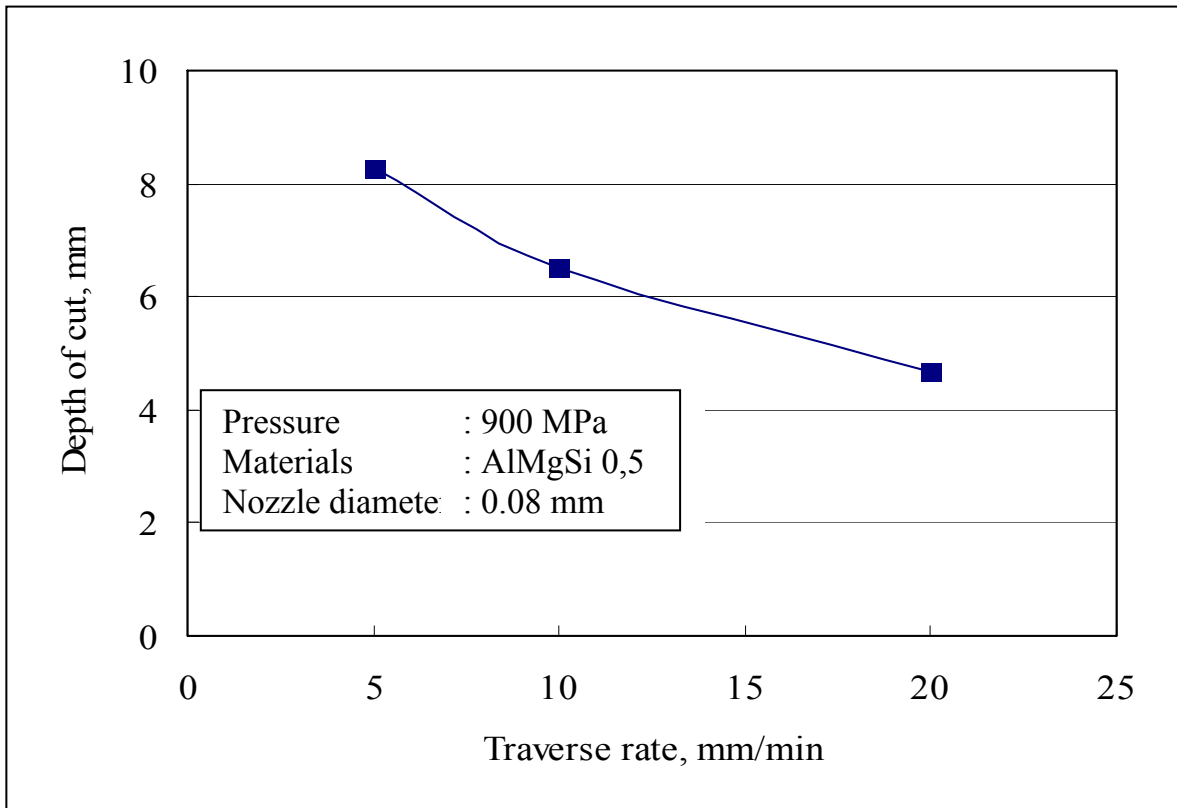


Fig. 5.7: The effect of traverse rate on the depth of cut for aluminium at 900 MPa.

### 5.1.4 Cutting quality at pressure 900 MPa

The cutting quality in relation to the surface finish for machining AlMgSi0.5, at nozzle diameter of 0.1 mm, traverse rate of 10 mm/min standoff distance of 2 mm and pressure of 900 MPa is shown in Figure 5.8. The surface roughness was measured at three positions. The first was at distance 0.5 mm from the top cutting ( $R_a$  3  $\mu\text{m}$  and  $R_z$  20.23  $\mu\text{m}$ ), the second position was at distance 2 mm at the beginning of the striated cutting zone ( $R_a$  10  $\mu\text{m}$  and  $R_z$  40  $\mu\text{m}$ ) and the third position at distance 3.5 mm from the striated cutting zone ( $R_a$  19.8  $\mu\text{m}$  and  $R_z$  188  $\mu\text{m}$ ).

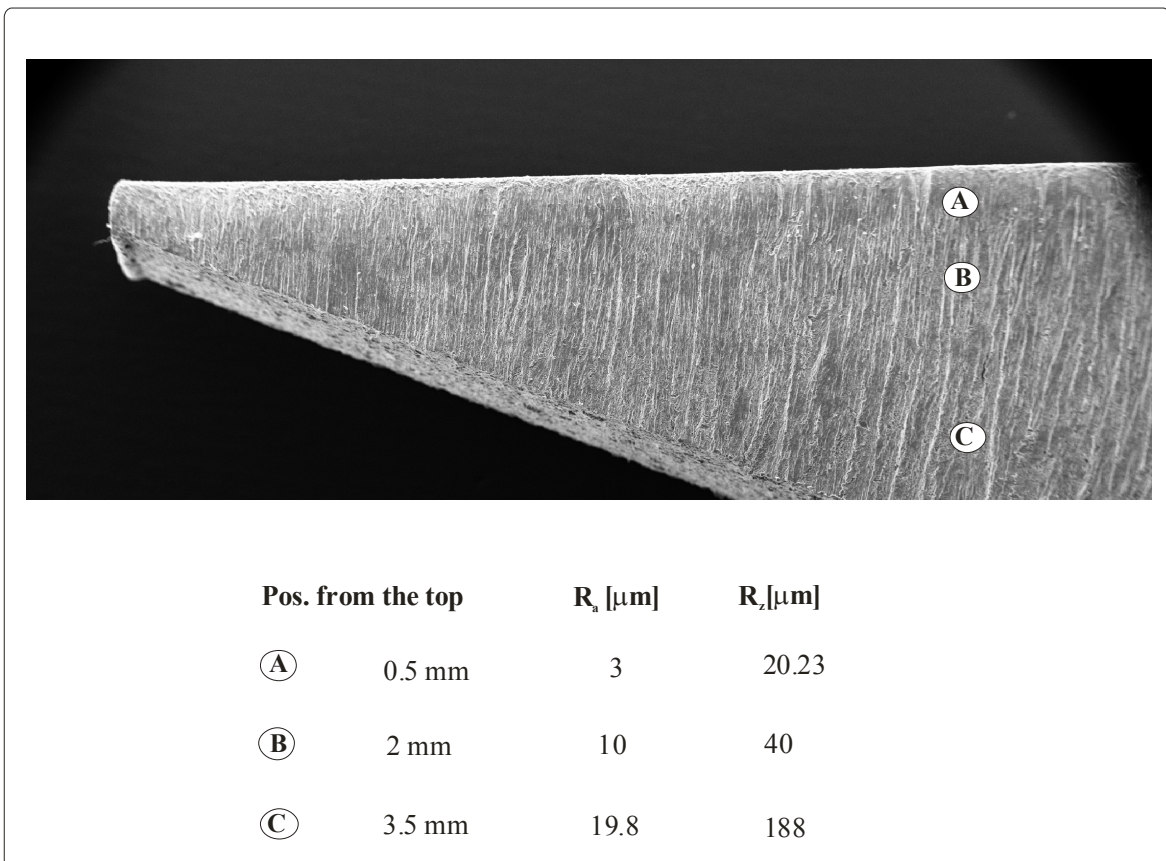


Fig. 5.8: Aluminium cut with waterjet at 900 MPa.



## 5.2 Abrasive Waterjet

This section discusses the experimental results of cutting by abrasive waterjet at ultra high pressure up to 600 MPa.

### 5.2.1 Effect of Pressure in the depth of cut

The effect of pressure on the depth of cut for pressures up to 600 MPa, a traverse rate of 100 mm/min, a sapphire nozzle of 0.1 mm diameter, focus diameter of 0.4 mm, focus length of 70 mm, Barton garnet 220 mesh, abrasive flow rate of 1 g/s and standoff distance of 2 mm to cut different workpiece of copper, austenite, aluminium is shown in Figure 5.9. It is clear that, with increasing pressure the depth of cut increased due to increasing velocity and acceleration of the abrasive particle. Linear relationship between the pressure and the depth of cut is observed for all the tested materials. The depth of cut increased from 2.2 mm at pressure of 400 MPa to 7.8 mm at pressure of 600 MPa for austenite and from 2.9 at pressure of 400 MPa to 9.7 at pressure 600 MPa for copper and from 5.9 mm to 17.2 mm for aluminium.

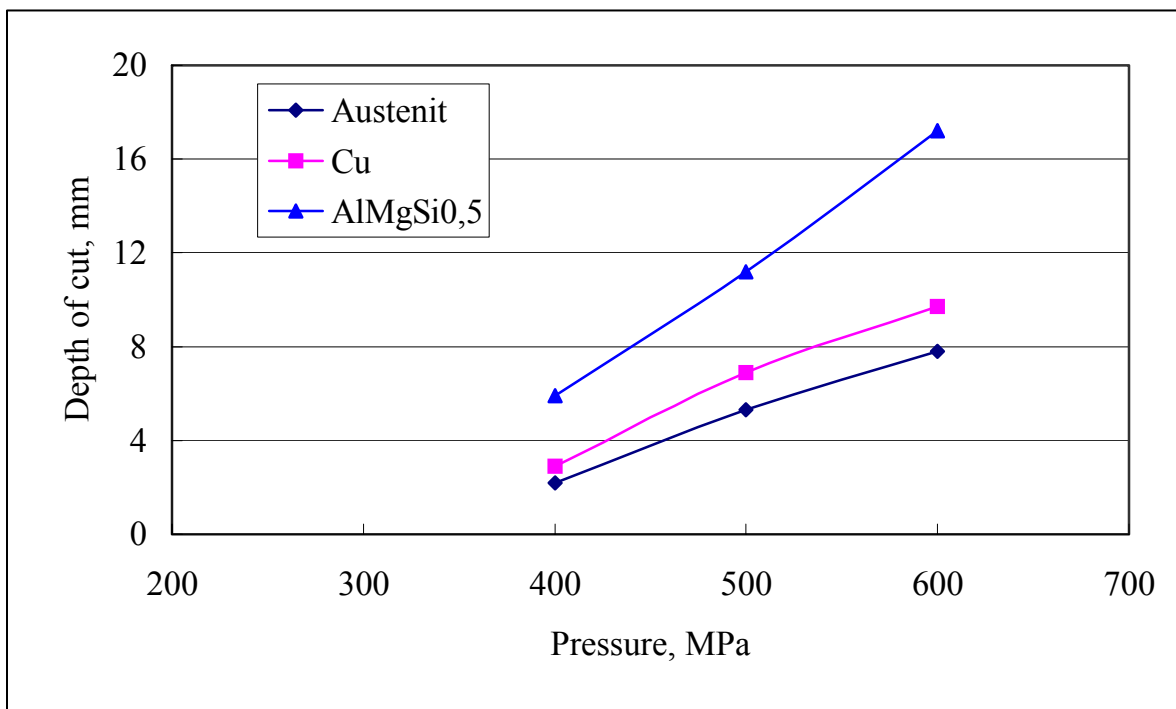


Fig. 5.9: The effect of the pressure on depth of cut for abrasive waterjet.

## 5.2.2 Abrasive waterjet optimizing

This section gives the experimental results to optimization the abrasive waterjet cutting by the way, first optimizations the abrasive flow rate for pressure 300 MPa and 600 MPa, the second optimization the water flow rate by using different nozzle diameter.

### 5.2.2.1 Optimizing the abrasive flow rate

The effect of abrasive flow rate on the depth of cut for pressures of 300 MPa and 600 MPa, a traverse rate of 100 mm/min, a sapphire nozzle of 0.1 mm diameter, focus diameter of 0.4 mm, focus length of 70 mm, Barton garnet 220 mesh, and standoff distance of 2 mm to cut aluminium are shown in Figures 5.10 and 5.11. The maximum depth of cut increased with increasing the abrasive flow rate up to critical value then decreased with increasing the abrasive flow rate. This phenomenon is found, [94–98], and can be explained by the following simplified momentum equation:

$$v_a = \frac{v_w}{1 + \frac{M_a}{M_w}} \rightarrow (5.1)$$

Where  $v_a$  is the velocity of abrasive particles after momentum transfer,  $v_w$  the velocity of water stream prior to momentum transfer,  $M_a$  and  $M_w$  the mass flow rates of abrasive and water respectively. The increase of the abrasive flow rate will increase the frequency of impact and consequently will increase the depth of cut. Beyond a certain point the benefit of higher impact frequency will be outbalanced by loss in particle velocity and therefore the depth of cut is reduced. This critical value increased by increasing the pressure, where the critical values were 0.55 and 0.8 g/s at pressures of 300 and 600 MPa respectively.

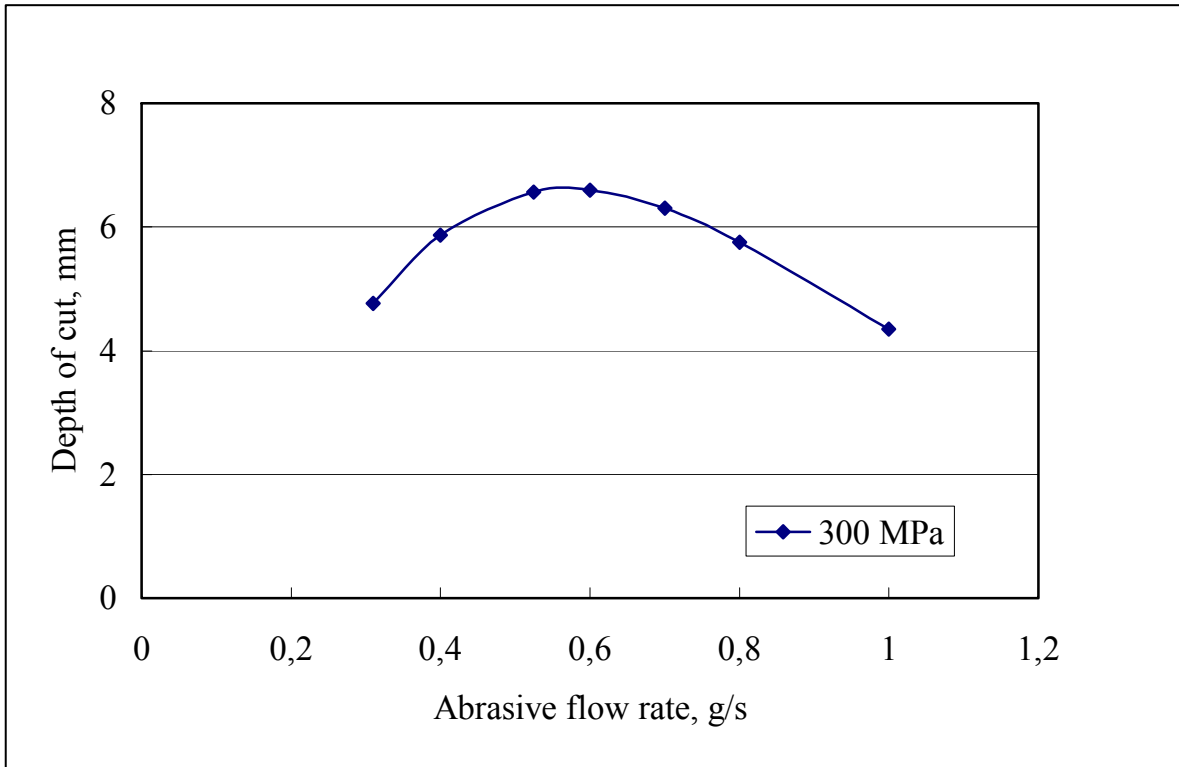


Fig. 5.10: The effect of abrasive flow rate on the depth of cut at 300 MPa.

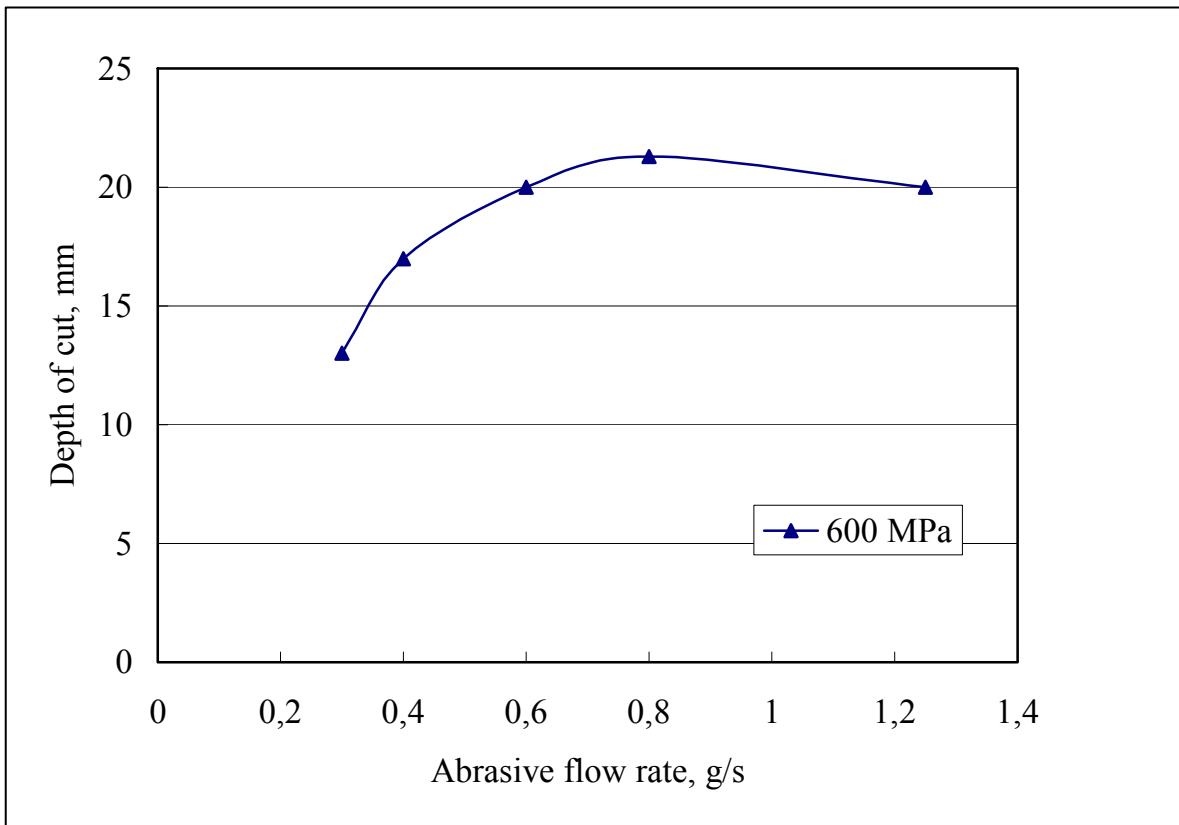


Fig. 5.11: The effect of abrasive flow rate on the depth of cut at 600 MPa.

### 5.2.2.2 Optimizing the waterjet nozzle diameter

The effect of nozzle diameter on the depth of cut at pressure of 300 MPa, a traverse rate of 100 mm/min, a sapphire nozzle of 0.1 mm diameter, focus diameter of 0.4 mm, focus length of 70 mm, Barton garnet 220 mesh, abrasive flow rate of 0.75 g/s, standoff distance of 2 mm for aluminium, copper and austenite is shown in Figure 5.11. The maximum depth of cut increased up to maximum values then decreased with increasing the waterjet nozzle diameter. Extrapolation of this data that there is an optimum nozzle diameter to given maximum depth of cut depending on the abrasive focus diameter. The maximum depth of cut occurred at nozzle diameter of 0.18 mm for all the tested materials.

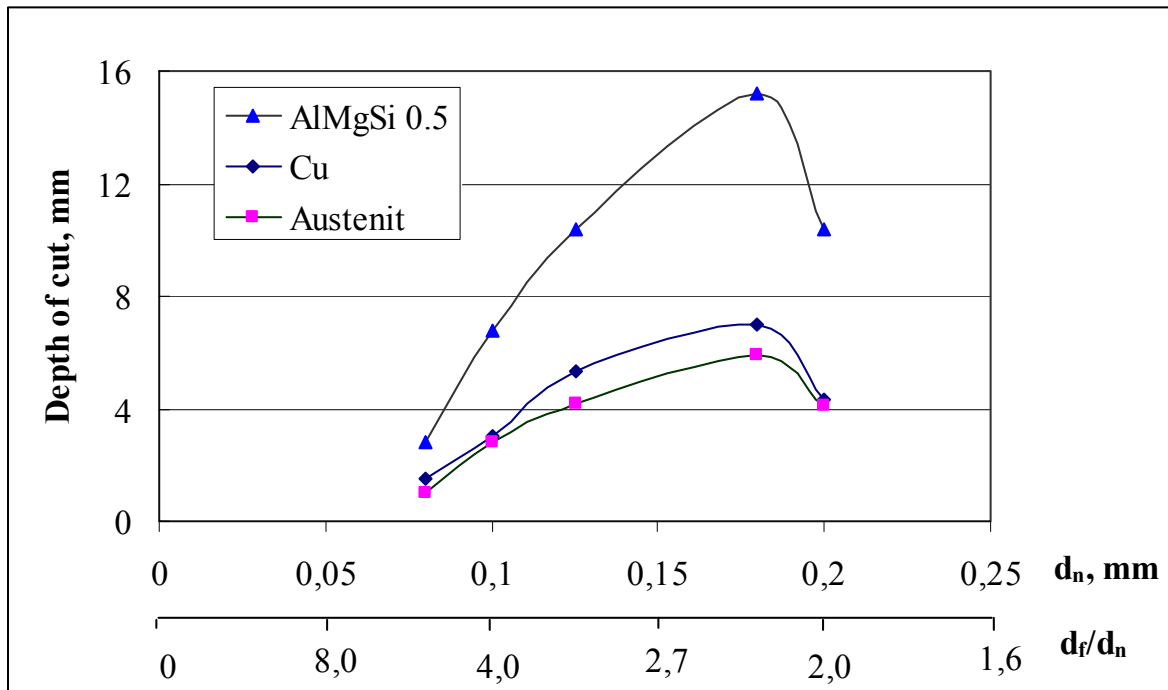


Fig. 5.11: The effect of waterjet nozzle diameter on the maximum depth of cut.

### 5.2.3 Effect of traverse rate in the depth of cut

The effect of the traverse rate on the depth of cut at working conditions, (pressure 600MPa, a sapphire nozzle of 0.1 mm diameter, focus diameter 0.4 mm, focus length 70 mm, Barton garnet 220 mesh, abrasive flow rate 0.8 g/s standoff distance 2 mm and workpiece aluminium) is shown in Figure 5.12. It is clear that with increase the traverse rate decrease the depth of cut. The depth of cut decreased from 34 mm at traverse rate 50 m/min to 16 at 150 mm/min.

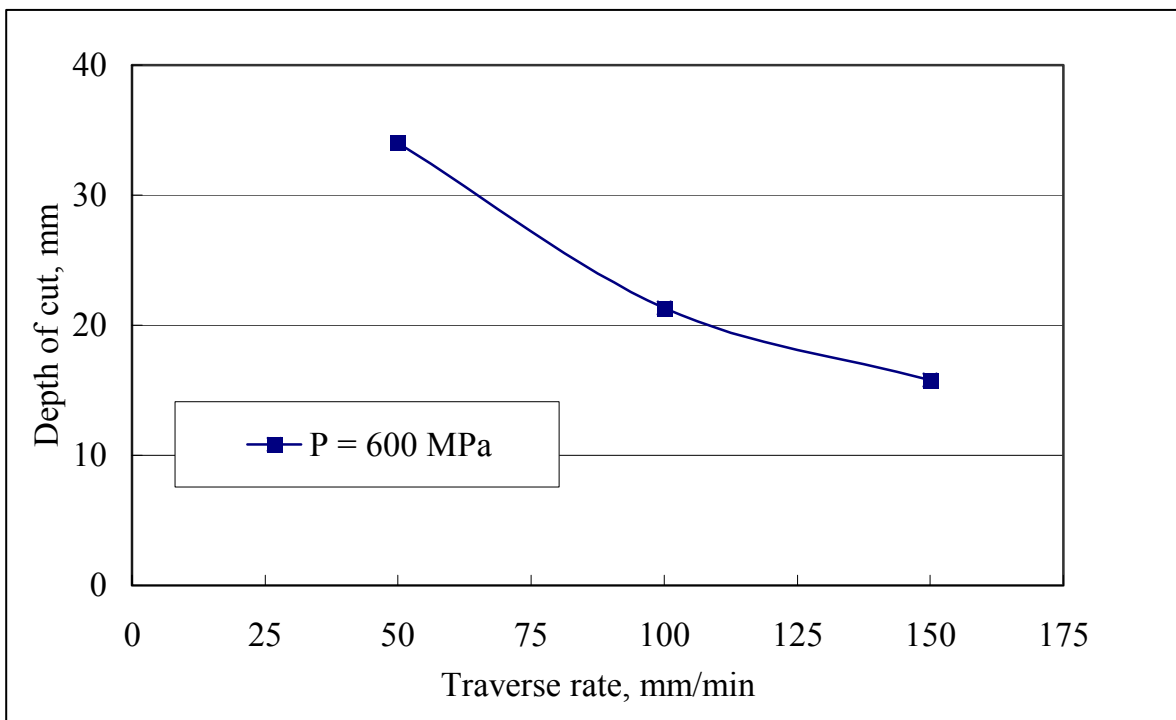


Fig. 5.12: Effect of traverse rate on depth of cut for aluminium at 600 MPa.

## 6. A THERMOGRAPHICAL MAP OF THE TOOL AND WORKPIECE

In this chapter the temperature distribution caused by the cutting with both plain waterjet and abrasive waterjet was studied experimentally. In plain waterjet the effect of both nozzle diameter and pressure were performed. In abrasive waterjet the effect of pressure is presented.

### 6.1 A Thermographical Map at Plain Waterjet

This section explained the temperature generation by both the various pressures and various nozzle diameters at nozzle holder and workpiece

#### 6.1.1 Effect of nozzle diameter on the maximum rise temperature

The effect of nozzle diameter on the maximum temperature at pressure of 300 MPa, for cutting workpiece of Al 99.5 and traverse rate of 10 mm/min is shown graphically in Figure 6.1. Schematically and photographically at scan area measurements is shown in Figure 6.2 (a and b). The temperature of the nozzle holder increased with increasing nozzle diameter. It can be explained on the basis that, as the nozzle diameter increased the flow rate increased leading to the increase of the frictional heating mainly generated from the friction of the water flow with the valves and pipe wall from the pump to the nozzle as shown in Figure 6.3.

Besides that, it is well known that the water mass flow rate given by  $\rho_0 c_d A \sqrt{\frac{2P}{\rho_0}}$ ,

where  $c_d$  is the coefficient of discharge. It was confirmed experimentally by hashish, [99], that the coefficient of discharge decreases with increasing both the pressure and the nozzle diameter. For example the coefficient of discharge is reduced from 0.75 to 0.66 when the nozzle diameter decreases from 0.152 to 0.582 mm at working pressure of 110 MPa. This means that by increasing the nozzle diameter the losses increase appears as significant rise in temperature.

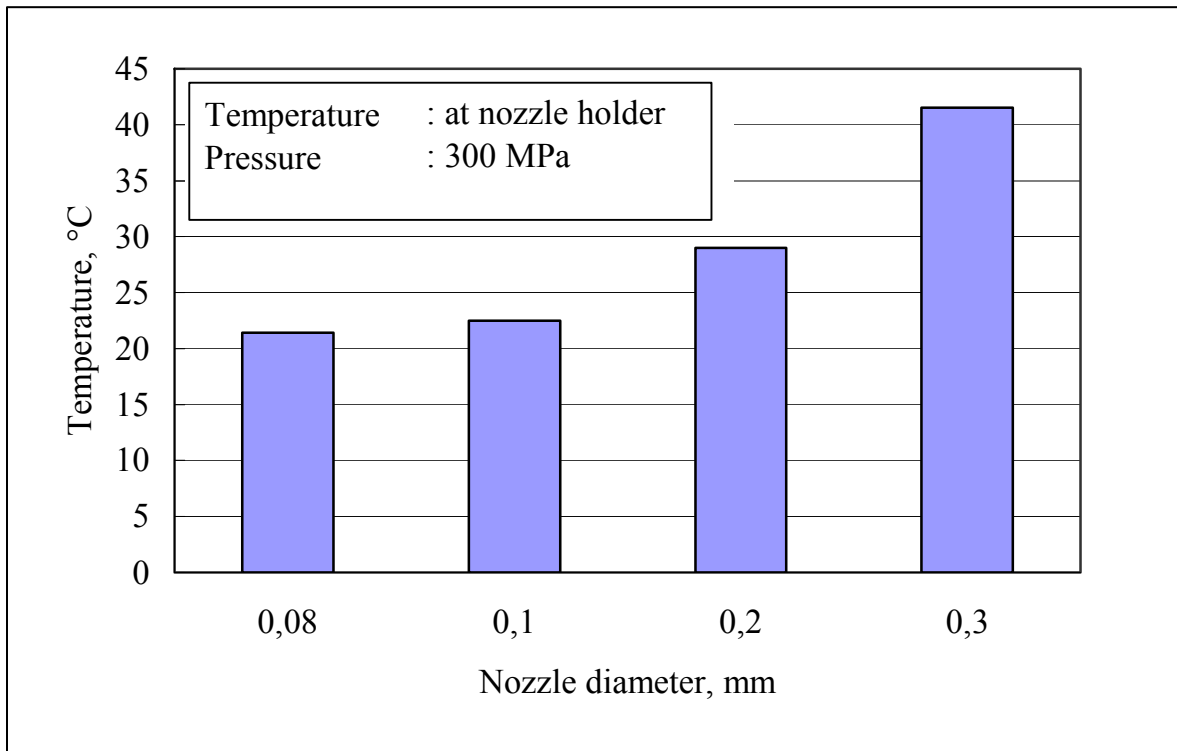


Fig. 6.1: Nozzle holder temperature at different nozzle diameter.

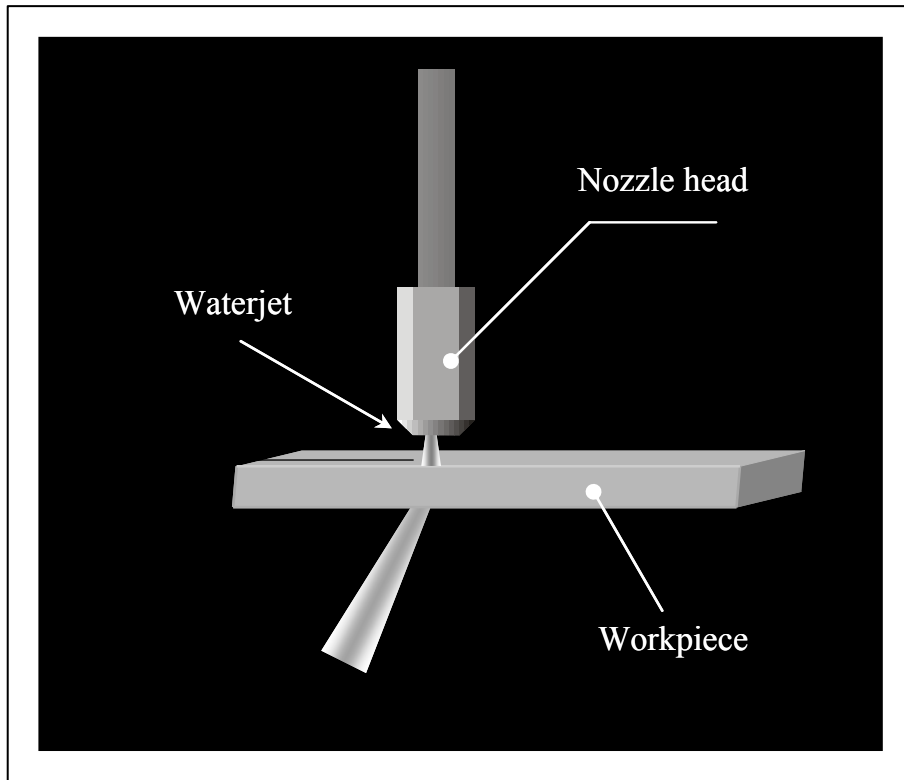


Fig. 6.2 (a): Schematically layout for temperature area measurements.

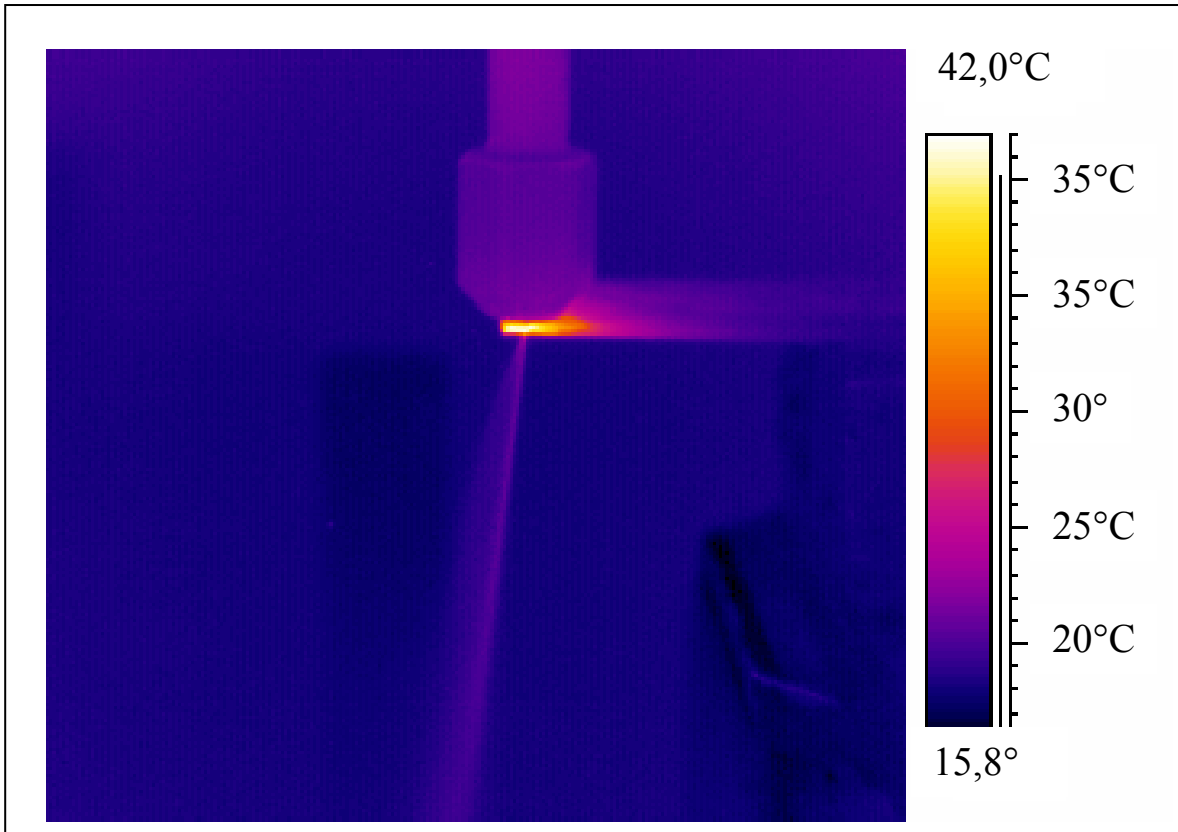


Fig. 6.2 (b): Photographically temperature area measurements at nozzle diameter 0.08 mm.

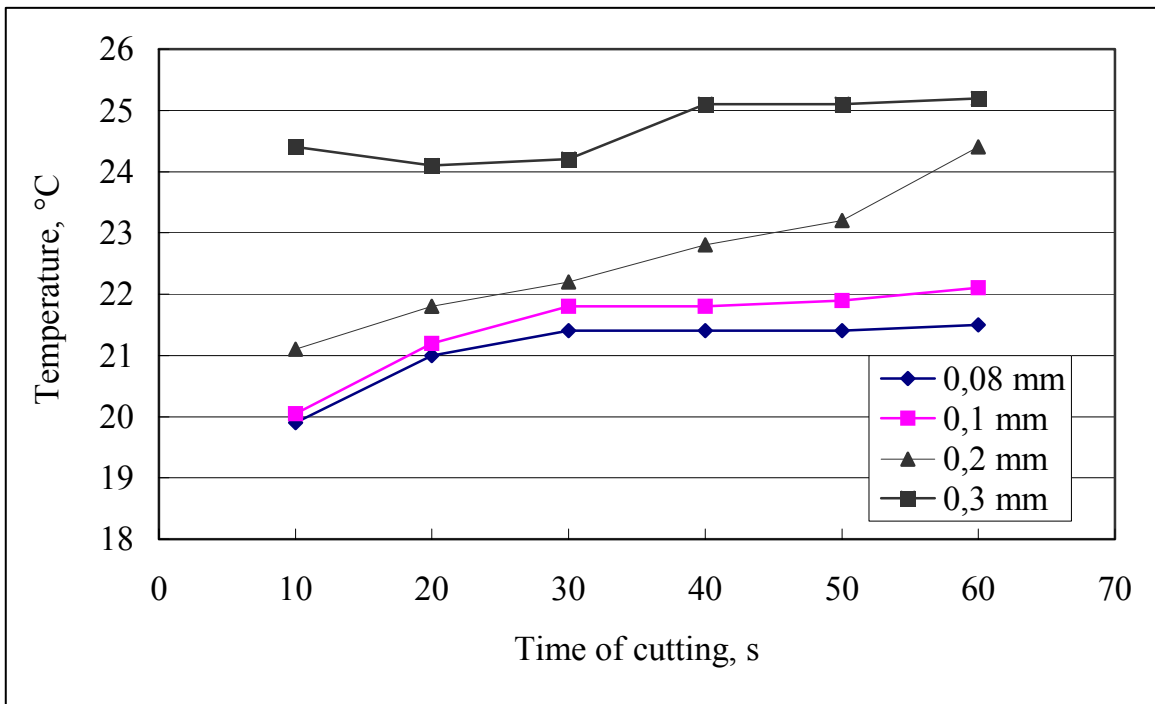


Fig. 6.3: Pipe temperature at position before nuzzle holder.



The workpiece temperature at different nozzle diameter with the same previous working conditions in section 6.1.1 is shown in Figure 6.4. The temperature of the workpiece increases with increasing the nozzle diameter from 0.08 to 0.2 mm. This can be attributed to the fact that as the diameter increases the number of the water concentric layers increases resulting in the increase of the friction and plastic deformation in the workpiece.

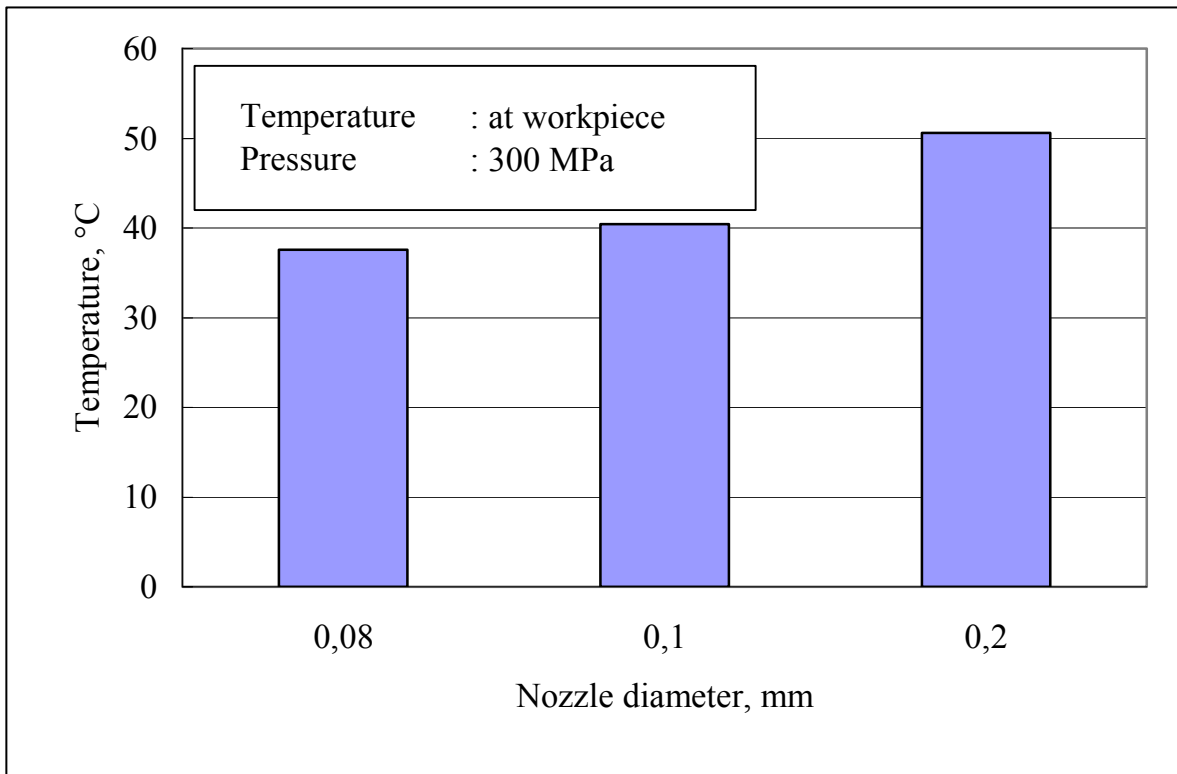


Fig. 6.4: Workpiece temperature at different nozzle diameter.

### 6.1.2 Effect of pressure on the maximum temperature

The effect of pressure on the maximum temperature in nozzle holder at nozzle diameter of 0.1 mm, and traverse rate of 10 mm/min for cutting workpiece of Al99.5 is shown in Figure 6.5. The temperature of the nozzle holder increased with increasing the pressure up to 900 MPa. As the pressure increases velocity of waterjet increases resulting in the increase of the frictional heating generated from the friction of the jet with the pipe wall [100-103]. The frictional heating increase is accompanied by significant temperature rise.

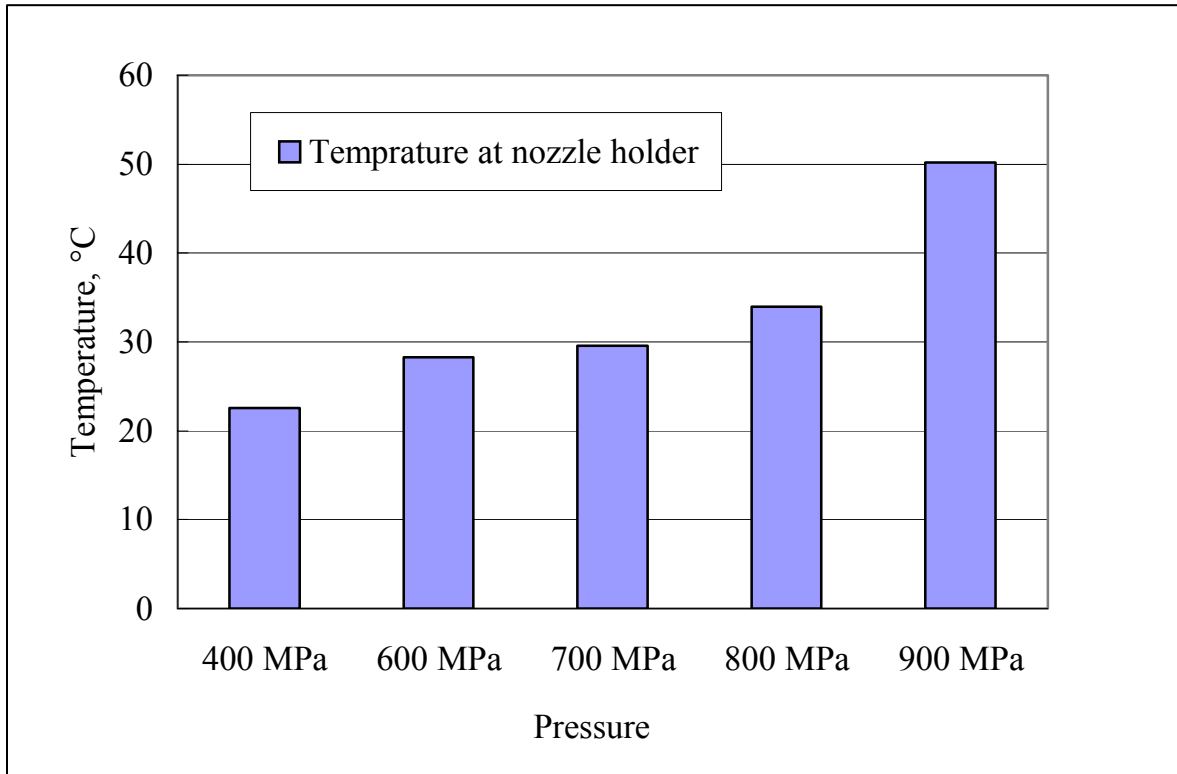


Fig. 6.5: Nozzle holder temperature at pressure up to 900 MPa and nozzle diameter 0.1 mm.

## 6.2 A Thermographical Map at Abrasive Waterjet

In this section, the generated temperature by the various pressures at abrasive focusing tube, abrasive waterjet and the workpiece were measured and explained.

### 6.2.1 Effect of pressure on the maximum temperature

Schematically and photographically for analysing the generation of heating-up of the cutting process is shown in Figure 6.6 (a and b). The effect of pressure on the maximum temperature in abrasive focus at machining parameter, nozzle diameter of 0.1 mm, focus diameter of 0.4 mm, abrasive flow rate of 0.5 g/s, abrasive mesh of 220 is shown in Figure 6.7. The temperature of the focus increases with increasing the pressure as the pressure increases both the abrasive particle and waterjet velocity increase resulting in the increase of the frictional heating generated from the friction and wear of the abrasive particles with the focus cylindrical wall.

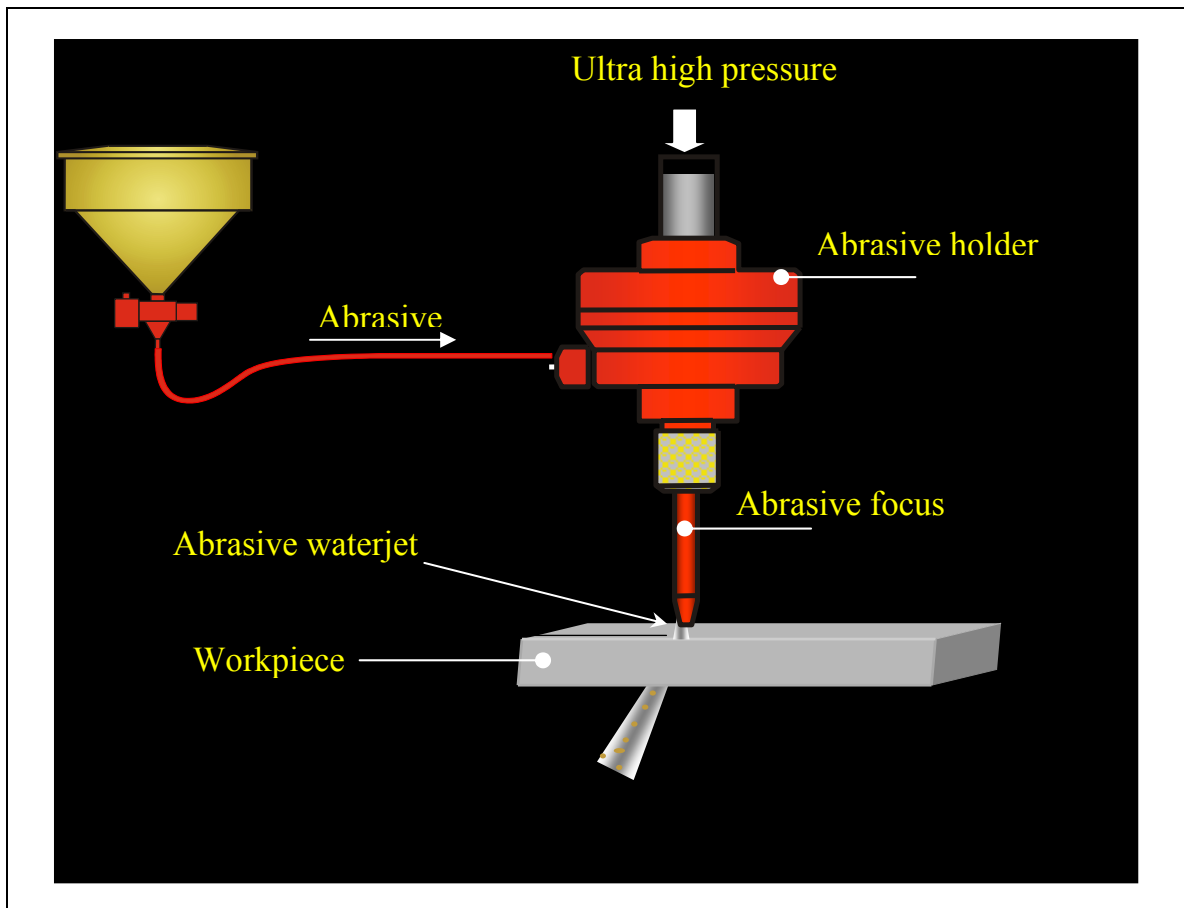


Fig. 6.6 (a): Schematically layout for temperature area measurements.

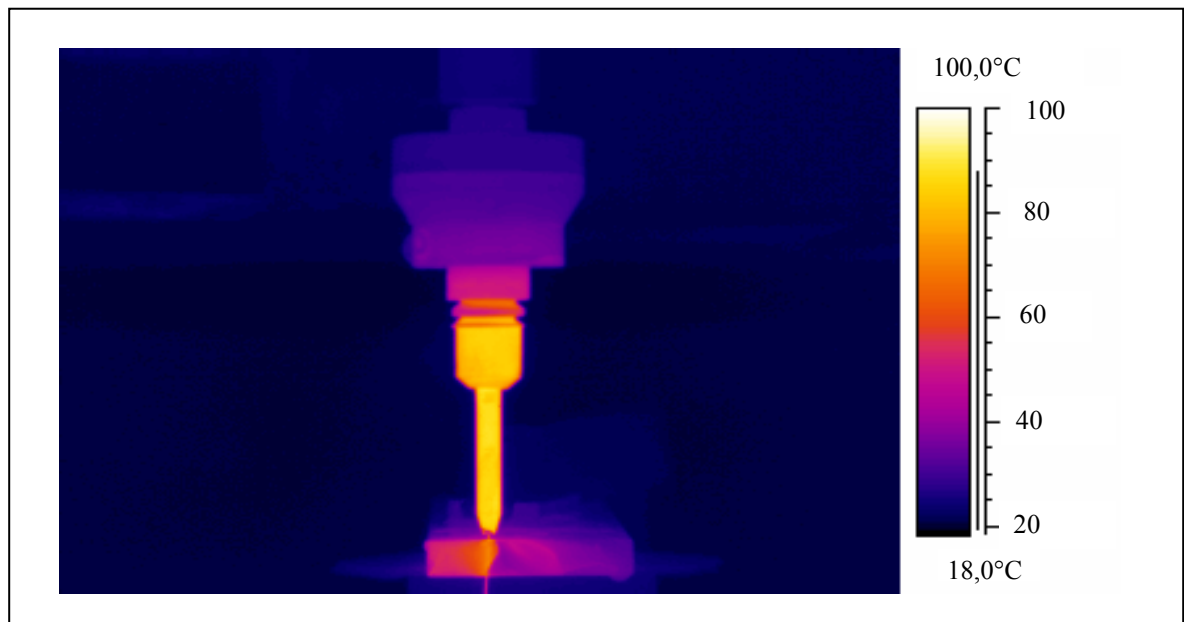


Fig. 6.6 (b): Photographically temperature area measurements for AWJ at pressure 600 MPa.

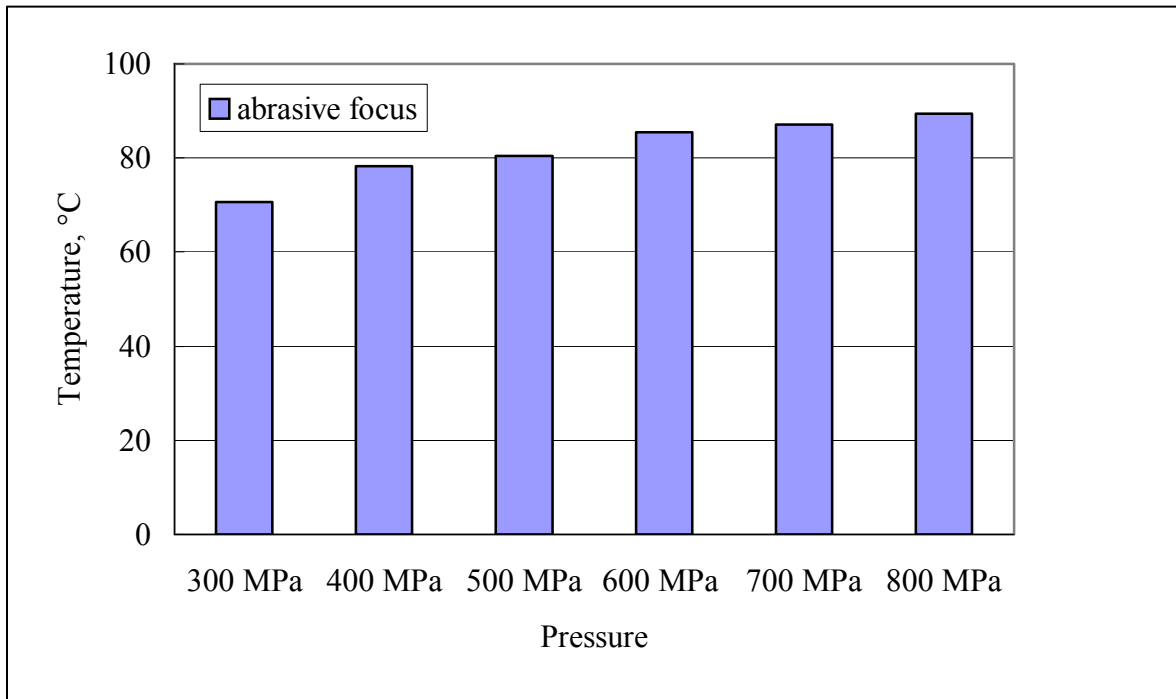


Fig. 6.7: Abrasive waterjet focus temperature at different pressure.

The effect of pressure on the abrasive waterjet temperature after focusing under the same working conditions above is shown in Figure 6.8. The temperature of the abrasive waterjet increases with increasing the pressure as explained before, as the pressure increases both the abrasive particle and waterjet velocity increase. It can be noted that the difference between the focus temperature and the abrasive waterjet temperature is due to the friction, for example at pressure of 400 and 800 MPa the difference is about 46 and 50 °C respectively. The effect of pressure on the maximum temperature in the workpiece (tested material is AlMgSi0.5 of 40 mm cutting length and 10 mm cutting depth) through the depth of cut at three position (at the start, the middle and the end of depth of cut) is shown in Figure 6.9.

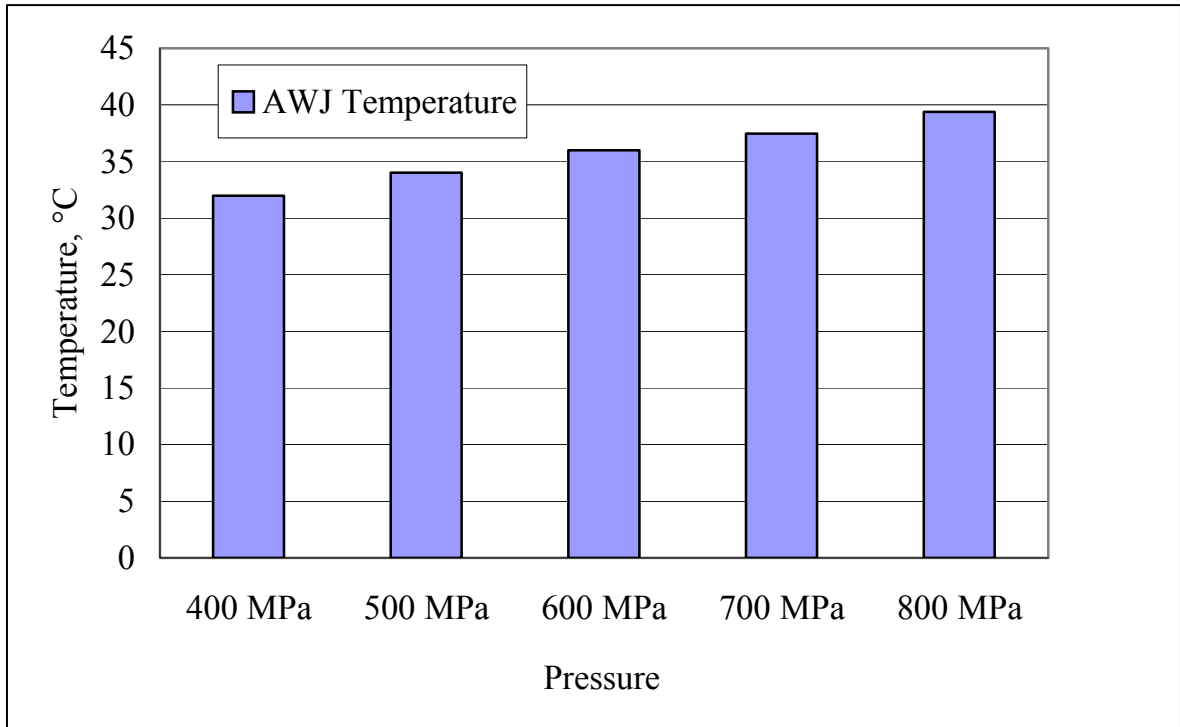


Fig. 6.8: The effect of pressure after focusing on abrasive waterjet temperature.

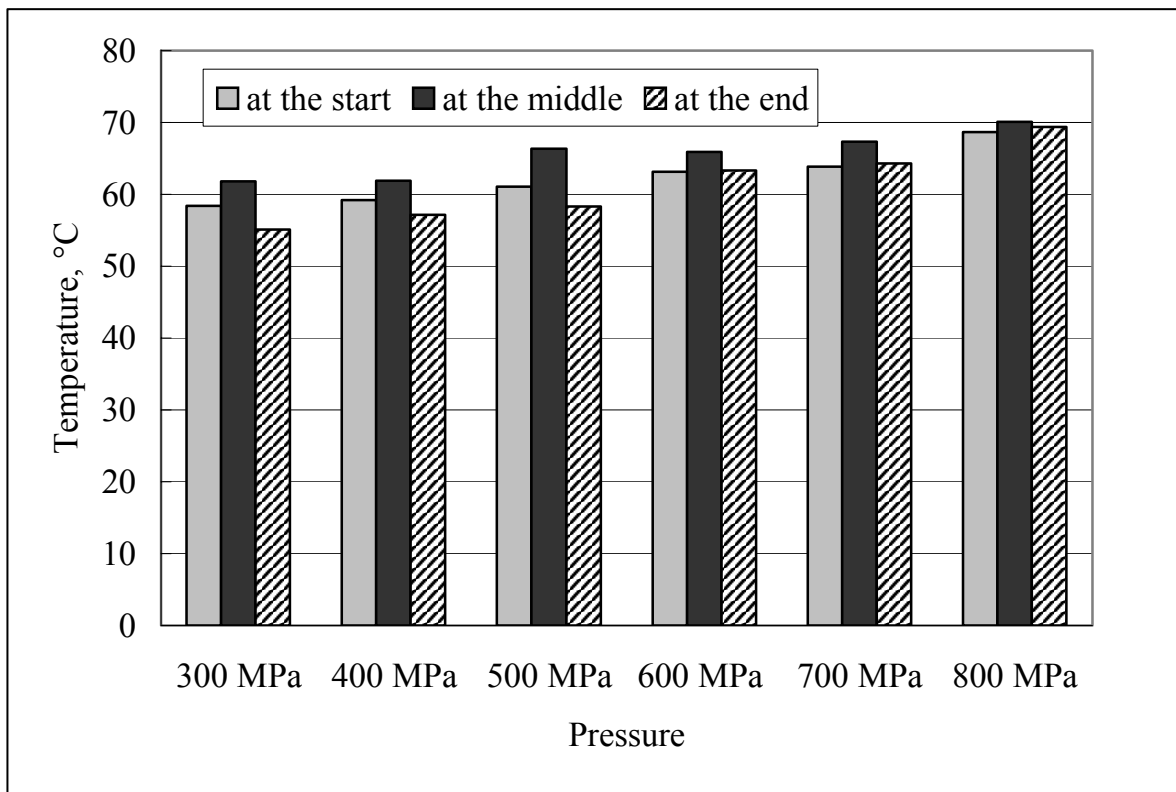


Fig. 6.9: Workpiece temperature at different abrasive waterjet pressure.

Generally, the temperature of the workpiece increases with increasing the pressure. It was observed that the temperature of the workpiece increases at the middle of the depth of cut more than the top (start) and bottom (end) of the depth of cut. This can be explained on the bases that at the top and bottom of the depth of cut the heat generated during micro-cutting process can easily transfer to the environment. The effect of pressure on the maximum temperature for the abrasive waterjet after cutting is shown in Figure 6.10. The abrasive waterjet temperature increases with increasing the pressure. This is due to increase in abrasive particle velocity

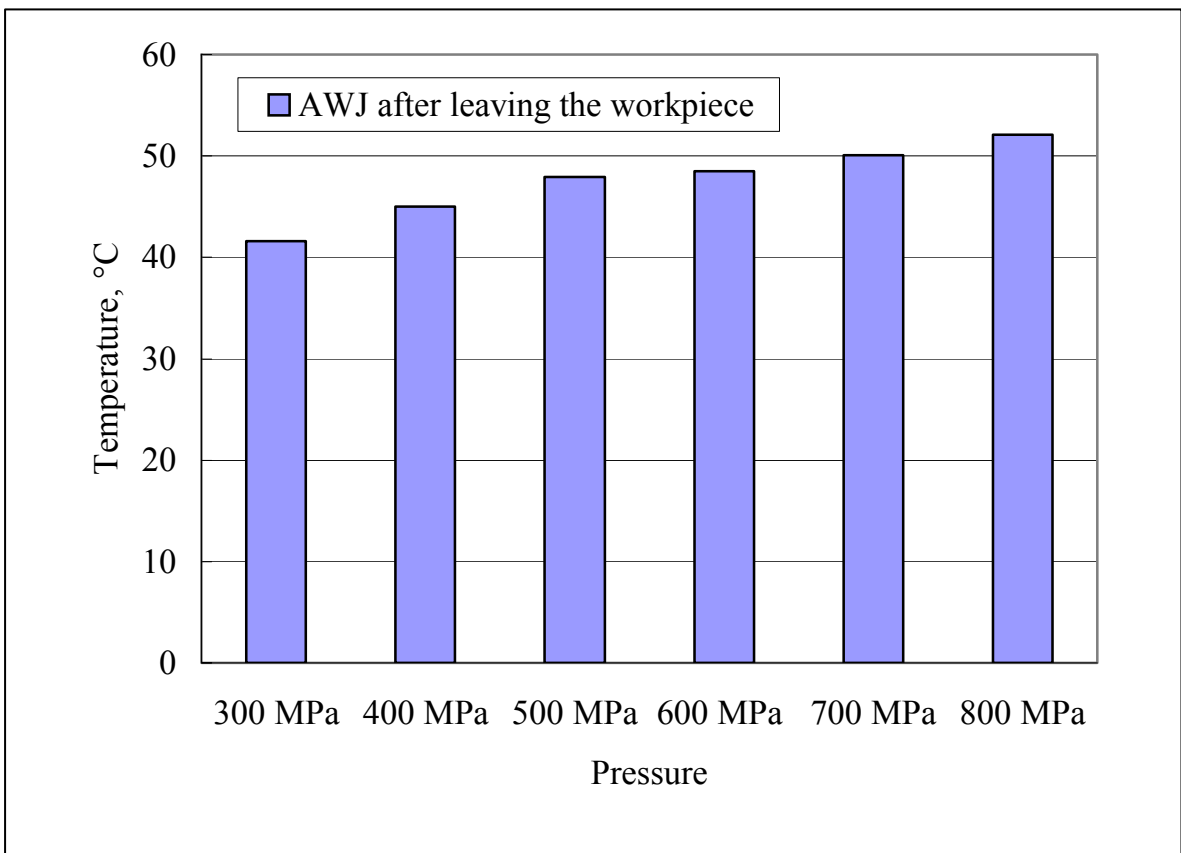


Fig. 6.10: AWJ temperature after leaving the workpiece at different pressure.

## 7. MODELLING OF PLAIN WATERJET CUTTING

This chapter deals with two models are derived to describe the relationship between the operating conditions and the maximum depth of cut for plain waterjet cutting. The first model is the energy model and the second is the semi-empirical model.

### 7.1 The Energy Model

The energy model is based on the penetration of the materials by the waterjet with specific energy, where certain amount of this energy is used to remove the material and the remaining energy is carried away by the exiting waterjet, [104 - 106]. The exiting waterjet contains the energy remained after the cutting process (which not able to removal the materials) and the energy carries the removed debris particles out of the depth of cut as shown in Figure 7.1.

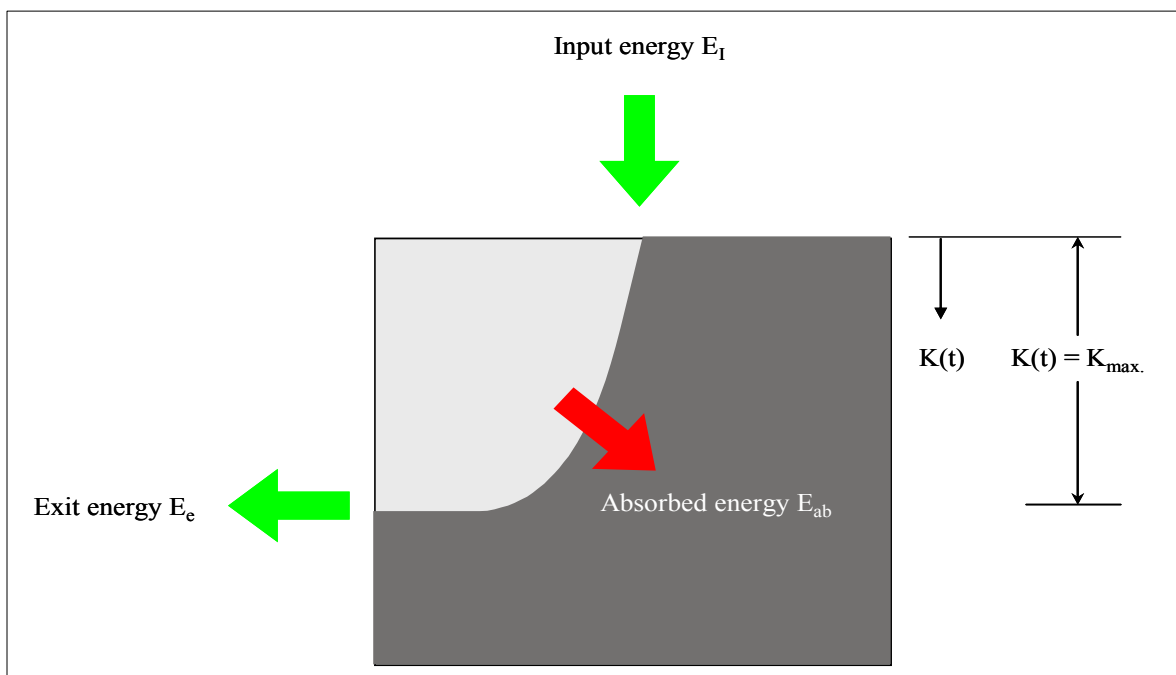


Fig. 7.1: Simplified energy balance during the waterjet cutting.

Based on this condition the energy balance for waterjet cutting can be defined as:

Input energy by waterjet = Absorbed energy in the materials + Exiting Energy

$$E_I = E_{ab} + E_e \quad \rightarrow (7.1)$$

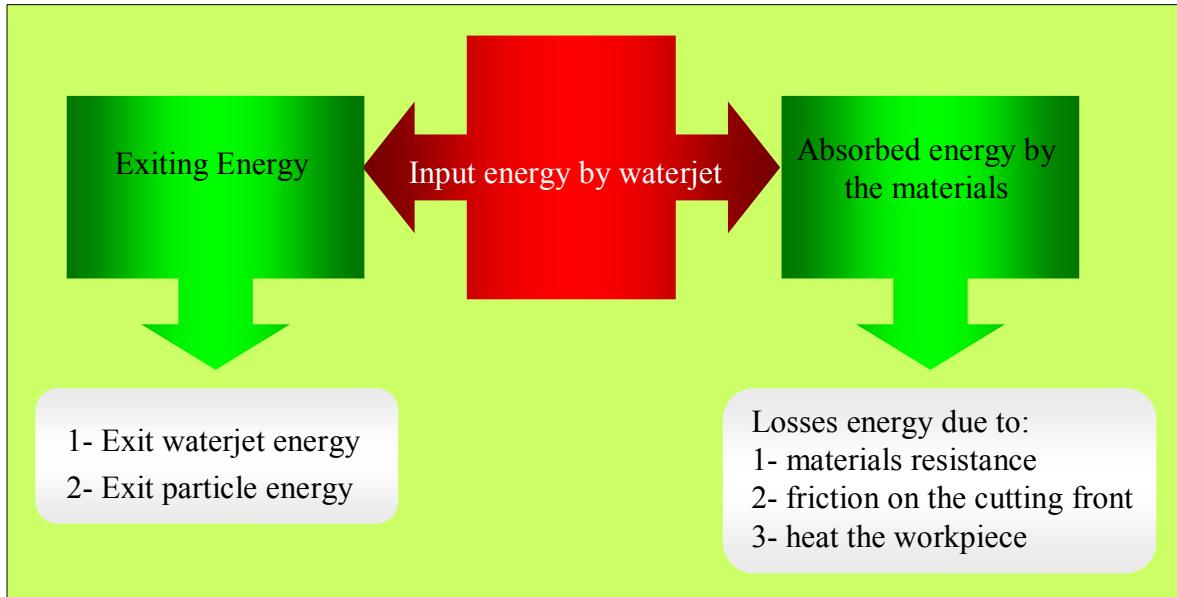


Fig. 7.2: Energy balance schematic diagram.

As shown in Figure 7.2 the absorbed energy in the materials balance as:

Absorbed energy in the materials =      Losses energy due to erosion debris formation (materials resistance)  
 + Losses energy due to friction on the cutting front  
 + Losses energy due to heat the workpiece

$$E_{ab} = E_r + E_f + E_q \quad \rightarrow (7.2)$$

Again we can balance the exiting energy as

Exiting energy = Exit waterjet energy + Exit particle energy

$$E_e = E_{exw} + E_{exp} \quad \rightarrow (7.3)$$



By replaced equations (7.2) and (7.3) to (7.1) can be rewritten as

$$E_I = (E_r + E_f + E_q) + (E_{exw} + E_{exp}) \rightarrow (7.4)$$

Equations (7.4) explained the energy balance at plain waterjet cutting process after estimation each term we can found relationship between the cutting parameters and the maximum depth of cut.

#### a) Calculation of the input energy

The velocity of the waterjet escaping from an orifice can be calculated according to the following Bernoulli's equation:

$$P + \frac{\rho_w}{2} v_0^2 + \rho_w g H_0 = P_{at} + \frac{\rho_w}{2} v_w^2 + \rho_w g H_1 \rightarrow (7.5)$$

For the present conditions, where  $H_0 = H_1$  and neglecting  $P_{at}$  and  $v_0$ . Therefore,  $v_w$  can be expressed as:

$$v_w = \mu \sqrt{\frac{2P}{\rho_w}}, \rightarrow (7.6)$$

where  $\mu$  is a momentum-transfer coefficient considered to compensate the velocity loss due to friction between the water flow and the orifice, fluid flow disturbances and compressibility of water. For the sapphire orifice used in this study  $\mu$  is taken to be 0.95, [101].

The water mass flow rate ( $m_w$ ) is derived from the continuity equation and is expressed as:

$$m_w = \frac{\pi}{4} d_n^2 v_w \rho_w, \rightarrow (7.7)$$

where  $d_n$  is the nozzle diameter.

So, the input energy of waterjet becomes

$$E_i = \frac{1}{2} m_w v_w^2 t \quad \rightarrow (7.8)$$

where  $t$  is the time that can be calculated as follows:

$$t = \frac{V_f}{d_j} \quad \rightarrow (7.9)$$

where  $V_f$  is the traverse speed and  $d_j$  is the waterjet diameter.

The dependency of the waterjet diameter on the standoff distance, ( $S$ ) should be considered. It was observed that the waterjet diameter increased with increasing the standoff distance. This relationship is expressed as follows:

$$d_j = f(S) \quad \rightarrow (7.10)$$

For  $S = 0$ ,  $d_j = d_n$ . Several investigators, [25], attempt to solve equation (7.10). The waterjet as a function of the standoff distance,  $d_{jet}(S)$ , can be reported as:

$$d_j(S) = 0.24 d_n \sqrt{S} \quad \rightarrow (7.11)$$

Substituting equation (7.9) into equation (7.8), the input energy of waterjet can be determined as:

$$E_i = \frac{1}{2} m_w v_w^2 \frac{V_f}{d_j} \quad \rightarrow (7.12)$$

### **b) Calculation of the absorbed energy by the materials**

To calculate the absorbed energy, it is necessary to calculate the material resistance as follows:

$$E_r = \sigma_m A_m k \quad \rightarrow (7.13)$$

where  $\sigma_m$  is the tensile stress and the  $A_m$  is the cross section of the cutting area ( $\pi r_j^2$ ), where  $r_j$  is the radius of the waterjet.

Then the energy losses due to friction on the cutting front, Figure 7.3, should be calculated as:

$$E_f = F_d \times v_j \quad \rightarrow (7.14)$$

where  $F_d$  is the friction drag force =  $\mu_f A \frac{\rho_w v_j^2}{2}$   $\rightarrow (7.15)$ ,

$A$  is the area of friction =  $\frac{\pi}{2} d_j k$ ,  $\mu_f$  is the coefficient of friction and  $v_j$  is the velocity of the waterjet in the cutting kerf. However, not only the velocity of the waterjet changes due to the frictional drag of the kerf on the jet itself, but also the direction of the gradual jet deflection changes. Equation (7.14) can be simplified the as:

$$E_f = \mu_f E_t \quad \rightarrow (7.16)$$

The friction coefficient,  $\mu_f$ , was calculated, [75], as:

$$\mu_f = \frac{0.074}{\left(\frac{v_j k}{\nu}\right)^{0.2}}, \text{ where } \nu \text{ is the liquid dynamic viscosity for hydraulically smooth}$$

$$\text{turbulent flows, and } \mu_f = \left(1.89 + 1.62 \log \frac{k}{k_s}\right)^{-0.25}, 10^2 < \frac{k}{k_s} < 10^6 \text{ for hydraulically}$$

rough turbulent flows where  $k_s$  is the absolute roughness. Typical cuts vary from smooth at the top cutting where the waterjet velocity represents the highest value to rough at the bottom where the waterjet velocity is the lowest. Therefore, the coefficient of frictions will be a mean value between the smooth and rough regimes but the best way is to be determined from experimental data.

As for the energy losses due to heat, there is little information about these losses. In the present study, their value will be assumed as constant determined from experimental data.

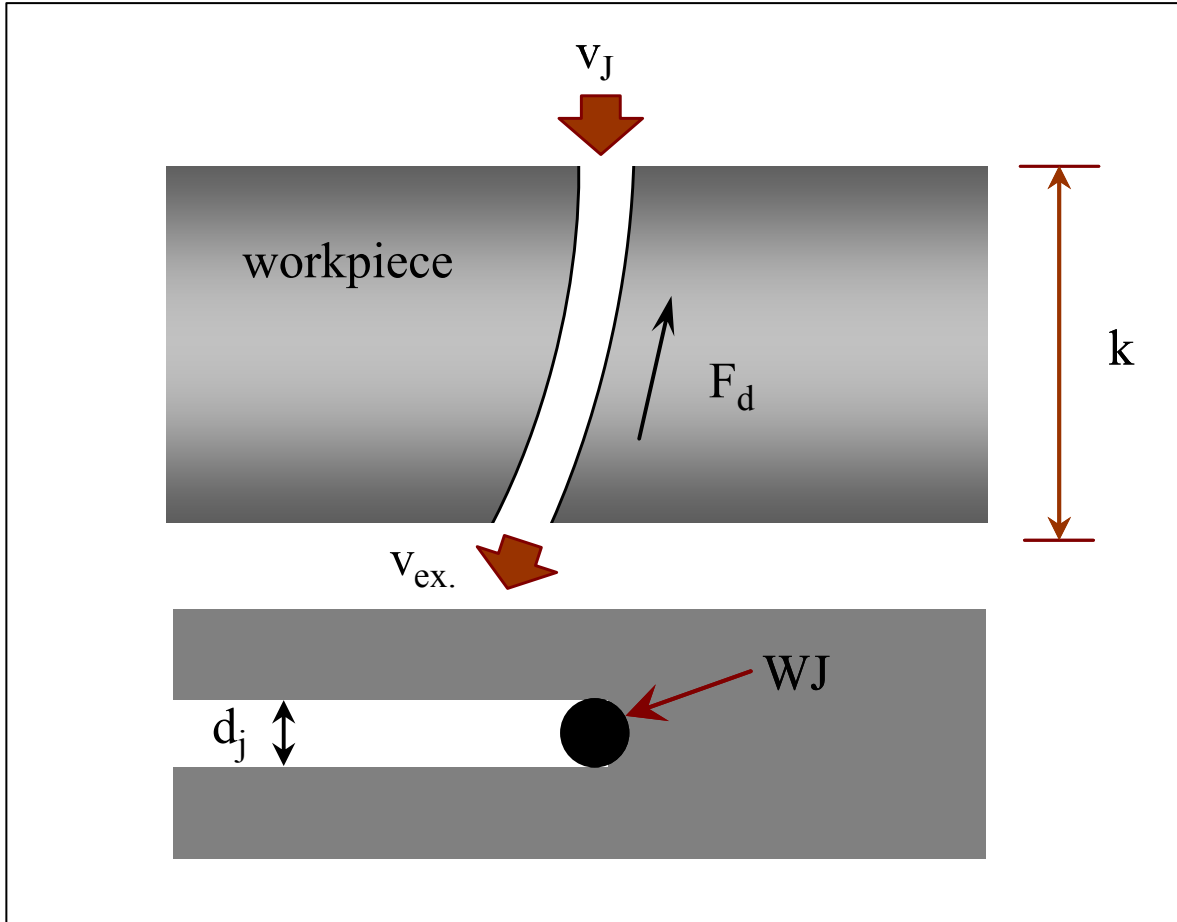


Fig. 7.3: Frictional force at the kerf-jet interface.

### c) Calculation of the exiting energy

The exiting energy can be determined through the calculation of the exit waterjet energy and the exit particle energy. Assuming that water flow rate is constant, the exit waterjet energy can be calculated as follows:

$$E_{exw} = \frac{1}{2} m_w v_e^2 t \quad \rightarrow (7.17)$$

Assuming that the debris particles leave the workpiece with the same velocity as the waterjet exit velocity, the exit particle energy is expressed as follows:

$$E_{\text{exp}} = \frac{1}{2} m_p v_e^2 \quad \rightarrow (7.18)$$

where  $m_p$  is the mass of debris particles

It is noted that the exit velocity of waterjet is equal to the critical velocity of waterjet. The critical velocity of waterjet can be determined by knowing the threshold pressure which represents the minimum value of pressure for cutting process. It was observed that the materials removal take place when the threshold pressure equal to half the yield strength of materials, [75]. It was reported that the threshold pressure for aluminium AlMgSi 0.5 is equal to 55.6 MPa, [48]. This value is about the half of the yield strength of the aluminium. So it is assumed that the threshold pressure  $P_c = 0.5 \sigma_y$  in the present study to determine the waterjet exit velocity.

After calculating all the known terms of the energy balance for waterjet cutting, the relationship between the maximum depth of the kerf and the cutting parameters can be determined as shown in equation 7.19 that derived only in the field of waterjet cutting applications with the following assumptions:

1. The waterjet penetrates the materials with an angle of  $90^\circ$ ,
2. the water flow rate is constant,
3. normally the standoff distance in waterjet cutting is 2 mm so it is assumed that there is no change in the input energy from the nozzle to the workpiece,
4. and there is no change in the width of cut,

$$k = \frac{\frac{c \cdot m_w \cdot d_j}{\rho_w V_f} [\mu^2 (1 - 2\mu_f) P - 0.5\sigma_y]}{A_m \left[ 0.5 \frac{\rho_m}{\rho_w} \sigma_y + \sigma_m \right]} \quad \rightarrow (7.19)$$

where  $k = \text{mm}$ ,  $m_w = \text{kg/min}$ ,  $d_j = \text{mm}$ ,  $\rho_w = \text{kg/litre}$ ,  $V_f = \text{mm/min}$ ,  $P = \text{MPa}$ ,  $\sigma_y = \text{MPa}$ ,  $\sigma_m = \text{MPa}$ ,  $A_m = \text{mm}^2$  and  $c$  is constant for unknown parameters =  $\text{liter/mm}^3$

Actually, the relation between the traverse rate and the kerf depth is not exactly inversely proportional, as given in equations (7.19). Therefore, the traverse speed was considered by a traverse exponent  $n$ . This traverse exponent expresses the energy loss of the jet flowing through the kerf, which increases with increasing the depth of cut. With respect to these considerations, equation (7.19) was modified to:

$$k = \frac{c \cdot m_w \cdot d_j}{\rho_w V_f^n} \left[ \mu^2 (1 - 2\mu_f) P - 0.5\sigma_y \right] \rightarrow (7.20)$$

$$A_m \left[ 0.5 \frac{\rho_m}{\rho_w} \sigma_y + \sigma_m \right]$$

The unknown parameters  $c$ ,  $\mu_f$  and  $n$  were determined and listed in Table 7.1 for sapphire nozzle of 0.08 mm diameter and standoff distance of 2 mm at different pressure, different traverse speed and different materials.

Table 7.1: The values of the constants in equation (7.20)

Materials	Constant $c$ liter/mm <sup>3</sup>	$\mu_f$	$n$
AlMgSi 0,5	4,77	0,02	0,87
Cu	7,63	0,0334	
Amrco-Eisen	5,62	0,0536	
Austenite	3,36	0,094	
Zink	6,92	0,37	

The experimental values of the depth of cut is compared to that calculated from equation (7.20) and plotted in Figure 7.4. It is clearly seen that there is a good correlation between the experimental and calculated depth of cut.

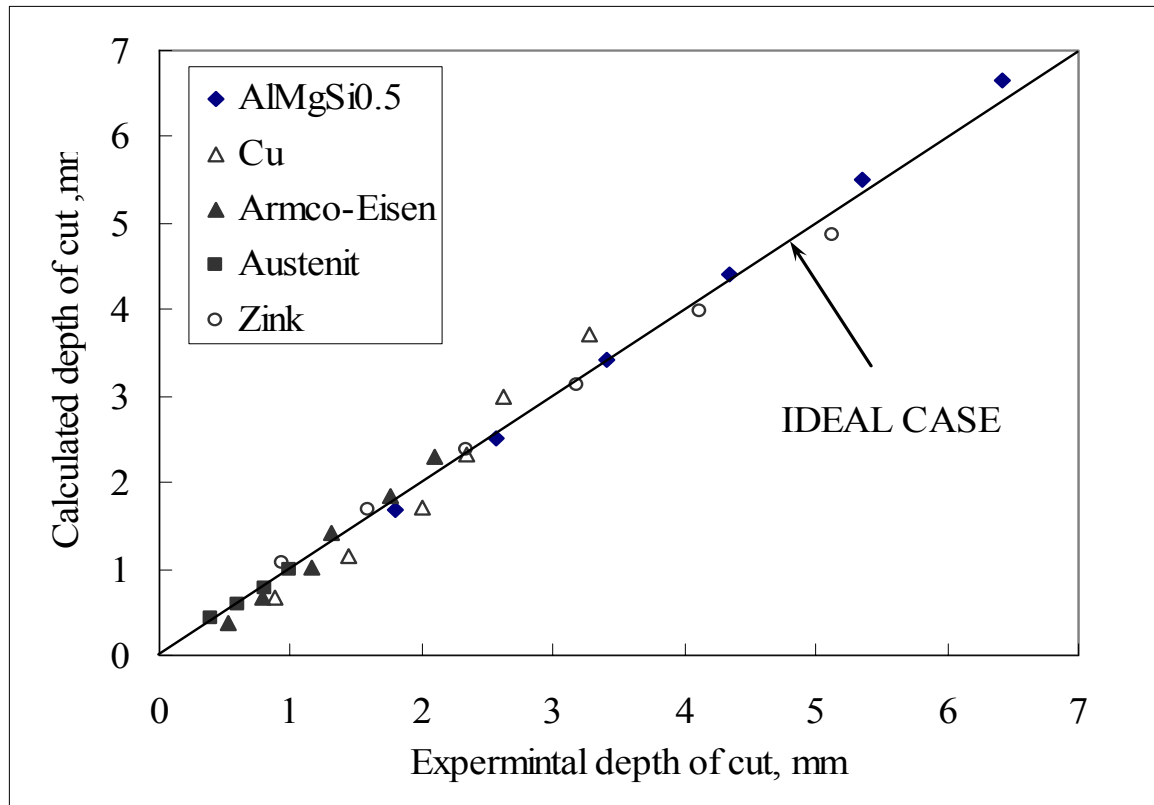


Fig. 7.4: Experimental and calculated depth of cut by equations (7.20).

Although equations 7.20 shows a good correlation between the theoretical and experimental work but it is not able to describe the effect of standoff distance to be used in a wide applications for waterjet such as cleaning and decoating. It is recommended that more investigations are required in the future work to determine the input energy as a function of standoff distance to modify equation 7.20.

## 7.2 The Semi-Empirical Model

Several theoretical attempts were made to model the abrasive waterjet cutting but little attention was exerted to model the plain waterjet cutting especially in the cutting process of metals. Even though all published formulae need specific coefficients, which have to be determined by experimental results. This indicates that basic problems in describing the cutting process obviously exist. On one hand the parameters, which are needed for a physically based analysis of the cutting process, like impact velocity and impact angle of the waterjet can only be evaluated with a wide

inaccuracy. From this background, in the present work, a semi-empirical equation for the prediction of plain waterjet cutting performance has been developed.

It is known that the maximum depth of cut is proportional to the pressure as well as the nozzle diameter and inversely proportional to the traverse rate and the standoff distance. So the empirical relationship can be written as

$$k = \frac{AP^a d_n^b}{V_f^c S^d} \rightarrow (7.21)$$

where A is an empirical coefficient depends on the properties of the materials and erosion mechanisms and symbolizes the resistance of materials against the loading by waterjet and a, b, c and d are factors calculated by a large number of experimental data. The constants in equation 7.21 are calculated for AlMgSi0.5 with a good correlation coefficient of 0.955 and can be rewritten as:

$$k = \frac{0,159P^{1.29}d_n^{1.42}}{V_f^{0.623}S^{0.093}} \rightarrow (7.22)$$

Equation 7.22 is modified to be applied using other engineering materials by material characteristic parameter named “Machinability Number”. It should have a unique value for a certain workpiece material. The value of  $N_m$  for any material can be determined from the experimental data and the following equation:

$$k = \frac{0,159N_m P^{1.29}d_n^{1.42}}{V_f^{0.623}S^{0.093}} \rightarrow (7.23)$$

The “Machinability Number” value calculated from experimental data for deferent materials is shown in Figure 7.5. It is clear that  $N_m$  decreases with increasing the strength of materials and is different from the value obtained by abrasive waterjet as reported before, [89]. For example, the Machinability Number for austenite for abrasive waterjet cutting is 0.40, but for plain waterjet it is approximately half the value observed for AWJ (0.19). The variation of the “Machinability Number” for



abrasive and plain waterjet may be attributed to the different cutting mechanisms. The experimental verification of the semi-empirical model is shown in Figure 7.6.

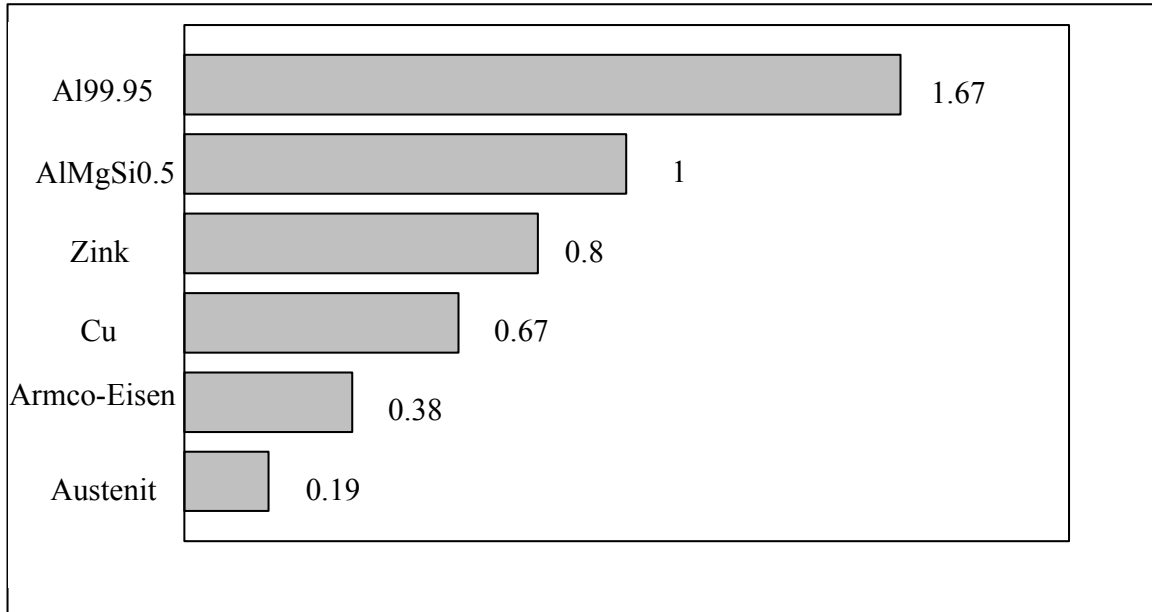


Fig. 7.5: Machinability Number ( $N_m$ ) for different materials cut by plain waterjet.

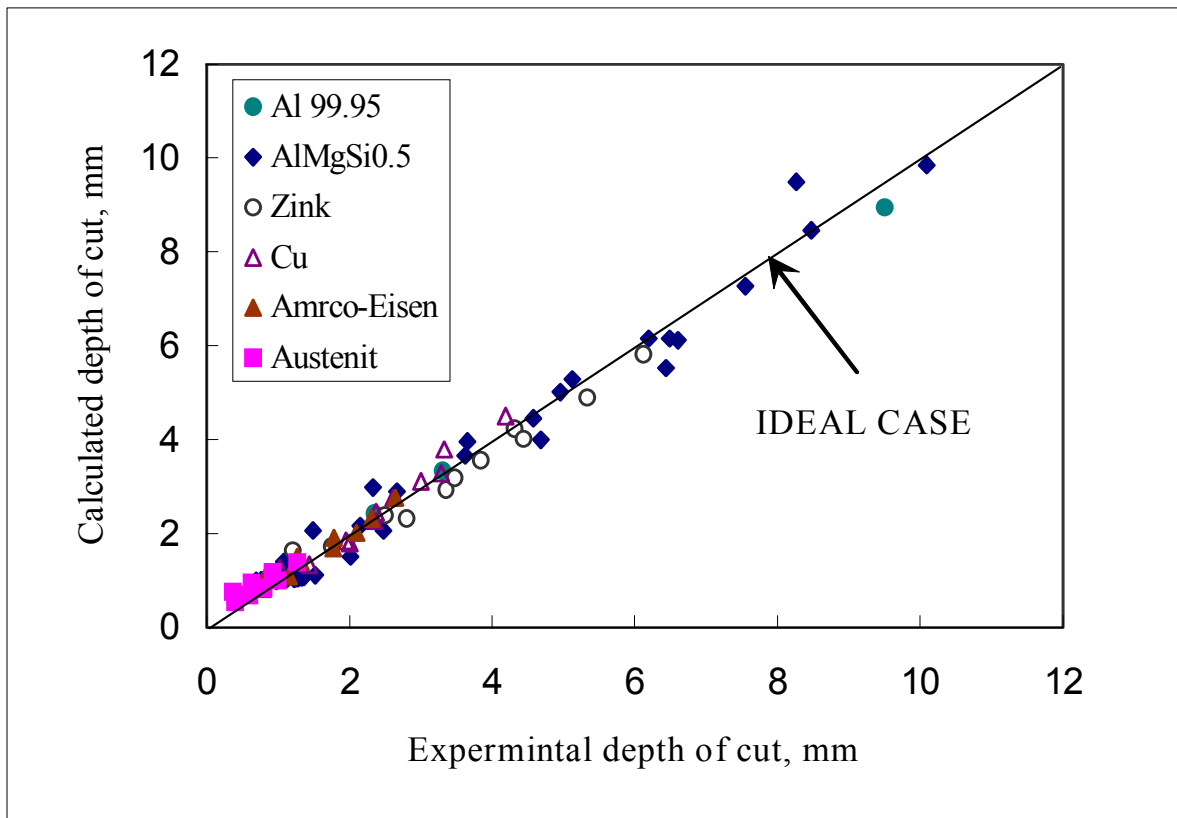


Fig. 7.6: Experimental verification of the semi-empirical model.

The verification of the effect of pressure on the depth of cut by a semi-empirical model, equations 7.23, is plotted in Figure 7.7. The data calculated assuming the machining parameters used in the experiments, 0,08 mm nozzle diameter, 2 mm standoff distance, 10 mm/min traverse rate and AlMgSi 0,5 as workpiece materials. The verification of the effect of nozzle diameter on the depth of cut using a semi-empirical model, equation 7.23, is shown in Figure 7.8. It is clear that a good correlation between the experimental and the calculated data was found.

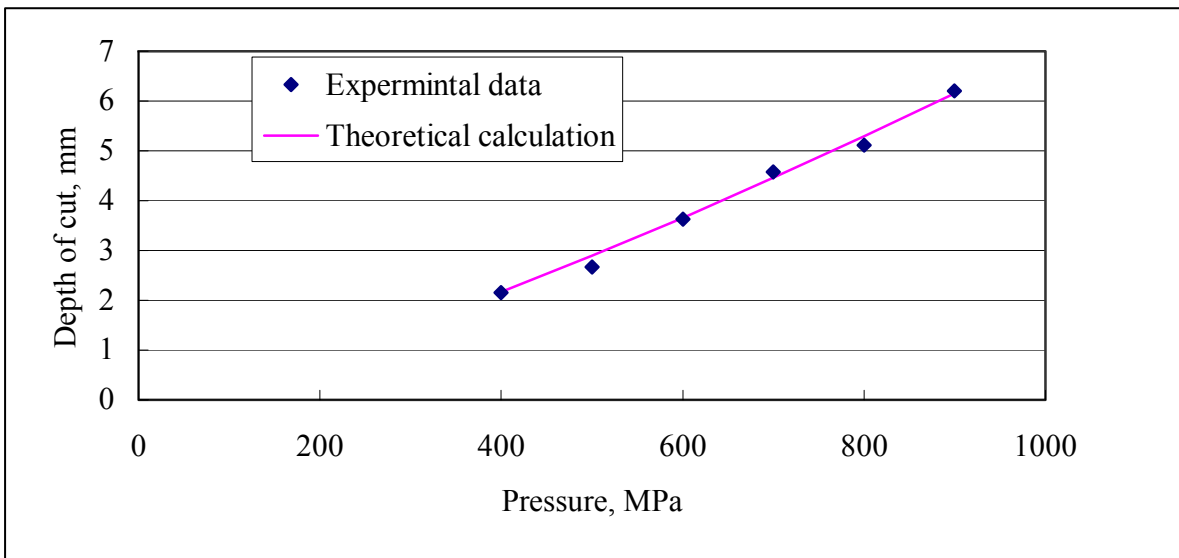


Fig. 7.7: Experimental and calculated data as a function of pressure.

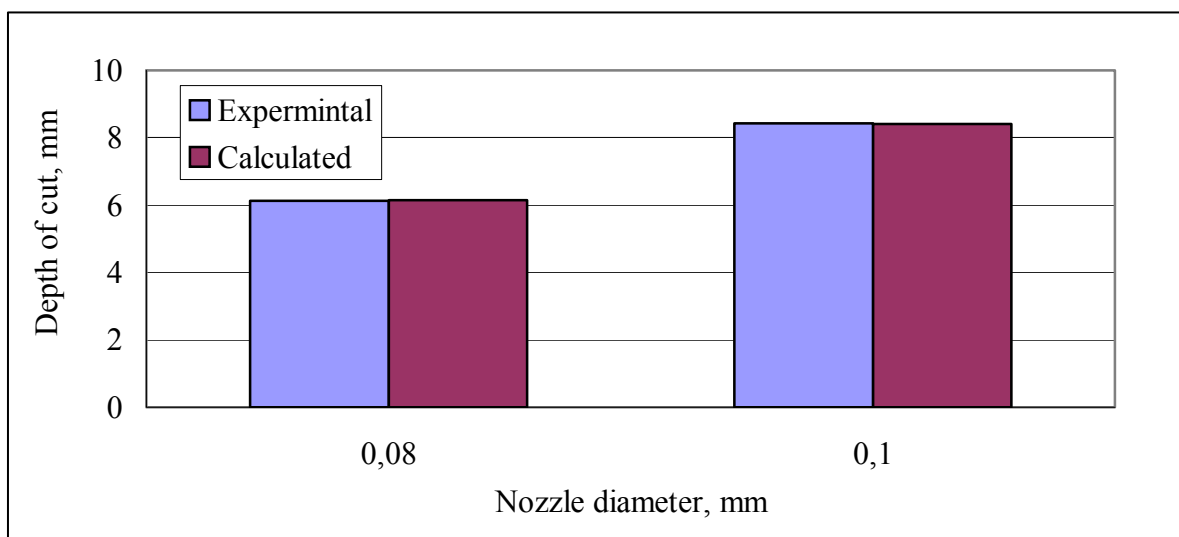


Fig. 7.8: Experimental and calculated data as a function of nozzle diameter.

## 8. OUTLOOK AND CONCLUSIONS

The last chapter in this thesis described the remaining difficulties either in the development or manufacture of the 900 MPa cutting system technology and the conclusions of the investigations.

### 8.1 A 900 MPa Cutting System Technology

Besides the benefit obtained from the increase of the working pressure up to 900 MPa, as explained in chapter 5 and summarized in section 8.2, the loading of the components has a negative influence on their lifetime. Inspection of the nozzle after experiments carried out using 900 MPa pressure reveals that the nozzle permanent plastic deformation and the length was reduced as shown in Figure 8.1. This reduction in the length is usually happened during experiments carried out with pressure above 600 MPa which exceeds the tensile strength of the nozzle body material (austenite). Also for the orifice used normally up to 420 MPa, this high pressure reaches their limits. Figure 8.2 (A, B, C and D) show that the nozzle suffered a kind of distortion due to working at 900 MPa Pressure.

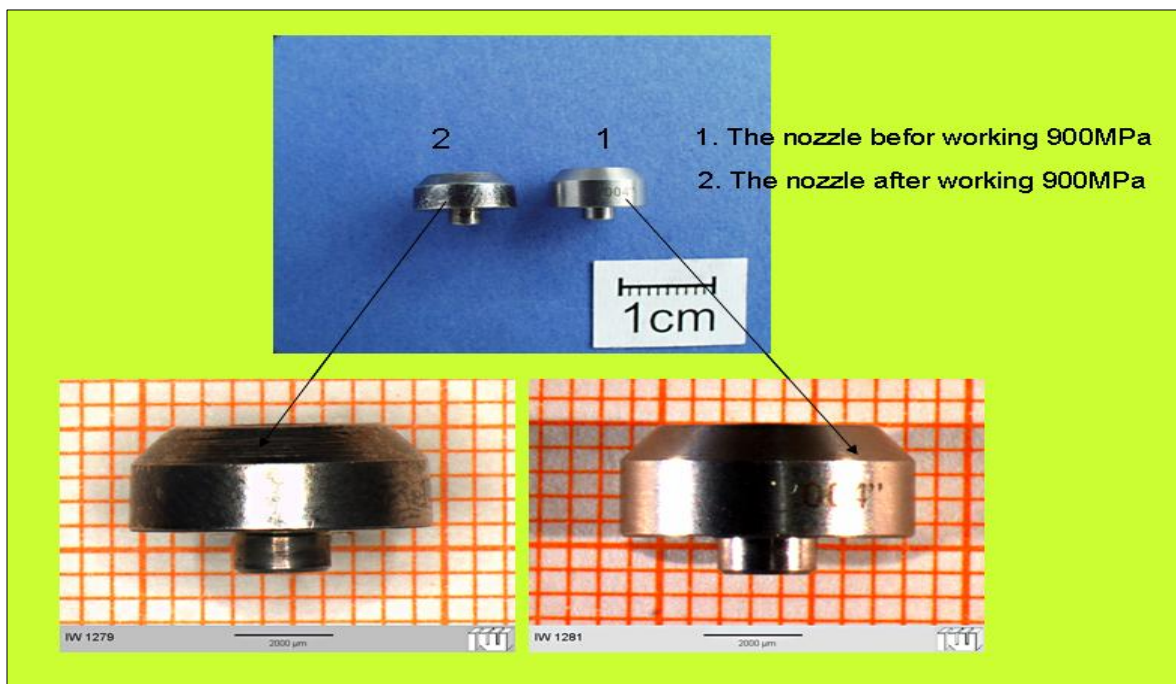


Fig. 8.1: Dimensional changes occurred to the nozzle after 900 MPa pressure.

Due to the high pressure difference from atmospheric pressure to 900 MPa, the dynamic loading applied to the nozzle during the process is very high. A special construction and materials of the nozzle system should be designed to protect the nozzle deformation as explained above.

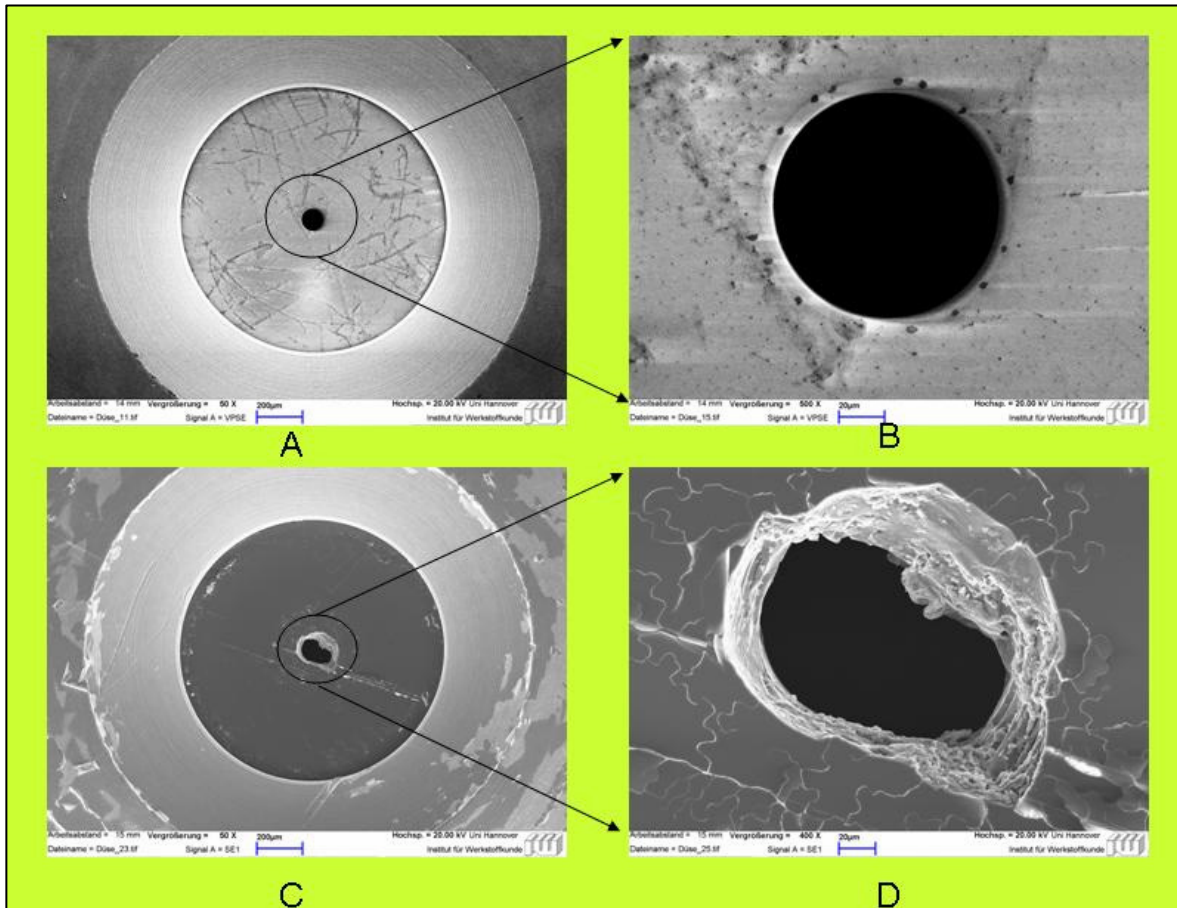


Fig. 8.2: (A and B): The nozzle before working with 900 MPa.

Fig. 8.2: (C and D): The failed nozzle after working with 900 MPa.

## 8.2 Conclusions

The conclusions can be summarized as follows:

1. The risk of water freezing at 900 MPa pressure at inlet temperatures between 10 and 15 °C is not relevant due to the adiabatic heating caused by the pressure and due to friction in the pump, the couplings and the hoses. The accompanied temperature rise prevented the ice formations.

2. Increasing pressure of water leads to an increase of cutting efficiency of plain waterjet as well as abrasive waterjet.
3. The mathematical relationship between the working pressure and the depth of cut is linear for all the tested materials in the case of waterjet or abrasive waterjet cutting.
4. Sheet metal can be cut to a certain extent (thickness, hardness) with plain waterjet. The depth of cut increased from 1.4 mm at pressure of 300 MPa to 8.2 mm at pressure of 900 MPa for cutting aluminium as explained in chapter 5.
5. The optimal value for abrasive flow rate increased by increasing the working pressure. The flow rate was 0.55 and 0.8 g/s at a pressure of 300 and 600 MPa respectively.
6. In abrasive waterjet cutting there is an optimal nozzle diameter to give maximum depth of cut depending on the used abrasive focus diameter.
7. The maximum temperature, for nozzle holder at plain waterjets and for focusing tube at abrasive waterjets, increased by increasing the working pressure.
8. Waterjet cutting and abrasive waterjet cutting are classified as cold cutting process. The analysis shows that this description from the technological point of view is correct, because the critical temperatures for the tested materials, which can influence the material structure or properties, are much higher than the temperatures measured during the cutting process using waterjet or abrasive waterjet.
9. Two models are derived to describe the relationship between the operating conditions and the maximum depth of cut for plain waterjet cutting. The first model is the energy model and the second is the semi-empirical model. The two models presented good correlations between the experimental results and theoretical calculations.
10. The surface topography generated by waterjet shows different appearance compared to the abrasive waterjet cutting because of the change of the cutting mechanism.

11. In the study of the cutting mechanism by waterjet cutting the material loaded by repeating dynamic loading and the material removal is occurred for all the tested materials by the effect of shear stress.
12. The topography of the machined surface depends on the type of the tested materials. The variation of the effect of waterjet impact for ductile materials (aluminium), for materials having less ductile (Armco-iron) and for brittle materials (zinc) was observed.
13. The standoff distance and traverse rate (loading time) are greatly influencing the topography of the surface, while increasing the working pressure and nozzle diameter has no significant effect to the surface topography.
14. The loading of components above 500 MPa has a negative influence on their lifetime as explained in section 8.1.

## REFERENCES

- [1] Louis, H.: Grundlagen der Wasserstrahlanwendung. Interdisziplinäres Symposium mit Live-Operationen und Work-Shop über Wasserstrahl-dissektion in der Medizin. (1999), S. 31/41
- [2] Momber, A. W., and Kovacevic, R.: Principles of abrasive water jet machining. Springer, 1998
- [3] Summers, D. A.: Waterjetting technology. E & F Spon, 1995
- [4] Hashish, M.: The waterjet as a tool. 14<sup>th</sup> International Conference on Jetting Technology. 1998
- [5] Brandt, St., Louis, H., Milchers, W., Mohamed, M., Pude, F., and von Rad, Chr.: Abrasive water jets a flexible tool for nonconventional machining. Proceedings of the 19<sup>th</sup> All India Manufacturing Technology, Design and Research Conference, (2000), S. 129/134
- [6] Hashish, M.: Cutting and drilling at 690 MPa. 10<sup>th</sup> American Waterjet Conference. (1999), S. 137/152
- [7] Hashish, M., Steele, D., and Bothell, D.: Machining with super-pressure (690 MPa) waterjets. In: International Journal of Machine Tools Manufacturing, Volume 37, No. 4, (1997), S. 465/479
- [8] Hashish, M.: Observations on cutting with 600-MPa waterjets. In: Journal of Pressure Vessel Technology, Volume 124, (2002), S. 229/233
- [9] Trieb, F., and Zamazal, K.: 800 MPa ultra high pressures for cutting applications. Anlage zum AWT-Forum, Arbeitskreis Wasserstrahl-technologie Uni-Hannover, 2000
- [10] Trieb, F., and Zamazal, K.: Waterjet cutting 300 MPa high pressure to 800 MPa ultra high pressures. 6<sup>th</sup> Pacific Rim International Conference on Water Jetting Technology. (2000), S. 186/190
- [11] Trieb, F., and Zamazal, K.: 800MPa pure waterjet and abrasive waterjet cutting-what's next. Proceedings of the 2001 WJTA American Waterjet Conference. (2001), S. 797/807
- [12] Oweinah, H.: Leistungssteigerung des Hochdruckwasserstrahl-schneidens durch Zugabe von Zusatz- Stoffen. Ph.D. Thesis, Technische Hochschule Darmstadt, 1989

- 
- [13] Rhagavan, C., and Ting, E.: Hyper pressure waterjet cutting of thin sheet metal. 6<sup>th</sup> American Waterjet Conference. (1991), S. 493/504
- [14] Koerner, P., Hiller, W., and Werth, H.: Design of reliable pressure intensifiers for water-jet cutting at 4 to 7 kbar. 16<sup>th</sup> International Conference on Water Jetting. (2002), S. 123/132
- [15] Imanaka, O., Fujino, S., Shinohara, K., and Kawate, Y.: Experimental study of machining characteristics by liquid jets of high power density up to  $10^{18}$  W/cm<sup>2</sup>. 1<sup>st</sup> International Symposium on Jet Cutting Technology. (1972), S. G3-25/G3-35
- [16] John, Xu., Kevin, O., Mark, H., Reynold, S., and Jude, L.: Hyper pressure waterjet and abrasive waterjet cutting. 10<sup>th</sup> American Water Jet Conference. (1999), S. 127/135
- [17] Tammann, G.: Über die Grenzen des festen Zustandes IV. In: Annalen der Physik, series 4, (1900), S. 1/31
- [18] Victor, F., and Robert, W.: Physics of ice. Oxford University Press Inc, New York, 1999
- [19] Bridgman, P.: The phase diagram of water to 45,000 kg /cm<sup>2</sup>. In: Journal of Chemical Physics Volume 5, Nr.1-12, (1937), S. 964/966
- [20] Bridgman, P.: The physics of high pressure. London: G. Bell and Sons, Ltd. 1952
- [21] Wagner, W., Saul, A., and Pruß, A.: International equations for the pressure along the melting and along the sublimation curve of ordinary water substance. In: Journal Physics Chemical Reference data, Volume 23, No.3, (1994), S. 515/525
- [22] Wagner, W. and Pruß, A.: The IAPWS formulation 1995 for the thermodynamic properties of ordinary water substance for general and scientific use. In: J. Phys. Chem. Ref. Data, Volume 31, No. 2, (2002) S. 387/535
- [23] Andreas Pruß: Eine neue Fundamentalgleichung für das fluide Zustandsgebiet von Wasser für Temperaturen von der Schmelzlinie bis zu 1273 K bei Drücken bis zu 1000 Mpa. Ph.D. Thesis, University of Bochum, Fortschritt-Berichte VDI, Reihe 6, Nr. 320. Düsseldorf: VDI-Verlag 1995



- 
- [24] Heide Koch: Einfluß von Hochdruck auf Phasenübergänge Wasser-Eis und dessen Nutzung zur Konservierung in der Lebensmittel- und Biotechnologie. In: DKV-Tagungsbericht. (1996), S. 141/160
- [25] Wayne Burnham, C., Holloway, J. R., and Davis, N. F.: The specific volume of water in the range 1000 to 8900 bars, 20° to 900°C. In: American Journal of Science, Volume 265-A, (1961), S. 70/95
- [26] Truckenbrodt, E.: Strömungsmechanik. Berlin, Heidelberg, New York, Springer Verlag 1968
- [27] Tait, P.G.: Report on some of the physical properties of fresh water and sea water. In: Phys. Chem. Z., (1888), S. 1/71
- [28] Bridgman, P.: Thermodynamic properties of liquid water to 80° and 12000 KGM. In: Proceedings of the American of Arts and Science, Volume XLVIII, No. 9, (1912), S. 309/362
- [29] Yanaida, K.: Flow characteristics of water jets. 2<sup>nd</sup> International Symposium on Jet Cutting Technology. (1974), S. A2-19/A2-32
- [30] Yanaida, K., and Ohashi, A.: Flow characteristics of water jets in air. 4<sup>th</sup> International Symposium on Jet Cutting Technology. (1978), S. A3-39/A3-54
- [31] Shavlovsky, D. S.: Hydrodynamics of high pressure fine continuous jets. 4<sup>th</sup> International Symposium on Jet Cutting Technology. (1978), S. A6/A81
- [32] Hlavág, L.M., Hlavágová, I.M., Mádr, V.: Quick method for determination of the velocity profile of the axial symmetrical supersonic liquid jet. 10<sup>th</sup> American Waterjet Conference. (1999), S. 189/199
- [33] Milchers, W.: Abtrag von Polymeren mit dem reinen Wasserstrahl. Ph.D. Thesis, University of Hannover. Fortschritt-Berichte VDI, Reihe 5, Nr. 639. Düsseldorf: VDI-Verlag, 2001
- [34] Louis, H., Polak, H., Pude, F., and Schenk A.: Pure WJ cleaning process characterization: approach and technologies. Proceedings of the 6<sup>th</sup> International Conference on management of Innovative technologies Piran, Slovenia. (2003), S. 111/118
- [35] Neusen, K. F., Gores, T. G., and Amano, R. S.: Axial variation of particle and drop velocities downstream from an abrasive water jet mixing tube. 12<sup>th</sup> International Conference on Jet Cutting Technology. (1994), S. 93/103

- 
- [36] Tikhomirov, R.A, Babanini, V.B., Pethukov, E.N.: High pressure jet cutting. ASME press, New York, 1992
- [37] Cheroudi, B., Onuma, Y., Chen, S. H., and Bracco, F. V.: On the intact core of fullcone sprays. SAE Paper 850126, 1985
- [38] Arai, M., Tabat, M., and Hiroyasu, H.: Disintegration process and spray characterisation of fuel jet injected by a diesel nozzle. SAE Paper 840275, 1985
- [39] Cadavid, R., and Wüstenberg, D.: Enhancing the coherent length of cutting waterjets. 16<sup>th</sup> International Conference on Water Jetting. (2002), S. 279/286
- [40] Christoph von Rad: Leistungssteigerung von Wasser-und Wasserabstrahlstrahlen durch Polymerzusatz. Ph.D. Thesis, University of Hannover. Fortschritt-Berichte VDI, Reihe 2, Nr. 638. Düsseldorf: VDI-Verlag, 2003
- [41] Wu, P.-K., Tseng, L.-K., and Faeth, G.-M: Primary break-up in gas/liquid mixing layers for turbulent liquids. In: Atomization and Sprays, Nr. 2, (1992), S. 295/317
- [42] Andrzej Perec: Possibilities of materials machining with an hydro abrasive waterjet under 1000 MPa pressure. Proceedings of the 3<sup>rd</sup> International Conference on Machining and Measurements of Sculptured Surfaces, Krakow, (2003), S. 435/444
- [43] Anuja Dorle, John Tyler, L., and David A. Summers: Measurement of particle velocities in high speed waterjet technology. 2003 American Waterjet Conference (released on CD), 2003
- [44] Chen, W.-L., E. S. Geskin: Measurements of the velocity of abrasive waterjet by the use of laser transit anemometer. 10<sup>th</sup> International Symposium on Jet Cutting Technology. (1990), S. 23/36
- [45] Neusen, K. F., Gores, T. J., and Labus, T. J.: Measurement of particle and drop velocities in a mixed abrasive water jet using a forward-scatter LDV system. 11<sup>th</sup> International Conference on Jet Cutting Technology (1992), S. 63/73
- [46] Swanson, R. K., Kilman, M., Cerwin, S., and Tarver, W.: Study of particle velocities in water driven abrasive jet cutting. 4<sup>th</sup> American Waterjet Conference. (1987), S. 103/107

- 
- [47] Liu, H.-T., Miles, P. J., Cooksey, N., and Hibbard, C.: Measurements of water-droplet and abrasive speeds in a ultrahigh-pressure abrasive-waterjets. 10<sup>th</sup> American Waterjet Conference. (1999), S. 201/216
- [48] Blickwedel, H.: Erzeugung und Wirkung von Hochdruck-Abrasivestrahlen, Ph.D. Thesis, University Hannover, 1990
- [49] Himmelreich, U.: Fluiddynamische modelluntersuchungen an Wasserabrasivstrahlen. Ph.D. Thesis, University of Hannover. Fortschritt-Berichte VDI, Reihe 7, Nr. 219. Düsseldorf: VDI-Verlag 1993
- [50] Louis H., Mohamed, M., and Pude, F.: Cutting mechanism and cutting efficiency for water pressures above 600 MPa. 2003 American Waterjet Conference (released on CD), 2003
- [51] Adler, W. F.: The mechanisms of liquid impact. In: Treatise on Materials Science and Technology, Volume 16, (1979), S. 127/183
- [52] Beutin, E. F., Erdmann-Jesnitzer, F., and Louis, H.: Material behaviour in the case of high-speed liquid jet attacks. 2<sup>nd</sup> International Symposium on Jet Cutting Technology, (1974), S. C1-1/C1-18
- [53] Beutin, E. F., Erdmann-Jesnitzer, F., Hassen A. M., and Louis, H.: A new technique in the application of high speed water jet. 3<sup>rd</sup> International Symposium on Jet Cutting Technology. (1976), S. F2-15/F2-22
- [54] Erdmann-Jesnitzer, F., Louis, H., and Wiedemeier, J.: Material behaviour, material stressing and principle aspects in the application of high speed water jets. 4<sup>th</sup> International Symposium on Jet Cutting Technology. (1978), S. E3-29/E3-44
- [55] Erdmann-Jesnitzer, F., Louis, H., and Wiedemeier, J.: The action of high speed water jets on materials. 5<sup>th</sup> International Symposium on Jet Cutting Technology. (1980), S. B3-75/B3-86
- [56] Franz, N. C.: The influence of standoff distance on cutting with high velocity fluid jets. 2<sup>nd</sup> International Symposium on Jet Cutting Technology. (1974), S. B3-27/B3-46
- [57] Beutin, E. F., Erdmann-Jesnitzer, F., and Louis, H.: Anwendung von Flüssigkeitsschlag. In: Metall 27, Volume 1, (1973), S. 14 /10
- [58] Thomas, G. P., and Brunton, J. H.: Drop impingement erosion of metals. In: Proc. Roy. Soc. London. (1970), S. 549/565

- 
- [59] Bowden, F.P., and Brunton, J. H.: The deformation of solids by liquid impact at supersonic speeds. Proc. Roy. Soc. London. (1961), S. 433/450
- [60] Kang, S-W., Reitter, T., and Carlson, G.: Target responses to the impact of high-velocity non-abrasive water jets. 7<sup>th</sup> American Water Jet Conference. (1993), S. 71/86
- [61] Bowden, F.P., and Field, J.E.: The brittle fracture of solids by liquid impact, by solid impact and by shock. Proc. Roy. Soc. London. (1964), S. 331/3521
- [62] Mabrouki, T., Cornier, A., and Raissi, K.: The study of HP pure waterjet impact as the primary mechanism of paint decoating process. 14<sup>th</sup> International Conference on Jetting Technology. (1998), S. 563/577
- [63] Mabrouki, T., Raissi, K., and Cornier, A.: Numerical simulation and experimental study of the interaction between a pure high-velocity waterjet and targets: contribution to investigate the decoating process. In: Wear, Volume 239, (2000), S. 260/273
- [64] Louis, H.: Beanspruchbarkeit fester Werkstoffe durch Flüssigkeitsstrahlen. Habilitationsschrift. Technische Universität Hannover, 1979
- [65] Peter J. Blau: Friction, lubrication and wear technology. In: ASM International-Handbook Committee. Volume 18, (1992), S. 221/232
- [66] Yong, Z., and Kovacevic, R.: Effects of water-mixture film on impact contact in abrasive waterjet machining. In: International Journal of Mechanical Sciences, Volume 39, No. 6, (1997), S. 729/739
- [67] Hashish, M.: A modelling study of metal cutting with abrasive waterjets. In: Journal of Engineering Materials and Technology, Volume 106, No. 1, (1984), S. 88/100
- [68] Hashish, M.: Visualization of the abrasive-waterjet cutting process. In: Experimental Mechanics. (1988), S. 159/169
- [69] Guo N. S., Louis, H., and Meier, G.: Surface structure and kerf geometry in abrasive water jet cutting: formation and optimization. 7<sup>th</sup> American Waterjet Conference. (1993), S. 1/25
- [70] Guo, N. S.: Schneidprozess und Schnittqualität beim Wasserabrasivstrahlschneiden. Ph.D. Thesis, University of Hannover, Fortschritt-Berichte VDI, Reihe 2, Nr. 328. Düsseldorf: VDI-Verlag 1994
- [71] Neelesh K. Jain and Vijaz K. Jain.: Modelling of material removal in mechanical type advanced machining processes: a state-of-art review. In:

- International Journal of Machine Tools & manufacture, Volume 41, (2001), S. 1573/1635
- [72] Hoogstrate, A. M.: Towards high-definition abrasive waterjet cutting. Ph.D. thesis, University of Delft, 2000
- [73] Hashish, M., and DuPlessis, M. P.: Theoretical and experimental investigation of continuous jet penetration of solids. In: Journal of Engineering for Industry, Volume.100, (1978), S. 88/94
- [74] Hashish, M., and DuPlessis, M. P.: Prediction equations relating high velocity jet cutting performance to stand-of-distance and multipasses: In: Journal of Engineering for Industry, Volume 101, (1979), S. 311/318
- [75] Mohamed Hashish.: Theoretical and experimental investigation of high velocity water jet cutting. Ph.D. thesis, University of Concordia, 1977
- [76] Hashish, M., and DuPlessis, M. P.: Jet cutting studies. Proceedings of the sixth Canadian of Applied Mechanics, Vancouver, (1977), S. 719/720
- [77] Cooly, W. C.: Correlation of data on jet cutting by water jets using dimensionless parameters. 2<sup>nd</sup> International Symposium on Jet Cutting Technology, (1974), S. H4-39/H4-48 H4
- [78] Frank, N. and P. D. Lohn: Fragmentation of native copper ores with hydraulic jets. 2<sup>nd</sup> International Symposium on Jet Cutting Technology, (1974), S. H3-29/H3-38
- [79] Matsui, S., Matsumara, H., Ikemoto, Y., Kumon, Y., and Shimizu, H.: Prediction equations for depth of cut made by abrasive water jet. 6<sup>th</sup> American Water Jet Conference, (1991), S. 31/41
- [80] Kovacevic, R.: Monitoring the depth of abrasive waterjet penetration. In: International Journal of Machining and Tools Manufacturing, Volume 32, (1992), S. 725/736
- [81] Zeng, J., and Kim, T. J.: Development of an abrasive water jet kerf model for brittle materials. 11<sup>th</sup> International Conference on Jet Cutting Technology. (1992), S. 483/501
- [82] Zeng J., and Kim, T. J.: Parameter prediction and cost analysis in abrasive waterjet cutting operations. 7<sup>th</sup> American Water Jet Conference. (1993), S. 175/189

- 
- [83] Hashish, M.: A model for abrasive water jet machining. In: Journal of Engineering Materials and Technology, Volume 111, (1989), S. 154/162
- [84] Finnie, I.: The mechanism of erosion of ductile metals. Proceedings of the 3rd National Congress of Applied Mechanics, ASME, (1985), S. 527/532.
- [85] Finnie, I.: Erosion and cavitations. ASTM STP 307. (1962), S. 70/82
- [86] Bitter, J. G. A.: A study of erosion phenomena-Part I. In: Wear, Volume 6, (1963), S. 5/21
- [87] Bitter, J. G. A.: A study of erosion phenomena -Part II. In: Wear, Volume 6, (1963), S. 169/190
- [88] Chung, Y., Geskin, E. S., and Singh, P.: Prediction of the geometry of the kerf created in the course of abrasive waterjet machining of ductile materials. 11<sup>th</sup> International Conference on Jet Cutting Technology. (1992), S. 525/541
- [89] Blickwedel, H., Guo, N.S., Haferkamp, H., and Louis H.: Prediction of Abrasive Jet Cutting Performance and Quality. 10th International Conference on Jet Cutting Technology. (1990), S. 163/179
- [90] Hlavac L.: Physical description of high energy liquid jet interaction with material. Geomechanics 91. (1992), S. 341/346
- [91] Bellman, R. Jr., and Levy, A.: Erosion mechanism in ductile metals. In: Wear, Volume 70, (1981), S. 1/28
- [92] Foley, T., and Levy, A.: The erosion of heat treated steels. Wear, Volume 91, (1983), S. 45/64
- [93] Preece, B. M., and Brunton, J. H.: A comparison of liquid impact erosion and cavitations erosion. In: Wear, Volume 60, (1980), S. 269/283
- [94] Guo, N. S., Louis, H., Meier, G., and Ohlsen, J.: Abrasive water jet cutting – methods to calculate cutting performance and cutting efficiency, Geomechanics 93. (1994), S. 291/299
- [95] Hashish, M.: Experimental studies of cutting with abrasive waterjets. 2<sup>nd</sup> American Waterjet Conference. (1983), S. 402/416
- [96] Hashish, M.: Optimization factors in abrasive-waterjet machining. Presented at the winter annual meeting of the Am society of mechanical engineering Chicago, Illinois. (1988), S. 163/180

- 
- [97] Zeng, J., and Munoz, J.: Optimization of abrasive waterjet cutting- the abrasive issues. Conference Waterjet Machining Technology Chicago, (1994), S. 274/258
- [98] Faber, K., and Oweinah, H.: Influence of process parameters on blasting performance with the abrasive-jet. 10<sup>th</sup> International Conference on Jet Cutting Technology. (1990), S. 365/382
- [99] Hashish, M.: The effect of pressure on the performance of abrasive-waterjet (AWJ) machining. Proceedings manufacturing international symposium on product and process design. (1988), S. 225/263
- [100] Kovacevic, R., Mohan, R. and Beardsley, H. E.: Monitoring of thermal energy distribution in abrasive waterjet cutting using infrared thermography. In: Journal of Manufacturing Science and Engineering, Volume 118, (1996), S. 555/563
- [101] Kovacevic, R., and Mohan, R.: Heat flux determination at the AWJ cutting zone using IR thermography and inverse heat conduction problem. HTD- Proceedings of the ASME heat transfer division. Volume 332, (1996), S. 245/254
- [102] Ohadi, M., Ansari, A. I., and Hashish, M.: Thermal energy distributions in the workpiece during cutting with an abrasive waterjet. In: Journal of Engineering for industry, Volume 114, (1996), S. 67/73
- [103] Gschwandtner, M., Höver, M., Louis, H., Pude, F., and Chr. von Rad: A thermographical view on tool and workpiece during the cutting process of abrasive waterjets. Proceedings of the 3<sup>rd</sup> International Conference on Machining and Measurements of Sculptured Surfaces, Krakow, (2003), S. 409/422
- [104] Hlavac, M. L: Physical analysis of the energy balance of the high energy liquid jet collision with brittle non-homogenous material. 8<sup>th</sup> American Water Jet Conference, (1995), S. 681/697
- [105] Vijay Krishna, M., and Ramesh Babu, N.: A model for production of striation free depth in abrasive water jet cutting. Precision engineering, narosa publishing house, New Delhi, India, (200), S. 211/221
- [106] Momber A. W: The kinetic energy of wear particle generated by abrasive-water-jet erosion. In: Journal of materials processing technology, Volume 83, (1998), S.121/126

# Lebenslauf

## Persönliche Daten

Name	Mohamed
Vorname	Mostafa
Geburtsdatum	19.04.1968
Geburtsort	Kena, Ägypten
Familienstand	verheiratet, 3 Kinder
Nationalität	ägyptisch

## Schulbildung

1974 – 1980	El Shuban El-Muslimen, Grundschule, Kena
1981 – 1983	El-Tahrier, Mittelschule , Kena
1983 – 1987	El-Shaheed Abdel Monem Reyad, Oberschule, Kena

## Hochschulausbildung

1987 – 1992	B.Sc. Maschinenbau an der Universität El-Minia, Ägypten
1992 – 1996	M.Sc. Maschinenbau an der Universität El-Minia, Ägypten

## Berufliche Tätigkeiten

1992-1999	Wissenschaftlicher Mitarbeiter im Fachbereich Maschinenbau (Production and Design department), an der Universität El Minia, Ägypten
seit 8/1999	Stipendiat der ägyptischen Regierung an der Universität Hannover mit dem Ziel der Promotion